Fermi National Accelerator Laboratory

JA

FERMILAB-Pub-94/390-A
November 1994

ON THE EVOLUTION OF THE LIGHT ELEMENTS I. D, ^{3}He, AND ^{4}He

Brian D. Fields

Department of Physics
The University of Chicago, Chicago, IL 60637-1433

NASA/Fermilab Astrophysics Center
Fermi National Accelerator Laboratory, Batavia, IL 60510-0500

and

Institut d'Astrophysique
98 bis, Blvd. Arago
Paris 75014
FRANCE

Submitted to
The Astrophysical Journal

Operated by Universities Research Association Inc. under contract with the United States Department of Energy

ABSTRACT

The light elements D, ^{3}He, ^{4}He, and ^{7}Li are produced in big bang nucleosynthesis (BBN) and undergo changes in their abundances due to galactic processing. Since one may observe most of these elements only in contemporary environments, knowledge of the intervening evolution necessary for determining the observational constraints on primordial nucleosynthe . Chemical and stellar evolution model dependences in light element evolution are systematically investigated via a comparison of 1460 possible chemical evolution scenarios and of stellar nucleosynthesis yields, all of which have been selected to fit solar neighborhood C, N, O, and Fe abundances as well as the observed local gas density and gas mass fraction. The light element evolution and solar system yields in these models are found to span a wide range, explicitly demonstrating the model dependence. The range of model dependence for D, ^{3}He, and ^{4}He solar abundances is calculated, and the sensitivity of this range to the heavy element constraints is noted. The chemical evolution contribution to the uncertainty in the observed primordial light element undances is estimated, and the effects of this uncertainty on big bang nucleosynthesis results are discussed. The predictions for the light elements are found to be correlated; the extent and physical origin of these correlations is discussed. D and ^{3}He evolution is found to have significant model dependence, however, the dominant factor determining their solar and interstellar abundances is their primordial abundance. In addition, ^{3}He is found to be very sensitive to the details of processing in low mass stars. ^{4}He yields are shown to be very model dependent: in particular, both the introduction of mass loss and the possibly very high ^{4}He stellar yields in the poorly understood mass range of $\sim 8 - 12\ M_\odot$ can lead to large enhancement of ^{4}He production and can lead to large slopes of $\Delta Y/\Delta$N and $\Delta Y/\Delta$O. It is found that the inclusion of secondary nitrogen leads to only a small distortion in the low metallicity $Y-$ N relation if there is also a significant contribution of primary N, as demanded by observations.

1 Introduction

A central element of the hot big bang cosmological framework is the prediction of light element (D, ^{3}He, ^{4}He, and ^{7}Li) synthesis during the epoch of big bang nucleosynthesis (hereafter BBN). This prediction is tested against observations of the light elements abundances, and the agreement between theory and observation provides major empirical support for the big bang. The comparison between prediction and measurement is not always simple, however. Many of the observations are of environments that are contemporary to the present, or nearly so, and galactic astrophysical production and destruction of the light elements may have changed their abundances. An understanding of these galactic processes is thus needed to in order to accurately interpret the light element observations and so to realistically constrain BBN. The study of the nuclear history of galaxies is the domain of galactic chemical evolution: here we will re-examine the galactic chemical evolution of the light elements.

Models for galactic chemical evolution were first constructed in the 1970's and for the most part studied the nucleosynthesis history of the heavy elements. Since such pioneering work as Cameron & Truran (1971), Talbot & Arnett (1971), and Tinsley (1980, 1972), chemical evolution has come to do a surprisingly good job of reproducing many solar abundance patterns and even many abundance histories as observed in and around the solar neighborhood (see, e.g., the recent work of Timmes, Woosley, & Weaver (1994); Matteucci & Francois (1989); and Ferrini et al. (1992)). These models also give reasonable predictions for stellar luminosity evolution (see, e.g. Tinlsey (1980); Colin & Schramm (1993)), and underpin the study of nucleocosmochronology (e.g. Thielemann et al (1993)).

The chemical evolution of the light elements has been studied since the work of Cameron & Truran (1971), and has been used to determine primordial abundances since the work of Reeves, Audouze, Fowler, & Schramm (1973) and Audouze & Tinsley (1974). These seminal papers made a critical comparison of light element abundances from deuterium to boron with the various cosmological and astrophysical processes suggested for their production. Since this early work there have been many calculations of light element chemical evolution, usually focusing on a few nuclides (see references in §§2.3–2.6). In this paper we will again take a comprehensive look at all of the light elements to see how consistent a picture of their joint chemical evolution can be made.

Chemical evolution models are physically based on important mass conservation principles, and have been refined considerably over the years. Unfortunately, however, chemical evolution is still a somewhat ambiguous enterprise. One should always be mindful of the uncertainties in the conventional prescription for these calculations. These uncertainties stem from unknown character of star formation rates and mass distributions, galactic inflow and outflow of gas, as well as from unresolved model dependent effects in stellar evolution nucleosynthesis calculations and cosmic ray distributions. Lacking a first principles calculation of these phenomena, we are forced to model them in a

phenomenological or schematic way.

As a result of these uncertainties, the commonly adopted framework for chemical evolution contains features that are not well understood in a theoretical and/or empirical way. Thus within this framework, there are a great many ways to construct specific models, and work has been done using a diverse variety of the possible scenarios. Encouragingly, the overall framework has been quite successful despite these difficulties. And indeed chemical evolution is a always a part of comparison of nucleosynthesis calculations with data (though sometimes its role is only implicit).

The effects of chemical evolution model dependences have been investigated to varying degrees. However, the larger studies of these effects (e.g. that of Tosi (1988)) did not concentrate on the light elements, and work on light element evolution has not examined model uncertainties as broadly. There has not yet been an emphasis on the full range of uncertainty in the predictions for a comprehensive description of light element chemical evolution.

In this paper we construct a chemical evolution framework for the evolution of all of lthe light elements, and we obtain estimates of the range of model uncertainties. We will follow the history of all of the light elements, D through ^{11}B. We also include the non-cosmological "heavy" elements ^{12}C, ^{14}N, ^{16}O, and ^{56}Fe, which serve as benchmark tests of potential models. We systematically examine a wide variety of model assumptions, examining many chemical evolution prescriptions and parameterizations (in the spirit of Tosi (1988)), as well as including many suggested galactic production and destruction mechanisms for each of the light elements (in the spirit of Reeves, Audouze, Fowler, & Schramm (1973)).

Our strategy is to choose a broad chemical evolution framework, allowing for many features that authors have considered in examining the histories of specific light elements. These features are chosen to be inclusive, without regard for their compatibility. With these we form a very large ($\sim$ 1200) set of models which include all combinations of these features. We then constrain these models to fit observed solar neighborhood characteristics, apart from those of the light elements. This reduces the set of potential models to $\sim$ 120 models which are viable descriptions of solar neighborhood chemical evolution (again, light element behavior aside). To each of these successful models we add a range of 18 variants of light element evolution. We then examine the predictions of this large battery of light element evolutionary schemes. Specifically: (1) we see which models fit light element observations; (2) we estimate the chemical evolution uncertainty and discuss its influence on the use of BBN observational constraints; and finally (3) we note correlations between the evolution of different light element nuclides. As part of this analysis we will consider as well the uncertainties in the solar system constraints themselves.

In addition to these considerations of the whole set of the light elements, we will also address specific issues particular to each of them For example, recent observations

of high-redshift quasar absorption line systems have approached the precision needed to give meaningful D abundances. This is an exciting prospect indeed, as these high-z environments are much more pristine than contemporary ones, and so give a new window to a much earlier epoch in D evolution (though still $\gtrsim$ 1 Gyr after BBN). The initial reported abundances by Songalia, Cowie, Hogan, & Rugers (1994) and by Carswell, Rauch, Weymann, Cooke, & Webb (1994) were tantalizingly high if taken at face value (see, e.g. Kernan & Krauss (1994) and Cassé & Vangioni-Flam (1994), and Steigman (1994)). However, the observers themselves have been careful to caution that the absorption line systems may be subject to contamination, and so the derived D abundances are best understood as upper limits to the actual levels of D/H. Clearly, the present situation is in flux and more observations are needed to determine the D abundance in these systems accurately; but just as clearly, this technique is quite promising and holds the key for a very accurate D abundances at very early epochs. We will examine D evolution in detail in this paper, and comment on the role of it chemical evolution in interpreting the quasar absorption line system observational program.

These new constraints on D evolution also call attention to conventional accounts of the evolution of ^{3}He. Recent improved observations of ^{3}He in Galactic H II regions can be puzzling in light of preceding discussions of this element. The data suggest that ^{3}He shows spatial variations, and that the abundance of ^{3}He today in the ISM is not significantly larger than that at the formation of the solar system—indeed, in some places, ^{3}He is even seen in (possibly) smaller amounts. This may call into question (Hogan (1994)) the conventional wisdom about ^{3}He production in low to intermediate mass stars (Iben & Truran (1978)). On the other hand, the high ^{3}He abundance seen in planetary nebulae (Rood, Bania, & Wilson (1992)) seems to support the notion of production in low mass stars at a level roughly consistent with that predicted by Iben & Truran (1978). Thus the H II region data may more likely point to a need to re-examine ^{3}He evolution in high mass stars (Olive, Rood, Schramm, Truran, & Vangioni-Flam (1994)). However, as the issue of low mass stellar production of ^{3}He is crucial, we will address it explicitly.

The much more abundant helium isotope, ^{4}He, is important because it is so powerful. Notably, an accurate assay of the ^{4}He content of the universe provides a bound on N_ν, the number of light neutrino families, as first shown by Steigman, Schramm, and Gunn (1977). Thus there are continual improvements in the accuracy of theoretical predictions for ^{4}He (e.g. Dicus et al. (1982), Walker et al. (1991), Kernan (1978), Seckel (1993), and Fields, Dodelson, & Turner (1993)), as well as in the observed abundances (Skillman et al. (1994)). A pressing issue now is the systematic uncertainty in these measurements (e.g. Copi, Schramm, & Turner (1994) and Sasselov & Goldwirth (1994)). There is also discussion of the correct means of extrapolating the primordial ^{4}He abundance, an issue in which chemical evolution plays a crucial role.

The least abundant light element having significant primordial production is ^{7}Li.

There are now many observations of Li in Pop II stars, and the existence of the Spite plateau(s) well established (Spite & Spite (1982), Thorburn (1994) and refs. therein). The recent determinations of ^{6}Li/^{7}Li ratio (Smith, Lambert, & Nissen (1992); Hobbs & Thorburn (1994)) most importantly give empirical support to the longstanding claim that the Li in these stars had to be predominantly ^{7}Li. Additionally, this measurement places an important constraint on stellar models (Pinsonneault, Deliyannis, & Demarque (1991)) which were used to argue that Li these stars had suffered a large depletion from true primordial value (Steigman et al. (1993)). As ^{6}Li plays such a key role, its production via interactions between cosmic rays and the interstellar medium needs also to be well understood. Fortunately, Be, ^{10}B, and ^{11}B are also produced by this mechanism and so serve to constrain it (Prantzos, Cassé, & Vangioni-Flam (1993); Walker et al. (1993)). These elements have now been observed in Pop II stars, and there remains a need for a full account of their history that agrees in detail with the observations.

In this paper we will describe our framework for constructing models of light element chemical evolution, and summarize our overall results on model dependences. We will then discuss in more detail our results for D, ^{3}He, and ^{4}He evolution and its uncertainties. In a forthcoming work (Fields (1994), hereafter Paper II) we will discuss our results for Li, Be, and B evolution, with particular focus on the range of available models for cosmic ray nucleosynthesis of these elements.

2 Light Element Evolution

2.1 BBN Predictions

The BBN predictions are crucial to our considerations, as the primordial yields set the initial conditions for the chemical evolution calculation. The basic BBN calculation itself is well established has not changed dramatically since the calculation of Wagoner, Fowler, & Hoyle (1967). For reviews we refer the reader to, e.g., Schramm & Wagoner (1977), Boesgaard & Steigman (1985), and to Smith, Kawano, & Malaney (1993). For recent calculations see Walker et al. (1991), Krauss & Kernan (1994), and Copi, Schramm & Turner (1994).

We consider here and throughout only the simplest and "standard" case, that of BBN in a universe that is spatially homogeneous in all particle species. Some models with baryon inhomogeneities are still allowed by the data, but even these more complicated cases lead to the same basic conclusions, as discussed in, e.g., Malaney & Mathews (1993) and Thomas et al. (1993).

In the standard calculation, the only free parameter is $n_B/n_\gamma \equiv \eta$, the baryon-to-photon ratio. In figure 1 we plot the light element abundances as a function of η; for reference, Copi, Schramm, & Turner (1994) found concordance between theory and data

for the range

$$2.4 \times 10^{-10} \leq \eta \leq 6 \times 10^{-10} \quad (1)$$

which we have indicated on the plot.

For our purposes there are several salient features to notice. First, the ^{4}He abundance does not depend strongly on η, with variations only at the 10% level; however, we will be interested in determinations of the ^{4}He abundance to this level, and so the small differences are important. Clearly significant as well is the precipitous decline in D and ^{3}He abundance with η. Thus there is a large range of initial values which these may take, particularly for D which varies more strongly with η. Indeed, in the allowed range D varies by a factor of 9. This simple point is an important one, as we will find that the a requirement of significant depletion of initially high D down to the solar and interstellar abundance is a serious constraint on chemical evolution models.

As we will see, the combined abundance D+^{3}He can most profitably and model independently be used to constrain η. Note that for the concordant range of η that this sum is dominated by the contribution from D. Knowledge of the primordial level of D is tantamount to knowledge of D+^{3}He: thus the D abundances obtained from quasar absorption line systems will provide a constraint on this sum. Such a constraint will be a crucial one in light of present determinations of the solar system and interstellar D and ^{3}He abundances.

The final BBN trend to notice is that of ^{7}Li, which in the concordance region lies at its minimum. Thus for BBN predictions to agree with theory the primordial ^{7}Li abundance cannot be much larger than the value at its minimum, ^{7}Li/H $= 10^{-10}$. This is indeed the value of the Spite plateau (Spite & Spite (1982); Thorburn (1994)), i.e. the ^{7}Li abundance seen in all old (i.e. metal poor Pop II dwarf) stars with $T \gtrsim 5500$ K and [Fe/H] $\lesssim -1$. If this plateau value in these primitive stars does faithfully reproduce the primordial ^{7}Li abundance—i.e., if no original ^{7}Li has been destroyed over the stars' lifetime—then all is well for BBN. Indeed, standard stellar models (e.g. Deliyannis et al. (1990)) do not indicate significant depletion of ^{7}Li. However, some stellar models including a mock-up of the effects of rotation show significant depletion, with the initial ^{7}Li abundance reduced by a factor of $\sim$ 10 (Pinsonneault, Deliyannis, & Demarque (1991)). If these models were correct, then primordial ^{7}Li would be at a much higher value than the Spite plateau indicates, and this would be a challenge to the standard BBN picture.

An important constraint on Li depletion Pop II stars is the determination of the ^{6}Li/^{7}Li isotopic ratio in several such stars (Smith, Lambert, & Nissen (1992); and Hobbs & Thorburn (1994)). These groups find ^{6}Li/^{7}Li ~ 0.05. ^{6}Li is only known to be made in cosmic rays; furthermore, its cosmic ray production can be estimated from the abundances of Be and B which have a similar origin (and are less fragile and so less subject to depletion). Thus we can (roughly) estimate the abundance of ^{6}Li expected for these stars, which is consistent with that observed. Moreover, the existence of *any* ^{6}Li is

a strong constraint on depletion models because ^{6}Li is more fragile than ^{7}Li (Steigman et al. (1993)). For our purposes, it is clear that in our chemical evolution models we will wish to include cosmic ray production of ^{6}Li, Be, and B as well as ^{7}Li.

2.2 Chemical Evolution Framework

The basic theoretical framework and observational constraints on models of chemical evolution is well reviewed in Tinsley (1980). We will for the most part adopt her notation. Our goal is to trace the history of the Galaxy's isotopic content. Ideally, we wish to model formation of stars in inhomogeneously distributed gas clouds, their return of material during their lifetime to the ISM via winds, and finally their deaths, which occur in stochastic bursts and return processed and unprocessed material to the ISM. In principle, all of these processes can depend on many variables, e.g. the metallicity of the gas, the temperature of the gas, and the strength and configuration of the galactic magnetic fields, to name a few.

However, the ideal description is quite out of our theoretical and computational reach, and to reduce to problem to a tractable one, simplifying assumptions are necessary. We will assume the Galaxy (or at least the solar neighborhood, which is all we are really interested in here) to be spatially homogeneous. We will assume that stars are born according to a given mass distribution, and that their lifetimes are a function of mass only. We will assume that all of the stellar ejecta are returned at once at the time of the star's death. These ejecta we will take to be instantaneously mixed in the interstellar medium (ISM). These assumptions, though strong, are adequate for many applications, and in any case are necessary to proceed.

A fundamental uncertainty in galactic chemical evolution arises due to our ignorance about the process of star formation from gas clouds. Lacking firm theoretical guidance, we are left to phenomenologically define a stellar creation rate

$$C(m,t)\,dm\,dt\ , \tag{2}$$

the number of stars born (per pc^2)[1] at the time interval $(t, t+dt)$ in the mass interval $(m, m+dm)$ (here and throughout, we will give mass in units of $M_\odot$, unless otherwise noted). The creation function conventionally divided into star formation rate (hereafter SFR, ψ) and initial mass function (hereafter IMF, ϕ)

$$C(m,t)\,dm\,dt = \psi(t)\phi(m)\,dm\,dt\ . \tag{3}$$

The SFR has units $[M_\odot \mathrm{Gyr}^{-1}\mathrm{pc}^{-1}]$, and gives the mass per unit time going into stars. The IMF gives the mass distribution with which these stars are formed. Questions of the

[1] We use surface densities of stars here and throughout rather than full volume densities as the former have the advantage of already accounting for different distributions of stellar populations according to Galactic scale height

time constancy of IMF are hard to answer theoretically or observationally (see, e.g. Scalo (1986)). We follow most work and assume it to be constant, however we will in our final discussions address the possible effect of a differing distribution at early times due to the low metallicity of the gas.

The literature is fraught with unfortunate variations in the convention for IMF normalization; we follow Tinsley (1980) in choosing

$$\int_{m_{\rm low}}^{m_{\rm up}} dm\ m\phi(m) \equiv 1 \tag{4}$$

Note the need to for lower and upper mass limits, $m_{\rm low}$ and $m_{\rm up}$, to the IMF. These are not well constrained by data, and so will be parameters we will have to choose. Note also the possibility that the lower and upper limits to form stars might be different from limits at which stars return material to the ISM. Clearly this is true for low mass ($M < 0.4M_\odot$) stars which never proceed beyond hydrogen burning and go straight to white dwarfs. Note as well that the *upper* limit to the IMF could be different from the upper limit at which material is returned, as it has been proposed that high mass ($\gtrsim 30M_\odot$) stars could proceed directly to black holes without becoming supernovae and not return any material to the ISM; on the other hand, mass loss could cause all stars above some mass $\sim 30 - 40\ M_\odot$to behave like a $30 - 40\ M_\odot$ star.

We will use a one zone model for the Galactic disk (more properly, the solar neighborhood), treating it as as homogeneous and instantaneously mixing. We will track the total disk mass in terms of its surface mass density $\sigma_{\rm tot}$, which evolves by

$$\frac{d\sigma_{\rm tot}}{dt} = f \tag{5}$$

where f is the rate for the infall of new material due to, e.g. the collapse of the disk or to accretion of extragalactic material. in units $[M_\odot {\rm Gyr}^{-1}\ {\rm pc}^{-2}]$.

We put the basic constituents of matter as stars (including their remnants) and gas,

$$\sigma_{\rm tot} = \sigma_{\rm s} + \sigma_{\rm g}\ . \tag{6}$$

Of these, we will explicitly track the gas, which evolves according to

$$\frac{d\sigma_{\rm g}}{dt} = -\psi + E + f \tag{7}$$

where

$$E(t) = \int_{m_t}^{m_{\rm up}} dm\ m^{\rm ej}\ \phi(m)\ \psi\,(t - \tau_m) \tag{8}$$

is the rate at which dying stars eject processed material back into the ISM. The lower mass limit, m_t, is the stellar mass m for which $\tau_m = t$, i.e. the smallest mass star which dies just at time t after being created at $t = 0$.

We will define the mass fraction

$$X_i \equiv \frac{\sigma_i}{\sigma_{\rm tot}}\ , \qquad \sum_i X_i \equiv 1 \tag{9}$$

and we write

$$\frac{d\,(\sigma_{\rm g} X_i)}{dt} = -\psi X_i + E_i + X_i^{\rm inf} f \tag{10}$$

where

$$E_i(t) = \int_{m_t}^{m_{\rm up}} dm\ m_i^{\rm ej} \phi(m) \psi(t - \tau_m) \tag{11}$$

is the rate of the ejection of isotope i to the ISM.

Note that the presence of the "retarded time" $t - \tau_m$ makes the equations unwieldy. Indeed, in practice one often makes ψ a function of $\sigma_{\rm g}$ and/or $\sigma_{\rm tot}$, thus rendering the basic equations as integro-differential. These are in not general soluble analytically, and thus a proper treatment requires numerical solutions. We have therefore numerically implemented the preceding equations, taking into account their full integro-differential nature. Our results are all based on these calculations.

In passing we mention an approximation that does allow for analytic solutions, the instantaneous recycling approximation. If the stellar lifetimes relevant to the problem are short compared to the galactic age, one may set $\tau_m = 0$ and putting $m_t = m_{t_1} = 1 M_\odot$ (a subscript 1 here and throughout denotes the present value, in this case t_1 being the age of the Galaxy today). While this approximation is a bad one for any calculation involving the long-lived low mass stars, it has the great utility if reducing the basic equations to ordinary differential equations, and so allows for analytical solutions. We do not make this approximation in our numerical results presented here, but some analytic results using it do provide some intuition for the full calculations.

It is useful to define the return fraction

$$R = \int_{m_{\rm low}}^{m_{\rm up}} dm\ m^{\rm ej} \phi(m) \tag{12}$$

the fraction of mass going into a generation of stars that will eventually be ejected back into the ISM. Note that $R < 1$ and that it is very sensitive to the choice of IMF form and mass limits. We will also use $\mu \equiv \sigma_{\rm g}/\sigma_{\rm tot}$ for the gas mass fraction.

Of the model features we have described, those most influential on the abundance predictions are the IMF, the SFR, infall, and the adopted nucleosynthesis yields. Of these, the IMF, SFR, and infall (or outflow) are not well understood theoretically, and so one must select a phenomenological prescription for each. The stellar nucleosynthesis inputs come from model calculations for different stellar masses (and sometimes different metallicities). For the most part only a limited number of metallicities are used, thus forcing chemical evolution models to interpolate and extrapolate. A better treatment would iteratively run both stellar models and chemical evolution models; such a program

has recently been done by Timmes, Woosley, & Weaver (1994), who emphasized heavy element yields which they calculated self-consistently using a supernova code.

Of the other input parameters, two are cosmological. The first is of course the BBN result of the initial abundances; our approach to this is discussed below (§4.4.2). The other cosmological parameter is the age of Galaxy including the collapse of the disk; we will take this 15 Gyr, and our results are not very sensitive to this choice. We will take the age of the earth to be 4.6 Gyr. Finally, we will use the τ_m vs. m relation of Scalo (1986), but again, our results are insensitive to this choice.

Having selected a set of models representing the range of choices of the major model features—IMF, SFR, and nucleosynthesis—we will want to constrain this set with observational data. Specifically, we will test these against solar system abundances of CNOFe, as well as the gas mass fraction. The confrontation with observations will select a set of viable models which we will then use to test different models of light element abundances. Thus we will want to include in our initial suite of models all variations of the major features— the IMF, SFR, and nucleosynthesis—which have been proposed to be well-suited to fit individual light elements. Therefore, we now will review the chemical evolution of the light elements, to identify features to include in the initial set of chemical evolution features.

2.3 Deuterium

2.3.1 D Data

Traditionally, D has been measured in the solar system and in the ISM. Important evidence for the solar system D abundance came as a result of the Apollo 11 mission (Geiss & Reeves (1972)), giving a measurement of the D+^{3}He content in the solar wind. These data are complemented by measurements of meteorites (Black (1972)), which allows determination of the presolar D level. The best numbers now are that the presolar D abundance is $(\mathrm{D/H})_\odot = 2.6 \pm 1.0$ (Geiss (1993)).

The D abundance in the ISM was first measured by Rogerson & York (1973). It has most recently been observed by the *Hubble Space Telescope*, with Linsky et al (1993) reporting $(\mathrm{D/H})_{\mathrm{ISM}} = 1.5^{+0.07}_{-0.18}$. This single, remarkably precise measurement will prove to set strong constraints on chemical evolution models.

Most D measurements to date have been of local and relatively recent epochs, viewed cosmologically. However, exciting new observations have reported possible detection of D in quasar absorption line systems (QSOALS). The absorption systems considered lie at high redshift ($z > 3$), and so are very young ($1 - 3$ Gyr). Thus one expects D to have suffered much less depletion. Indeed, initial reports (Songalia, Cowie, Hogan, & Rugers (1994); Carswell, Rauch, Weymann, Cooke, & Webb (1994)) suggested the possibility of a very high D, at levels of $\mathrm{D/H} \lesssim 2.5 \times 10^{-4}$. Both of these groups have been careful to caution that this result can only be regarded with surity as an upper bound on D, as

low column density intervening clouds can pollute or even mimic wholesale the D line.

2.3.2 D Chemical Evolution

Deuterium was originally thought not to be primordial, but to be produced in the T-Tauri phase of stellar evolu (Fowle., Greenstein, & Hoyle (1962)). However, this process was shown to fail (Ryter, Reeves, Gradstajn, & Audouze (1970)), and Reeves, Audouze, Fowler, & Schramm (1973) argued that D was likely of cosmological origin. This argument was cemented by the work of Epstein, Lattimer, & Schramm 1976), who showed that a fundamental nuclear proper. of D, namely having the minimal binding energy for a complex nucleus, sets very strong constraints on any process which can form it. Indeed, these authors pointed out that not only is D destroyed in stellar burning, but moreover, *any* known or likely astrophysical process destroys D—except the big bang.

Indeed, as recently emphasized by Copi, Schramm, & Turner (1994), from the perspective of BBN, D is best baryometer, i.e., the constraints on η which arise from D observations are particularly reliable. This reliability stems from the uniquely straightforward evolution of D in galaxies: all of the D in the universe was produced in BBN, and all subsequent processes destroy it. This fundamental fact greatly simplifies the chemical evolution of D, which has no sources and so is absent from any processed material that is returned to the ISM. The D abundance thus provides a clean indication of the amount of material that has not been processed in stars. (The galactic evolution of D and the other light elements is summarized in table 1).

To get a feel for D evolution, we note that in the instantaneous recycling approximation, the D evolution can be solved exactly as

$$\frac{X_2}{X_2^{\rm P}} = \mu^{-R/(1-R)} \quad . \tag{13}$$

Note that this result does not depend on the form of the star formation rate ψ. Furthermore, since the the gas fraction μ is constrained by observation, the entire character of the depletion comes from R, the return fraction. This is in turn completely determined by the initial mass function. Physically, the D abundance is a measure of the fraction of gas which remains unprocessed. Thus as material is cycled into stars, the D depletion will depend on how much (D-free) material is returned to the ISM to dilute the unprocessed component.

The main chemical evolution feature to consider in order to capture the range of D evolution is that which determines the return fraction R, namely the IMF. We will want to consider the gamut of possible IMF forms and mass limits. Indeed, we will expect all the light element evolution to depend strongly on the adopted IMF.

2.4 Helium–3

2.4.1 ^{3}He Data

The solar system information on both ^{3}He and D come together and are derived from measurements of the solar wind and meteorites (Geiss (1993); Black (1972)); the presolar abundance is $(^3\mathrm{He/H})_\odot = 1.5 \pm 0.3$. In the ISM, ^{3}He is observed in Galactic H II regions, and measured via its hyperfine line. Although these measurements are difficult, they apparently show real variations, with $(^3\mathrm{He/H})_{\mathrm{ISM}} \sim (1-5) \times 10^{-5}$ (Bania, Rood, & Wilson (1987)). ^{3}He has also been detected by Rood, Bania, & Wilson (1992) in a planetary nebula, and is found at very high levels: $^3\mathrm{He/H} \sim 10^{-3}$.

2.4.2 ^{3}He Chemical Evolution

As noted in §2.4, BBN yields a fairly low ^{3}He abundance, but not much lower than contemporary observations; i.e. BBN theory does not leave a lot of room for the increase of ^{3}He. On the other hand, stellar models firmly show that all initial D in a star is processed to ^{3}He in the pre-main sequence phase when the star is fully convective. Some of this ^{3}He survives to be ejected at the star's death, and indeed in low mass stars there is likely to be ^{3}He production. Thus while D suffers astration and ^{3}He is produced over time, the sum of the two, D+^{3}He, is more stabile; furthermore, D+^{3}He is at first dominated by D and then galactic evolution increases the ^{3}He to the point that the ISM today has about equal measures of each.

Yang et al. (1984) get a bound on $(\mathrm{D}+^3\mathrm{He})_\mathrm{p}$ by noting that in all stars, any initial D goes to ^{3}He in the pre-main sequence phase. Some fraction $g_3(m) < 1$ of that ^{3}He survives in the ejecta at the star's death. If we consider one stellar generation, and let $\langle g_3 \rangle$ be the average of $g_3(m)$ over the mass function, it may be shown that

$$\left(\frac{\mathrm{D}+^3\mathrm{He}}{\mathrm{H}}\right)_\mathrm{p} \leq \frac{1}{\langle g_3 \rangle}\left(\frac{^3\mathrm{He}}{\mathrm{H}}\right)_\mathrm{i} + \left(\frac{\mathrm{D}}{\mathrm{H}}\right)_\mathrm{i} \tag{14}$$

(Yang et al (1984)). The inequality (eq. 14) comes from disregarding ^{3}He production, and so guaranteeing that X_{23} decreases with time. If we do allow for possible production, it is no longer appropriate to use the Yang et al (1984) argument to get a *bound* on X_{23}: instead, one is getting an estimate of X_{23}; nevertheless, the bound is a safe one.

Indeed, within our formalism, we may get another perspective on it by seeing how the D+^{3}He argument plays out not for a single stellar generation, but in the approximation of instantaneous recycling (see preceding section) for a closed box chemical evolution model. We have

$$\frac{d(\sigma_\mathrm{g} X_3)}{dt} = -\psi X_3 + R\langle g_3 \rangle \psi \left(\frac{3}{2} X_\mathrm{D} + X_3\right) \tag{15}$$

and when substituting from eq. 10 we have

$$\frac{(\frac{3}{2}X_2 + X_3)}{(\frac{3}{2}X_2 + X_3)_{\rm p}} = \left(\frac{X_2}{X_2^{\rm p}}\right)^{1-\langle g_3\rangle} \tag{16}$$

and so in term of observable number ratios,

$$\frac{({\rm D} + {}^3{\rm He})}{({\rm D} + {}^3{\rm He})_{\rm p}} = \left(\frac{\rm D}{\rm D_p}\right)^{1-\langle g_3\rangle} \left(\frac{X_1}{X_{\rm p}}\right)^{\langle g_3\rangle} \approx \left(\frac{\rm D}{\rm D_p}\right)^{1-\langle g_3\rangle} \tag{17}$$

Whether D+^{3}He increases or decreases with time depends on the sign of $1 - \langle g_3\rangle$. For $\langle g_3\rangle > 1$, i.e. net ^{3}He production. D+^{3}He increases with time. For $\langle g_3\rangle < 1$, the opposite is the case. Note, however, that because low mass stars are crucial here, that the IRA is inappropriate. At any rate, there is a close relationship between D and ^{3}He, and we see that it is crucial to know whether ^{3}He is created or destroyed with time.

The physical explanation for the different fate of ^{3}He in high and low mass stars is that for $M < 2M_\odot$, p–p is the dominant form of hydrogen burning, and the $p(p,\nu e){\rm D}(p,\gamma)^3{\rm He}$ chain makes ^{3}He. However, for $m > 2M_\odot$, the CNO cycle dominates the hydrogen burning, and ^{3}He is destroyed. Indeed, Iben & Truran's (1978) calculation for low mass stars suggests that ^{3}He is produced copiously. Dearborn, Schramm, & Steigman (1986) find that ^{3}He is destroyed in high mass stars, particularly at low metallicity. Woosley & Weaver (1994) give more detailed but qualitatively similar results.

These conventional notions about ^{3}He evolution have recently been called into question as the interstellar ^{3}He abundances have become more accurate. Until recently, the production of ^{3}He in low mass stars was not considered in chemical evolution studies, e.g. that of Steigman & Tosi (1992). Vangioni-Flam, Olive, and Prantzos (1994) let the contribution to $\langle g_3\rangle$ from low mass stars be a free parameter, and used the Dearborn et al (1986) high mass yields. They found that to fit the data require net destruction by low mass stars, a mechanism for which is suggested by Hogan (1994). Indeed, with the Iben & Truran (1978) and Dearborn et al (1986) results, Galactic ^{3}He which starts with the espoused BBN value is apparently overproduced in many chemical evolution models (Olive et al (1994)). However, in the face of this apparent need for ^{3}He destruction is the observed prescence of high ^{3}He in planetary nebulae (Rood, Bania, & Wilson (1992)) at a level in rough agreement with Iben & Truran's calculation.

Another ^{3}He puzzle is the observed and apparently real dispersion in ^{3}He abundances. Bania, Rood, & Wilson (1987) present this dispersion as a ^{3}He abundance gradient, with ^{3}He decreasing towards the galactic center. This trend runs counter to intuition, if ^{3}He is to be formed by low mass stars which are more prevalent towards the galactic center. Moreover, for stars having lifetimes this long, it is hard to see how this gradient could happen at all, as such stars will have traveled a significant fraction of disk in their lifetimes and so should be well spread throughout the Galaxy.

A possible explanation for "what is wrong with ^{3}He" was offered by Olive et al (1994). They point out that the correlation of ^{3}He with galactocentric distance might be better understood as a correlation with the mass of the H II region. Then the ^{3}He in the higher mass regions will contain more ejecta from high mass stars. In this scenario, one expects ^{3}He to be lower wherever there is more ejecta from massive stars, i.e. more stellar processing. Thus the ^{3}He abundance should go down towards the center of the galaxy, where the density and so the star formation rates are higher. Note that this could also answer the puzzle of the existence of the gradient despite the long lifetime of low mass stars. The point is that there is not a gradient in ^{3}He production (by low mass stars), but instead there is a gradient in destruction by short-lived, high mass stars.

For our chemical evolution models, we will wish to consider want to use our apparatus to address the important issue of the effect of low mass processing on ^{3}He evolution, allowing for different possibilities as done by Vangioni-Flam, Olive, & Prantzos (1994). We will also include infall, as was done in Steigman & Tosi (1992).

2.5 Helium-4

2.5.1 ^{4}He Data

The ^{4}He observational situation well reviewed elsewhere, e.g. Pagel (1993), Pagel et al (1992), Walker et al (1991), Davidson & Kinman (1985), Skillman & Kennicutt (1993); Skillman et al (1994); and Copi et al (1994). Briefly, accurate observations of ^{4}He are hard to come by. Observations are best in H II regions, nebulae of ionized hydrogen. Here the He should also be ionized, and accurate abundances should be attainable. Although there have been observations of ^{4}He in Galactic H II regions, systems with lower metallicity are expected to reduce contamination from stellar ejecta. The sites of choice have proven to be metal poor extragalactic H II regions.[2]

The solar system abundance of ^{4}He is $Y_\odot = 0.274 \pm 0.016$ (Anders & Grevesse (1989)). ISM abundances are hard to come by, and furthermore, the ionization structure of gas regions causes ^{4}He to be systematically underestimated. (Wilson & Rood (1994)). Thus we have no information on ^{4}He in the ISM that is accurate enough to be an important constraint on chemical evolution models.

2.5.2 ^{4}He Chemical Evolution

As the second most abundant nuclide in the universe, next to hydrogen, ^{4}He comprises about a quarter of the universe's baryonic mass. It is also the only nuclide made in significant amounts in stars of a broad range of masses, with the dominant production

[2]Jakobsen et al. (1994) have recently reported detection ^{4}He in a quasar absorption line system. The uncertainties in the measurement render it a qualitative confirmation of BBN, but with more accuracy this type of observation could be extremely powerful.

in stars of middle masses. Despite this ubiquitous stellar synthesis, however, stars only make a small ($< 10\%$) contribution to the total helium abundance (Hoyle and Tayler (1964)): most ^{4}He is primordial. Nevertheless, to fully test BBN and moreover to use its power to constrain particle physics and/or test conditions in the early universe, one needs to know the abundance of ^{4}He exceedingly well.

Even in low metallicity H II regions, stellar pollution exists; the question is how best to determine it and so deduce the primordial He abundance. To this end Peimbert & Torres-Peimbert (1974, 1976) noted that He production should be correlated with heavier element production. In H II regions one observes both He and oxygen, nitrogen, and carbon. Following Peimbert & Torres-Peimbert, one deduces the primordial helium mass fraction $Y_{\rm p}$ from extrapolating the low metallicity end of the Y vs. Z plot, exploiting the relation

$$Y = Y_{\rm p} + \frac{dY}{dZ} Z \tag{18}$$

Equation (18) should be valid for sufficiently small Z, for which this procedure should succeed in extrapolating $Y_{\rm p}$. The challenge for chemical evolution is to determine which Z are sufficiently small, and which "metals" C, N, and/or O are the best surrogates for Z. The challenge for observers is to make precise enough measurements to allow for a meaningful extrapolation.[3]

Analysis using this technique has for the most part avoided the explicit use of detailed chemical evolution calculations. Instead, the approach has been an empirical one: Y and Z are measured for different regions; the Y vs. Z relation is plotted, fit, and extrapolated to get $Y_{\rm p} = Y(Z = 0)$. Two complications to this procedure immediately arise. First, one does not directly measure the metal fraction Z, and so one uses as a surrogate either oxygen or nitrogen (and carbon—see Steigman, Gallagher, & Schramm (1989)). Second, and moreover, one must adopt an expected Y vs. O (and N or C) relation to use in fitting the data and making the extrapolation.

While everyone recognizes that the fits need not be linear, this is the simplest two parameter fit, and so this has been the first to be tried. A glance at the data (see figure 10) suggests that this might not be a bad first guess. Indeed, the Y vs. O/H relation is well described by a linear fit. In contrast, the case of nitrogen as a metallicity tracer has generated vigorous debate as to the appropriate fitting function. At issue is whether to choose a linear fit, in which the slope $\Delta Y/\Delta$N is constant, or a nonlinear one, in which N $\propto Y^2$, and thus the slope is not constant and has the possibility of being quite steep for small N, i.e. at early times (Fuller, Boyd, & Kalen (1991); but see Olive, Steigman, & Walker (1991)).

[3]The difficulties of measuring He and metal abundances to the desired accuracy ($Y_{\rm p}$ good to the third decimal place!) cannot be overstated. For attempts to correct for some of these errors by culling points from the data set see Pagel (1993), Pagel & Kazlauskas (1992), Pagel, Simonson, Terlevich, & Edmunds, (1992), and Olive & Steigman (1992).

Put differently, the question regarding the $Y - \mathrm{N}$ relation is, what is the $\mathrm{N} - \mathrm{O}$ relation? The nonlinear fit for Y vs. N arises by assuming that N production is proportional to the C and O abundance, leading to the "secondary" relationship $\mathrm{N} \propto \mathrm{O}^2$. We wish to know the relative size of the primary and secondary stellar contributions to N, an issue not yet resolved. Consequently, we will want to allow test the viability both primary and secondary origins for N.

The ^{4}He used in deriving Y_p is observed for the most part extragalactic H II regions. To fit these regions requires a model appropriate for these galaxies. However, we will be fitting our model to the solar system. Thus, while we can expect our results to be indicative of the range of model uncertainties, we should not necessarily expect a close fit to the extragalactic data. Indeed, the few models that do exist, e.g. those of Mathews Boyd & Fuller (1993), and Balbes, Boyd, & Mathews (1993), are qualitatively similar to those studied here.

Another outstanding problem in ^{4}He evolution is the ability to reproduce theoretically the slope $\Delta Y/\Delta Z$. The theoretical dY/dZ depends on how many high mass stars are included in the calculation (e.g. Maeder (1983, 1992, 1993); Brown & Bethe (1994); and Prantzos (1994)). Note that the stellar yields for massive stars give a much lower ratio $dY/dZ \sim 1.3$ than that for intermediate and low mass stars, $dY/dZ \sim 6$. Averaged over a typical IMF with mass limits of 0.4 and 100. $M_\odot$ gives

$$dY/dZ \sim 2 \tag{19}$$

This theoretical slope is to be compared with an observed slope (calculated assuming $Z \propto \mathrm{O}$) of $dY/dZ \sim 4 - 6$ (Pagel (1993)). The discrepancy between theory and observation is well known.

One attempt to address this issue is to note that many models for high mass stars (e.g. Weaver & Woosley (1993)) do not include mass loss. For stars above $\sim 30\ M_\odot$ this can have a significant impact on all abundances but particularly ^{4}He, as suggested by the results of Maeder (1992). Indeed, stars above $\sim 30\ M_\odot$ are thought to rapidly lose mass until reaching $30 M_\odot$; thus one need only compute stellar yields up to this mass. For our purposes, we will explicitly include the possibility of mass loss in high mass stars.

Finally, an unfortunate aspect of stellar evolution is that there is a great deal of uncertainty as to the gross behavior–let alone the nucleosynthesis yields–of stars in the 8–10 $M_\odot$ mass range (further discussed below, §3.1.1). It has been suggested (Woosley & Weaver (1986)) that these stars might dominantly produce helium. This could have a large effect on the net ^{4}He production and so it is worth trying $8 - 10 M_\odot$ yields with very large yields helium, to see the sensitivity to this range.

2.6 Lithium, Beryllium, & Boron

Lithium, beryllium, and boron evolution are closely allied and so best considered together. Furthermore, the evolution of these elements is not strongly coupled to that of D, ^{3}He, and ^{4}He. Thus we shall defer a detailed discussion of Li, Be, and B until Paper II. Briefly: as discussed in the introduction and §2.1, ^{6}Li provides crucial insight into Pop II Li abundances. Li, Be, and B are all produced in cosmic rays, which allow for a wide range of models. Also, it is well known that to reproduce the the Pop I abundances of ^{7}Li and perhaps ^{11}B requires sources in addition to cosmic rays, which we include as well.

3 The Suite of Models

Our goal is to allow for a broad selection of physically plausible scenarios, including at least the variations that have been commonly used in the literature. This approach is inspired by that of Tosi (1988), although her study made infall a central feature whereas we will be more inclusive of other scenarios.

We classify model features as "global" in scope for particular to the light elements. We will designate "global" model features to be: (1) those that affect all elements (e.g. choices of SFR or IMF) and the gas consumption; or (2) those that affect the yields of C, N, O, and Fe (CNOFe), i.e. the nuclides we will be following which are not light elements but serve as chronometers or tracers for the light elements. Upon identifying the set of global model variations, we combine all of these features independently to create a large set of potential models for the solar neighborhood. By systematically investigating every possible combination of our chosen global features, we will be assured to properly estimate the full model variation inherent within the span of model options we have allowed.

Our strategy is to calculate the chemical evolution of the galaxy in all of these global models. We demand that the results conform to the features of the solar neighborhood. By selecting those models which reproduce the solar characteristics (as yet ignoring the information on the light elements themselves), we will construct a suite of observationally acceptable global models. To each of these global models is then added a wide variety of light element evolutionary prescriptions. We then calculate the chemical evolution for every light element variant, obtaining an inclusive measure of the model dependence of light element evolution.

3.1 Selection of Global Model Features

In her study, Tosi (1988) found that all aspects of chemical evolution models affect the absolute abundances. However, she found that the choice of IMF, and of course the selection of nucleosynthesis yields, had the most profound influence, affecting the

abundance ratios as well as the absolute abundances. Therefore we will want to be particularly thorough in our consideration of these model features. Our global model properties are summarized in table 2.

3.1.1 Nucleosynthesis Yields

The tabulated nucleosynthesis yields are those of low to intermediate mass stars, with masses $\sim 0.8 M_\odot$ to $\sim 8 M_\odot$, and high mass stars with masses $M > 12 M_\odot$. The former are understood to be stars whose lives progress to the point of planetary nebula ejection and becoming carbon-oxygen white dwarfs; the latter, high mass stars end their lives explosively as type II supernovae. Standard results for this study are those of Renzini & Voli (1981) for intermediate mass stars, and Weaver & Woosley (1993) for high mass stars.

There are uncertainties in the yields pointed out in these standard references. The Renzini & Voli (1981) results, for example, were found to depend on the adopted parameterization of convection in the form of the mixing length. However, we find that this level of detail is not a major source of uncertainty for our purposes. It would be desirable to compare results for different stellar models and yields; unfortunately this is not possible for the low mass stars, as Renzini & Voli (1981) are the only current models with detailed results reported. In addition, for the massive stars, several groups have published nucleosynthesis yields; however these models have very different degrees of emphasis on their nuclear yields, with Woosley & Weaver (1993) presenting particularly meticulous results.

As motivated in §2.5, we allow for a wide range of N evolution, including both primary and secondary sources for N. We thus will follow the approach of Mathews, Boyd, & Fuller (1993) in writing the mass fraction of ejected N, $X^{\rm ej}$, as

$$X^{\rm ej} = X_0^{\rm ej} \left\{ \alpha + \beta (X_C(t)/X_C^\odot) \right\} \tag{20}$$

where X_0 is the usual N yield, $X_C(t)$ is the calculated C mass fraction and $X_C^\odot$ is the solar carbon mass fraction from Anders & Grevesse (1989). The constants α and β are chosen as follows:

$$(\alpha, \beta) = (1.0) \ ; \ (0.5, 1) \ ; \ (0, 1) \ : \ (0.2) \tag{21}$$

where the first option is the standard case of purely primary N, the second is a mixed case of some primary and some secondary N, and the final two cases are variation on purely secondary N. Note that our procedure differs somewhat from that of Mathews, Boyd, & Fuller (1993) who used O as the seed nucleus for secondary N, instead of C. Carbon is the more appropriate choice (Audouze, Lequeux, & Vigroux (1975); Vigroux, Audouze, & Lequeux (1976); and Dearborn, Tinsley, & Schramm (1978)), and we have used it.

3.1.2 Initial Mass Function

The selection of an initial mass function is a crucial feature of any chemical evolution model. Unfortunately, there is no convincing physical theory of star formation, and so the nature of the IMF and the star formation rate over the history of the Galaxy are poorly understood. It is unclear, for example, whether the IMF has changed with time, what its upper and lower mass limits are (and have been), and whether it depends upon the composition of the gas which will become stars. Furthermore, it is very difficult to untangle the behavior of the IMF and the SFR, which could in fact be inseparable and better left in the form of a creation function, as in eq. (2).

Lacking any good theoretical or observational guidance as to these questions, we will adopt eq. (2), i.e. we will assume that the IMF is constant in time. We will, however, allow for it to take different forms. We will try the classic Salpeter (1955) function,

$$\phi(m) \propto m^{-(1+x)} \tag{22}$$

and we will allow the index ("slope") x to vary, trying $x = 1.1.35$, and 1.7. We will also try an IMF ϕ derived from the observed, present-day mass function (PDMF, $\phi^{\rm pd}$), as given by, e.g. Scalo (1986). The relationship between the two depends on whether the stellar lifetime τ_m is short enough that some of the stars of mass m have died; specifically,

$$\phi(m) = \begin{cases} \phi^{\rm pd}(m), & \tau_m \geq t_0 \\ \phi^{\rm pd}(m) / \int_{t_0-\tau_m}^{t_0} dt\ b(t), & \tau_m < t_0 \end{cases} \tag{23}$$

where the age of the Galaxy is t_0 and $b(t) = \psi(t)/\langle\psi\rangle$. We remind the reader that this procedure is only practicable when the star formation rate ψ is a given, explicit function of time, because of the role of ψ in eq. (23).

We also will try different mass limits to the IMF. Here we are guided by common choices that have appeared in the literature. We will wish to have a broad, medium, and narrow range in mass. We choose limis of

$$(m_l, m_u) = (0.2, 100); (0.1, 60); (0.4, 30) \tag{24}$$

which we feel to be representative.

3.1.3 Star Formation Rate

As star formation is ill understood, the form of the SFR is not well set by theory, although there have been some attempts to do so. As with the IMF, there are many variants, but we will select what we feel to be typical choices:

$$\psi = \nu\sigma_{\rm tot}\left(\frac{\sigma_g}{\sigma_{\rm tot}}\right)^0 = \nu\sigma_{\rm tot} \tag{25}$$

$$\psi = \nu\sigma_{\rm tot}\left(\frac{\sigma_{\rm g}}{\sigma_{\rm tot}}\right)^1 = \nu\sigma_{\rm g} \quad (26)$$

$$\psi = \nu\sigma_{\rm tot}\left(\frac{\sigma_{\rm g}}{\sigma_{\rm tot}}\right)^2 \quad (27)$$

$$\psi = a\ \exp(-t/\tau) \quad (28)$$

where we pick the $\tau = 7.5,\ 15$ Gyr as the timescale for the exponential case. Note that these always decrease for a closed box ($\sigma_{\rm tot} = {\rm const}$), but that for infall models with accreting gas, these will show a rise at early times.

3.1.4 Infall

There is very little known about the existence, nature, and composition of infall and/or outflow from our Galaxy. There is perhaps evidence for infall is given by the observation of the High and Very High Velocity clouds. However, there is certainly a need for infalling matter at early times, if one views infall to disk as just the outflow from the halo as it collapsed. In this case, one imagines a metal-poor (i.e. BBN composition) infall on a short (~ 2 Gyr) timescale. Another justification for infall is more pragmatic: it provides a possible solution to the G-dwarf problem (discussed in §3.2).

We will adopt models with and without infall, which we parameterize according to the widely used form $f(t) = f_0 \exp(-t/\tau_{\rm inf})$. We will vary the infall strength f_0, and the timescale $\tau_{\rm inf}$. Namely, we will try $\tau_{\rm inf} = 2,\ 4$ Gyr, and we will use different f_0 such that infall contributes 50% and 99.9% of the total disk mass today. We will also consider "closed box" models with no infall, i.e. for which $f_0 = 0$.

3.1.5 Supernova Rates

We will assume that all supernovae arise either from the core collapse of massive stars (type II) or from accretion onto a CO white dwarf in a binary system (type Ia). All stars above $\sim 12 M_\odot$ are thought to become type II supernovae, whereas the CO progenitors of type Ia supernovae are arise from binary systems of intermediate ($3 - 8\ M_\odot$) mass. The rates for these events are given by (Matteucci & Greggio (1986)), and are of the form

$$R_{\rm Ia}(t) = \lambda\, \mathcal{F}[\phi, \upsilon, f] \quad (29)$$

where $\mathcal{F}$ is a functional of the IMF and SFR, as well as f, the primary-to-secondary mass distribution in binaries.

The amplitude of the type Ia rate is controlled by the dimensionless parameter λ which is the probability for binary systems in the appropriate mass range to undergo supernova events. This number is not well understood theoretically and in practice is adjusted to reproduce the present ratio of type II to type Ia events ~ 1. We will examine the sensitivity of our results to this parameter, by choosing two values for λ:

a high value of $\lambda = 0.05$ near the value recommended by Matteucci & Greggio (1986), and a low value $\lambda = 0.007$ used by Timmes, Woosley, & Weaver (1994).

The type II nucleosynthesis yields are what is calculated for high mass stars as discussed in §3.1.1, and are directly included in eq. (10). Type Ia yields of nuclide i are added by putting

$$E_i^{\rm Ia} = M_i^{\rm ej} R_{\rm Ia} \tag{30}$$

with $M_i^{\rm ej}$ the mass ejected in i in a type Ia event. We use the yields for the W7 model of Thielemann, Nomoto, & Yokoi (1986).

3.2 Constraints on the Global Models

We first constrain the global models to fit the solar neighborhood properties within fairly generous tolerances, excluding for the moment any consideration of the acceptability of the global models' light element yields. The available constraints on the gross features of the models are $\sigma_{\rm g}^1$, μ_1, and the CNOFe abundances and their ratios.

Note that we want to be not too restrictive on our models, as the data, even the solar system abundances, are likely to be subject to systematic errors. For example, Olive & Schramm (1981) suggest that the solar system may have been formed from a young OB association; as a result its elemental and isotopic content would be a biased indicator of the larger solar neighborhood. Indeed, it seems unwise to dwell on one constraint at the exclusion of the rest. Consequently, we wish to be generous in choosing models with which to check chemical evolution uncertainties in the light elements.

We will demand that all models fit the local gas mass fraction, which is determined to be $\mu = 0.1 - 0.2$. Specifically we require $\mu = 0.13 - 0.17$. This fixes the overall mass consumption. Given that the a central feature explicitly built into chemical evolution models is the mass consumption and the conservation of overall mass, this is a most important constraint. We therefore have tuned all of the SFR normalizations to satisfy this constraint.

As for the quantitative means of evaluating a model, the χ^2 analysis of Tosi (1988) is interesting but perhaps premature given that the data is likely to be fraught with systematic errors. Instead, we will make the generous (and implementationally simple) demand the solar CNOFe abundances within a ± 0.4 dex[4] range. This is to be compared with the factor of 2 that Timmes, Woosley, & Weaver (1994) allowed themselves in a model tuned to give good results.

We will also constrain some of our models with observed G-dwarf distribution. G-dwarf stars are long lived, with ages comparable to the Galactic age now. Consequently, their provide a record of the integrated star formation history of the galaxy; the metallicity distribution of these stars is as seen in figure 13. It has long been known that

[4]dex = base 10 logarithmic units; i.e. a logarithmic variation by ± 0.4 dex is a linear variation by a factor of $10^{0.4} = 2.5$

the simplest models of galactic chemical evolution are unable to reproduce the G-dwarf distribution. In particular, such models cannot avoid overproduction of low metallicity stars, whereas the data shows that there is a dearth of G-dwarfs below a metallicity of [Fe/H].

One of the solutions to this classic "G-dwarf problem" is the introduction of infall. In models with infall, low metallicity stars are still formed, but as material is added subsequently, the fraction of low metallicity G-dwarfs becomes acceptably small. We will thus apply a G-dwarf constraint to our models, but only on models with infall. For these we will demand a solution to the most emphasized part of the G-dwarf problem, namely the need for a small number of low metallicity G-dwarfs. We will ask that our models not exceed the observed fraction of such stars at [Fe/H] = -0.8 by more than a factor of 0.4 dex $\simeq$ 2.5; this will prove to be a restrictive condition. We will not make the stronger demand that the models fit the full G-dwarf distribution to a high accuracy, as this is not done even in models which allow themselves tuning which we lack.

We will not impose the G-dwarf constraint on models without infall, as it is well established (e.g. Tinsley (1980); Pagel (1989)) that such closed box models are unable to meet this constraint without further modification (although Mathews & Bazan (1990) show that the G-dwarf problem is somewhat mollified by the inclusion of metallicity dependent stellar ages). We keep the closed box models since their ubiquitous presence in the literature demands that one examine their results, and again, we want to err on the side of inclusiveness in our selection of viable models.

3.3 Light Element Model Features

Having assembled a set of possible models and determined constraints on their gross characteristics, we now turn to the model features we will use to encompass the possibilities for light element evolution. For the most part, these introduce small enough changes in the CNOFe abundances that each model's CNOFe prediction will remain valid despite the modification of light element evolutionary features. An exception to this rule comes from mass loss.

The evolution of all light elements is affected by their initial BBN abundance as set by the choice of η. We use three different values of η, guided by the analysis of Copi, Schramm, & Turner (1994) (cf. eq. (1)). We choose central, high, and low values $\eta = (2, 4.6) \times 10^{-10}$; these values bracket the Copi, Schramm, & Turner's "sensible" limit. The low limit is intentionally chosen to be slightly below their recommended value (but above their "extreme" lower limit), in order to allow comment on recent speculation of the possibility of a low η.

In addition to systematically varying η, we will include the following features for each element:

3.3.1 D

As we have discus[illegible] evolution is uniquely simple beca[illegible]se there are no stellar sources of D; the range in [illegible] ults thus stems only from the choice of η and from global model features.

3.3.2 ^{3}He

For high mass ^{3}He yields we used the results of Weaver & Woosley (1994), which span a grid of masses from $\sim 11 - 40\ M_\odot$ and very complete range of metallicity from $Z = 0$ $Z = Z_\odot$. The metallicity dependence of these models is strong and thus a crucial feature to include; these results update the work of Dearborn, Schramm, & Steigman (1986).

As noted in §2.4, ^{3}He evolution hinges on the effect of low mass stars on ^{3}He. To investigate this effect we have chosen an approach similar to that of Vangioni-Flam, Olive, & Prantzos (1994), as well as Olive et al. (1994). Namely, we specify the ^{3}He survival fraction g_3 at $m = 1$, 2, and 3 $M_\odot$. We choose to allow for: (1) modest ^{3}He destruction (Vangioni-Flam, Olive, & Prantzos found they must); (2) "break even," with all ^{3}He surviving but no net production; and (3) modest ^{3}He production. Specifically, the three ranges we choose are

$$g_3(1M_\odot, 2M_\odot, 3M_\odot) = \begin{cases} (1, 0.7, 0.7) \\ (1, 1, 1) \\ (1.33, 1.33, 1.33) \end{cases} \tag{31}$$

We chose the production to be small (i.e. somewhat less that the Iben & Truran (1978) [illegible]ls, corrected to include initial D, would suggest) in order to be conservative. It is clear, as pointed out in Olive et al. (1994) that the yields at face value do not work, assuming the conventional ^{3}He high mass yields. In an effort to allow for uncertainties in the Iben & Truran (1978) calculation, we wish to see if even a modest production can work.

3.3.3 ^{4}He

As discussed in §2.5, Calculations of ^{4}He production must allow for its production by stars having a wide range of masses; because of this broad range, ^{4}He is particularly sensitive to systematic problems in nucleosynthesis yields over the whole mass range. One such problems is that tabulations of stellar nucleosynthesis yields usually do not include results for stars in the range of roughly $8 - 12\ M_\odot$. There is not a firm understanding of the basic nature of these stars' final fate: whether they become white dwarfs or explode as supernovae is a delicate and unresolved question. The nucleosynthesis results for these stars are therefore quite uncertain, and indeed possibly quite different

from those of stars either more or less massive. This is a regrettable state of affairs, as a typical IMF places a good deal of weight on the yields from stars in this range. Thus whatever assumptions one adopts about these yields can prove important for chemical evolution. Therefore we will examine two possible scenarios.

Traditionally, one obtains yields in this mass range by interpolating the results from the closest tabulated masses. Such an interpolation can be viewed as hedging one's bets about the accuracy of estimates for the onset of core collapse. We will include this case, however, note that it has also been suggested that stars in this range produce ^{4}He almost exclusively (Woosley & Weaver (1986)). We therefore mock up this behavior by assuming that *all* of the ejecta from these stars is in this form.

Other important model uncertainties regarding ^{4}He production arise due to the omission of mass loss in high mass stellar models Consequently, we use the stated Woosley & Weaver (1993) high mass yields, which do not include the effects of mass loss, but we also mock up the effects of mass loss by adding Maeder's (1992) calculation of these. Note that while Maeder also calculated supernova yields which included mass loss, the models were far less detailed and thorough than those of Woosley & Weaver; thus we choose to import only the mass loss addition.

3.3.4 Li, Be, and B

A detailed discussion of our model choices for Li, Be, and B can be found in Paper II. In brief, in order to make Pop I ^{7}Li, we have included both AGB star and supernova production mechanisms (specifically, the ν-process yields of Weaver & Woosley (1994)). These supernova yields also give an an additional source for Pop I ^{11}B.

The main emphasis of our Li, Be, and B study is on cosmic ray model variations. We have chosen three basic scenarios, which implement the suggestions of Fields, Olive, & Schramm (1994a). Two of these scenarios look at cosmic ray nucleosynthesis with and without time evolution of the cosmic ray confinement; the third scenario considers the possibility that the cosmic rays have an enhanced CNO component. For each of these scenarios we tried a wide range of cosmic ray source spectra types and spectral indices. Our wide range of cosmic ray evolution leads to a very wide range in predicted Li, Be, and B abundances.

4 Results

4.1 Effect of the Chemical Evolution Model Features

The effect of our global model features are for the most part well documented in the literature; we will discuss only the highlights. For a more complete discussion we refer the reader to, e.g., Talbot & Arnett (1971), Tinsley (1980), and Tosi (1988). Note that

unless otherwise indicated, all of the figures in this section are for models which vary only the parameters discussed while keeping the others constant.

A sample of SFR behaviors appears in figures 2 and 3; Figure 2 displays the case of a closed box model. We see that for SFRs of the form $\psi = \nu\sigma_{\rm tot}\mu^n \propto {\sigma_{\rm g}}^n$, there are progressively higher initial bursts and more rapid declines for progressively higher n. Also, we note that the $\psi = \nu\sigma_{\rm g}$ model is remarkably similar to the $\psi = a\exp(-t/\tau)$ model for $\tau = 2$ Gyr; this is not surprising given that (in the IRA) we expect the $\psi \propto \sigma_{\rm g}$ model to have an exponential SFR.

The presence of infall changes the behavior of the SFRs whose form depends upon the total and/or gas masses. As seen in figure 3 (a), for $\psi = \nu\sigma_{\rm tot}$ the SFR is monotonically increasing with time as the disk mass grows through infall, in contrast to the decaying SFR forms in a closed box. For $\psi = \nu\sigma_{\rm g}$ (figure 3 (b)), in the case of infall the SFR initially rises to a peak, but then falls off as the gas is converted to stars and remnants.

The total and gas mass evolution is illustrated in figure 4. Our SFR boundary conditions and infall prescription fix the $\sigma_{\rm tot}$ plot as well as the endpoints of the $\sigma_{\rm g}$ plot. Note that the spread in $\sigma_{\rm g}$ at $t_1 = 15$ Gyr is an indication of this spread in μ_1, which arises due to slight differences in the SFR tuning for different models. The effect of infall on the gas and total mass is clear from figure 4. Without infall, the total mass is of course constant, and the gas mass monotonically decreases. With infall, the total mass rises rapidly, withe the gas mass initially following, then reaching a peak, turning over, falling in a convergent way to the present value.

The relation between iron abundance and time (the "age-metallicity relation") is an important one: iron is readily observable whereas t is not, and the maximal binding energy of Fe ensures that its abundance will increase monotonically with time. Thus the iron abundance is traditionally used as a chronometer (although its origin in both type Ia and type II supernovae makes it a somewhat problematic one, with O perhaps being a more suitable choice. See Wheeler, Sneden, & Truran (1989)).

In figure 5 we plot [Fe/H] versus t for all of our SFR options, with data from Edvardsson et al. (1994). In general, we see that the Fe rises very quickly, with most of the production happening at very early times and very little new Fe being added today. The sharpness of this rise is seen to depend on the SFR ψ. For $\psi \propto \sigma_{\rm tot}\mu^n$, Fe rises faster with increasing n. This is indeed sensible: the stronger the SFR dependence on μ (which monotonically decreases), the sooner the SFR decreases. Since a fixed amount of mass has to be processed, this requires that the processing happen earlier, and hence the earlier rise in Fe. Note that Fe abundance shows very little sensitivity to the timescale of the exponential SFR.

In comparing the curves in figure 5 to the data it is immediately clear that all of the models are viable. There is also a great deal of scatter in the data, indeed, as much as the overall trend. Edvarsson et al. (1994) emphasize that this scatter is real, and is not well explained in most chemical evolution models which invoke, as we have, the

assumption of instantaneous mixing of stellar ejecta at a given epoch. We can only expect to reproduce the average trends in the observations, and one should recall that individual stars can show considerable excursions from the average trend.

The evolution of deuterium provides a good example of the effect of different IMFs; the D history for three different IMFs is displayed in figure 6. The three choices have different return fractions, with $R = 0.32, 0.42$, and 0.57. As expected (cf. eq. 13), the D evolution is very sensitive to this parameter, with the overall depletion at the solar system (i.e. at $t_\odot = 10.4$ Gyr) varying from a factor of about 1.4 to a factor of 2.3. As we will see, this spread accounts for a large portion of the model uncertainty in the D evolution (for a fixed η). Note that the largest D depletion comes from using the Scalo (1986) IMF, which is derived from the present-day mass function. This IMF is bimodal and so has a lot of power at large masses which eject most of their mass; consequently, this yields a large return fraction and considerable D depletion.

In figure 7 (a) we show ^{3}He and D+^{3}He for the same models. The tradeoff between D and ^{3}He is clearly seen, with ^{3}He being progressively higher in models having progressively lower D. Indeed, despite the large variation in the individual D and ^{3}He cases for the three IMF choices, we see that all show a very similar—and nearly constant—evolution of D+^{3}He. In figure 7 (b) we show the ^{4}He evolution for the same models. These models show a correlation between the D and ^{4}He evolution, as the models with larger D depletion also have larger ^{4}He production. We will investigate this relationship in detail in §4.3.

Deuterium together with ^{3}He provides a good barometer of the effects of infall on the evolution of an isotope. The infall of primordial material enriches the depleted Galactic D, while it dilutes the increasing Galactic ^{3}He. This behavior is evident in figure 8 which shows the slower decline of D in the infall models, mirrored by the inhibited growth of ^{3}He. Note, however, that in the case of D the spread (at the time of the formation of the solar system) due to different treatments of infall is only about 15%, much less than that caused by different IMF choices.

The different behaviors of nitrogen in our models are illustrated in figure 9. We focus on N behavior at the same low metallicities which are observed extragalactic H II regions, and we include data from Pagel et al. (1992) and Skillman et al. (1994). While there is a large scatter in the data, the trend seems better fit by the models with mixed and the purely primary N. Note in particular that the mixed model does a surprisingly good job at the low metallicities; this is the regime of the Skillman et al. (1994) data, not available in previous analyses. While the fit is to somewhat an accident of our particular choices for the primary/secondary N mix, it is amusing that the lowest metallicity region—the bone of contention—comes out as well as it does.

The effect of secondary N on the Y−N relation is shown in figure 10, along with the Y−O relation for the same models. For these plots we have chosen models with elevated ^{4}He production, as this provides a better fit to the data, as discussed below (§4.4). The

models with pure secondary N do indeed have a sharp increase at low metallicities; this arises from large early helium production in concert with suppressed N production as its seed nucleus C is first being made. Note, however, that the low metallicity $Y-N$ relation is much more gentle for the case of partial primary and partial secondary N, the case that best fits the observations. The small departure from linearity in this case suggests that linear $Y-N$ fits might not be in much error, a point we will return to in §4.4.

4.2 Global Constraints and Model Uncertainties

Having sketched some of the effects of the global model features, we now explore the range of abundances calculated for the initial suite of candidate global models and for the subsequent set of light element models. In finding the range of light element predictions we obtain a rough quantitative estimate for the model uncertainties inherent in the chemical evolution arguments used to deduce the primordial abundances of these elements.

We created the suite of candidate global models by making every allowed combination of features shown in table 2: this produces 1184 models. We ran all of these models, using one particular choice of light element model features. Results of this run are summarized in figure 11, in which we plot the abundances for each element, calculated at the birth of the solar system ($t_\odot$, 4.6 Gyr ago). Abundances are expressed in terms of the logarithm with respect to the observed solar abundance $\mathrm{A/H}_\odot^{\mathrm{obs}}$:

$$[\mathrm{A/H}] = \log \frac{\mathrm{A/H}(t_\odot)}{\mathrm{A/H}_\odot^{\mathrm{obs}}} \tag{32}$$

(solar data is from Geiss (1993) for D and ^{3}He, and from Anders & Grevesse (1989) for all other elements). Note the wide range of all calculated abundances, including those for the light elements. Indeed, the only element without large excursions is ^{4}He, since it is the only element whose solar system abundance is mostly primordial and so on this scale does not show large effects of uncertainty due to chemical evolution. The low ^{7}Li abundance arises because these models lack a source for Pop I ^{7}Li: the ^{7}Li abundance reflects only the primordial and cosmic ray contributions, which are known to be inadequate by themselves to reproduce the Pop I level. This omission is remedied in the full light element models.

We now impose the constraint that our models reproduce the solar abundances of CNOFe within 0.4 dex, i.e. within a factor ~ 2.5. While this may seem generous, recall that we have not tuned our models to fit any elements in particular, yet even models that do so (e.g. Timmes, Woosley, & Weaver (1994)) allow themselves a factor of 2. Also, the scatter in the age–metallicity relation suggests that there is a large spread of metallicities at a given time. Thus, we must be aware of the possibility that the solar

data will not necessarily reflect the average at the solar neighborhood, so we do not want to exclude potentially good models on the basis of a single element. Thus we make our criteria loose.

When impose this constraint on the candidate global models, we reduce the field to 267 models. A plot of the solar abundances for these models appears in figure 12. The light element uncertainties are seen to be greatly reduced, while still being considerable. The spread in D and ^{3}He is of particular interest, as we have not added any model variance in the D or ^{3}He evolution (e.g. different η or different low mass ^{3}He stellar processing). Thus the range abundances of D and ^{3}He reflect only the variance due to the global models. Quantitatively, we have a variance in D of a factor of 2.0. As we have noted, this is very close to the range due solely to the IMF, which we see to be the largest source of D variation. We also find ^{3}He to vary by a factor of 1.9, and ΔY to vary from 0.018 to 0.046.

As discussed in §3.1.4, we also constrain the models with infall to fit the G-dwarf distribution, again with a loose tolerance. We focus on the ability the models to avoid a large number of low metallicity G-dwarfs, comparing our results to the data of Rana (1991). A plot of the distributions for one model that passes and one that fails can be found in figure 13. As discussed in §3.1.4, we do not apply this constraint to models without infall. With the constraint, we reduce the number of models to 114, with 28 of these being infall models.[5]

We now have a set of 114 chemical models which fit the solar system behavior within the tolerances we have set. To investigate the range of light element evolution allowed by these models, we run each of them for 18 different varieties of light element evolution models. Note that this is far less than the possible number of allowed combinations of options for light element evolution. However, to run such a number of models would not only be tremendously time consuming, but it would also be redundant. We do not expect, for example, the various LiBeB yields in the cosmic ray models to depend on η in an important way compared to the other large uncertainties. Thus we have reduced the number of light element variations to only those 18 most likely to give interesting results. In total, therefore, we have 18 light element models $\times$ 114 global models = 2052 overall models to run.

Results for the 2052 models appear in figure 14. Notice that a problem has developed in the CNO abundances—some light element evolution features have affected them. The problem arises due to the extra CNO contribution from massive stars with mass loss. For consistency with our protocol of constraints, we again constrain the models to give CNOFe within 0.4 dex of solar.

[5]The only single features clearly important in determining whether a given model would pass or fail were the IMF slope and mass limits. We found no models with $x = 2$ survived; for $x = 2.35$, no models with the widest mass limits passed; for $X = 2.7$, mostly the models with the smallest mass limits passed. Aside from the IMF, no other model feature was prominent in either its presence or absence from the passing models.

This reconstraint reduces the number of models by about 25% to 1460. Results appear in figure 15. Note that even for this smaller number of models, the range in the light element abundances remains very similar, although with fewer models the extreme variations are less populated. The models depicted in figure 15 will be the basis for the analysis in the sections below, except where otherwise noted: for brevity we will refer to these as the "final set" of models.

The source of the gap in the D abundances in figure 15 becomes clear when we plot the results for a particular η. As figure 16 makes clear, the D gap arises due to the very high initial D at $\eta = 2 \times 10^{-10}$. It is also clear that it is hard for our models to reduce such a high initial D to i presolar abundance, a point we will explore in more detail in the next section. Note tha. ^{3}He also shows sensitivity to its initial abundance; ^{4}He does as well, but it is not clear on this plot; we will examine the matter more closely below. We caution the reader that the apparent η dependences in LiBeB are artifacts of our model distributions. That is, we varied LiBeB production mechanisms simultaneously with, and not independently of, variations in η.

The spread in the light element abundances, particularly the spread beyond that in the "control" group CNOFe, gives a sense of the spread due to model dependence. Note, however, that one must be careful in interpreting these limits. While we have tried a broad sample of models, the lack of a firm theory of star formation leaves open the possibility that one might construct other ones. Moreover, recall that we have not used chemical evolution to get limits on the primordial abundances. Instead, we have assumed BBN yields and seen how well these fit the solar system. What one really would like to know is not this but rather the opposite case. Namely, one would construct models with variable primordial light element abundances (i.e. not necessarily given by BBN values at a given η), and constrain these models to reproduce the solar system values for the light elements and everything else. The resulting spread in the primordial abundances would be an indication of the model uncertainties incurred when setting limits on η. This procedure suffers, of course, from a dangerously heavy reliance on the veracity of chemical evolution models. Furthermore, we may estimate the model ranges such a calculation would give, as we now discuss.

Table 3 summarizes the model variations in the light element production for each η. We see that, for all η, D varies almost exactly by a factor of 2 and ΔY varies by 0.063 units. The variation in D+^{3}He depends somewhat on η, but is small, varying by $< 20\%$ from ~ 2.8. The η-independence of these quantities are evidence that the range model variations does not depend on the light element initial values. This gives us confidence that, were we to do a light element evolution study by allowing the primordial values to float (as described in the preceding paragraph), we would find similar ranges. That is, we pect the reduced quantities in table 3, namely D_{max}/D_{min}, $(D+^3He)_{max}/(D+^3He)_{min}$, and $Y_{max} - Y_{min}$, to be generic estimates for the chemical evolution model ranges of these elements. Of course a different selection of model features will give different numbers,

but these results at least give a quantitative estimate for the model dependence within a large scale of models, and serve as a benchmark for others.

We emphasize that the D variation is due solely to variation of global model features, in particular the IMF and also infall. Thus to reduce the variation in D requires better chemical evolution modeling as a whole. By contrast, the span in the ^{3}He and ^{4}He ranges are due in part to the effects of different stellar processing features for these elements. Improvements in these features could reduce the ranges given, independently of improvements in the global chemical evolution framework.

It is encouraging to note that the variations in D, ^{3}He, and ^{4}He, while large, are significantly smaller than the 0.8 dex (i.e. factor of 6.3) overall variations allowed for CNOFe in our global model constraints. This implies that the light elements through ^{4}He have less model uncertainty than do the heavy elements. However, the relationship between the heavy and light element uncertainties is not necessarily a simple one.

To get a feel for the connection between the heavy and light element model variations, we examine the effect of tightening the fiducial tolerances in the heavy elements. Specifically, we now require that our models reproduce solar CNOFe to within 0.3 dex, i.e. to within a factor of 2, a 20% tightening of the constraint. Results appear in figure 17. The reduction in the number of models is drastic, going from 1460 models at 0.4 dex tolerance to 479 models at 0.3 dex tolerance, a 66% reduction in models from only a 20% tightening of the constraint. One can understand this large reduction by noting that our heavy element yields generically are scattered around the solar levels. For example ^{12}C is produced on "average" above the solar level, while ^{16}O is produced in a large range centered below solar: in other words, the O/C ratio is typically subsolar. Thus our models have some range of error in reproducing the solar $O/C_\odot$, and will never have all abundances any more accurate than this range. Indeed, demanding simultaneous fitting of both abundances for smaller and smaller tolerances would eventually squeeze out all models when the constraints become too stringent given the heavy element yields we have used.

Despite the large reduction in number of models which survive the stronger heavy element constraint, the spreads in the light element abundances remain roughly the same. This reinforces the notion that the CNOFe spreads are to some degree decoupled with the light element spreads. More quantitatively, we find for these models that D varies by about a factor of 1.76 and ^{3}He by a factor of 3.1, values closer to the range for models with the $\pm$ 0.4 dex CNOFe tolerance than the 20% tightening would naively allow. In other words, by making the variation in CNOFe smaller by 20%, we do not reduce the variation in D and ^{3}He by as large a factor. Thus the model variation in the heavy and the light elements are not related by a simple linear scaling, but instead the relationship between the two seems to be more subtile.

4.3 Correlations in Light Element Evolution

We now study in detail the results from the set of 1460 models comprising the "final set" having all allowed light element variation while also fitting CNOFe. In particular, we will be interested looking at D, ^{3}He, and ^{4}He (pre)solar and ISM predictions simultaneously to see better the correlations in their evolution and to show the interplay of the observational constraints.

In figure 18 we plot the solar D abundance versus the solar ^{3}He abundance for each model. One notices immediately that the choice of η (different shaped points) is the largest effect controlling the solar abundance of both elements. Furthermore, the correlation between D and ^{3}He is evident: the negative slope in the lines traced out in the figure points out the well-known tradeoff that D destruction leads to ^{3}He production. The steepness of these lines (which radiate out from the primordial values at each η), depends on the degree of low mass destruction or production of ^{3}He. The highest of the three "prongs" for each η comes from the case of ^{3}He production in low mass stars. The middle prong is the "break even" case, and the lowest one from net ^{3}He destruction. We clearly see that the ^{3}He solar yields are very sensitive to the low mass stellar behavior, which we have only varied by 30% either way from break even. Our models thus confirm the results of Vangioni-Flam, Olive, & Prantzos (1994) and Olive et al. (1994), and extend them to include a very wide range of models.

Figure 18 also includes lines marking the $2-\sigma$ variation in the observed presolar D and ^{3}He abundances, as calculated by Geiss (1993). The figure provocatively shows that none of the low-η, i.e. high initial D and ^{3}He, models are able to fit the presolar data to within this tolerance. Indeed, the majority of the moderate-η models also seem to fail. At face value, this might suggest that low values of η are ruled out and that higher ones are favored. The question is whether this strong conclusion holds up under scrutiny.

As we have discussed in the previous section, it is a subtle matter to use our models to constrain the possible BBN abundances. We have not included all possible chemical evolution models (e.g. IMF and SFR schemes) and one cannot conceivably do this, given the freedom one has to adjust each. One cannot exclude the possibility that some possible schemes are viable. Also, recall the observed scatter in Fe abundances for stars which are presumably coeval. If the solar D is a low variation to the mean we have calculated, we would be incorrectly constraining our results. Finally, as we have noted, significant uncertainties and assumptions underlie the entire chemical evolution framework we have adopted (and variants thereof). Even if one could show that if no such models work to explain the low-η D and ^{3}He, such a conclusion would not be founded upon a first principles calculation, since none exists.

Nevertheless, it is not terribly surprising that $\eta = 2 \times 10^{-10}$ fails for our study. Indeed, as we have noted, this value is outside of the "sensible" range in η given by Copi, Schramm, & Turner (1994), although it is within the "extreme" range. Also, while chemical evolution models are uncertain, as we have argued, the D evolution is

perhaps the most certain of any nuclide considered. Thus there is no obvious reason to disbelieve the D results, particularly when other abundances can be fit reasonably well.

Furthermore, while chemical evolution is known to be uncertain, our results as presented help one to quantify the size of the model dependence. At $\eta = 2 \times 10^{-10}$, the D abundance varies by a factor of ~ 2; but the lowest D abundance for this η is still a factor of ~ 1.5 away from upper limit to the solar system observation (and with an undesirable ^{3}He abundance at that). It is incorrect to think of the spread in our results as some sort of distribution around a mean model, as we have not just performed smooth parameter variations, but we have also changed whole prescriptions for, e.g., the SFR. Thus it is hard to say more than that the presolar value of D for BBN with $\eta = 2 \times 10^{-10}$ is not reachable in our models and seems hard to reach by models similar to ours.

While presolar D is a strong constraint on models with high η, we see that presolar ^{3}He is a very strong constraint for all η. Because ^{3}He survives processing of both D and ^{3}He, its abundances grows with time.[6] However, the presolar ^{3}He is not much larger than its primordial level, and so demands that models produce very little ^{3}He. We see that models with high η, i.e. with the lowest initial ^{3}He, are the only ones that can fit the presolar constraint. Within these, the different ^{3}He processing becomes important, with ^{3}He production in low mass stars often overproducing ^{3}He. Since this low mass behavior nevertheless seems to be demanded by planetary nebula data, the data seems to favor models which have very little processing in general. There are therefore models which have higher D, as borne out by the plot: ^{3}He is lowest where D is the highest.

We may also examine correlations between the calculated solar abundances of other pairs of light elements. Figure 19 shows D and ^{4}He solar abundances. Here again, the largest segregation of points is due to the different initial D abundances for different η. The shapes of the point distributions are similar for the different η values, though the higher η regions are more compressed. Note that the regions are shifted upwards for increasing η, reflecting the higher Y_p for these models. However, it is clear that the shift due to different Y_p values is a much smaller effect than the spread due to chemical evolution effects, which give ΔY anywhere from 0.04 to 0.08.

For a given η, the D–^{4}He correlations are not as immediately clear as for the D–^{3}He plot. One can understand the trends by separating the points according to the ^{4}He model features to be varied, namely the $8 - 12\ M_\odot$ yields and the presence of mass loss in massive stars. For models with no extra ^{4}He yields (i.e. using just the adopted yields without mass loss and interpolating between $8 - 10\ M_\odot$), the predictions appear as the lowest band of points; data for these models alone appears in figure 20 (a). These models do indeed show an appreciable correlation, as we have argued they should: D depletion is the measure par excellence of the amount of material processed through stars, and ^{4}He production is one consequence of this processing. Thus we expect and

[6]This is true for sufficiently early epochs and for sufficiently high g_3, both of which are the case in our study.

find a negative correlation for the "standard" case.

Figure 21 (b) shows the models with one or both of the helium enhancing features. We see here, like the D-^{3}He plot, there are three "prongs" for each η. These correspond (for the most part), to The three different cases of "nonstandard" ^{4}He yields. The lowest trend is for mass loss only, the intermediate (and some of the highest) prong is due to high $8-10\ M_\odot$ yields, and the highest points come from a combination of the two. Here again, we see the negative correlation we expect. We also note that many models appear to fit the solar ^{4}He. Indeed, while some are high and some low, a good number of both standard and nonstandard ^{4}He yields give a successful fit.

We should emphasize that the physics that underlies the D–^{4}He correlation is different from that behind the D–^{3}He correlation. In the latter case, we have demanded that D be made into ^{3}He, and so we have explicitly built in the correlation between the two. The relation between D and ^{4}He is somewhat less direct, as Galactic ^{4}He does not come from primordial D, but rather the destruction of D happens in processes which also produce ^{4}He independently of the level of D.

Having found correlations between D and ^{3}He as well as D and ^{4}He, it is reasonable to look for correlations between ^{3}He and ^{4}He producition. Figure 22 plots ^{3}He versus ^{4}He for standard and nonstandard ^{4}He yields. Note that in the set of light element variations, the possible combinations of D and ^{3}He evolution features were not explored with equal numbers of models; however, the distribution of points should be representative. The correlations are evident, as is the familiar prong structure, which arises due to the different low mass stellar ^{3}He yields. There is also a bifurcation of the prongs due to different IMF slopes and mass limits. The physical interpretation of the plots is fairly clear: both ^{3}He and ^{4}He are sensitive to how much matter is processed through stars, ^{3}He because it is the ash of all of the D that is destroyed, and ^{4}He because it is made ubiquitously.

Having examined the correlations between different model calculations at the epoch of solar birth, we now turn to correlations at the present epoch. Here the underlying physics is the same and so we of course expect similar relationships between the model yields, but the observational constraints are different, and in the case of D, more severe. In figure 23 we plot D versus ^{3}He for the present epoch, i.e. we plot the abundances calculated for the ISM now. One notices the same features as the plot for the solar system, now smeared out with the intervening evolution. For ^{3}He the observational situation is uncertain as the data shows a large dispersion; if one included the range of abundances spanned by the observations it would not constrain any of these points. This contrasts with the power of the presolar ^{3}He, which offers a tighter constraint than the presolar D.

The D observations in figure 23 are from the *HST* observation of Linsky et al. (1993), with the $2-\sigma$ variation shown. (Unfortunately, we are unaware of accurate ^{4}He abundances in the ISM, and so we are unable to constrain our models with this isotope.) If

this number is to be taken seriously, it is a strong constraint on chemical evolution models. Here again, we find that the low-η points are very disfavored by the D observations, with the lowest points in this regime needing to move at least a factor of 2 to meet the data. On the other hand, the spread in these points is larger than at solar, being almost a factor of 3. Recalling the caveats above, we note that our models have trouble fitting the ISM D abundance given an initial D from a low-η BBN model.

One final set of correlations of interest is a comparison of the same nuclide at the solar birth and at the present epoch. In figure 24 we plot D calculated at the birth of the solar system again D calculated for the ISM today. Unsurprisingly, we find that the two are strongly correlated. Note that all of the points lie below a line of unit slope; this is to be expected since a given model should have more D at the solar birth than at present. The departure of a given model to a line with unit slope is a measure of the destruction of D in that model since the birth of the solar system. This plot emphasizes the strong constraints imposed on our models by the D observations.

The stringency in the observed presolar and ISM abundances for D, illustrated in figure 24, bears further investigation. As we have noted, D is the nuclide whose chemical evolution is the simplest, and thus we can expect a given model to calculate D evolution the most accurately of all the nuclides. It is thus interesting to ask what models survive the constraint that both the presolar and ISM D observations are fit to within $2-\sigma$. As is clear from figure 24, the more stringent of the two cuts is comes from fitting the ISM observation.

Demanding that models fir presolar and ISM D reduces the number of models from 1460 to 231. In figure 25 we plot the calculated solar D versus ^{3}He for these models. Comparing these results to those of figure 18, we see that some of the models which could otherwise fit the (also stringent) presolar ^{3}He are removed. However, many of these models still remain. Correlations between ^{3}He and ^{3}He solar abundances in these models are shown in figure 26. Encouragingly, most of the models which successfully fit the presolar and ISM D also fit the (pre)solar ^{3}He and ^{4}He.

While it is not our purpose to find the "best models" for light element chemical evolution, it is useful to consider the reason for the success fo the models which fit the observed (pre)solar D, ^{3}He, and ^{4}He abundances, as well as the ISM D. Most importantly, these models all have a high η and so begin with a very small amount of D and ^{3}He—indeed, at $D/H_p = 2.3 \times 10^{-5}$, they are already smaller than the $2-\sigma$ upper limit to the presolar abundance. Thus these demand very little stellar processing of D to reduce it to the observed abundance, and therefore need not produce much ^{3}He.

Interestingly, these models have very few other strong identifying characteristics. All low mass ^{3}He prescription are represented in an even way, as are all combinations of ^{4}He prescriptions. The global characteristics include all SFR prescriptions and infall as well as closed box models. The two steepest IMF slopes are both represented as well, although the only mass limit range is the most restricted one (type 2 in table 2).

We are left to conclude that D evolution is a strong constraint on chemical evolution models, but also that models meeting this constraint can still fit ^{3}He and ^{4}He. We have demonstrated that comprehensive evolution of the light elements is possible within our adopted framework of chemical evolution, although this framework allows for substantial variation in its results according to the adopted model prescriptions and parameters.

4.4 Additional Considerations

4.4.1 D

The program of observation of D in quasar absorption line systems now just beginning, is likely to revolutionize how BBN is observationally constrained. The power and potential importance and of this method impel a close scrutiny of its assumptions. In particular, it is implicitly assumed that the observed D abundance in high redshift systems is a direct record of the primordial abundance. However, by a redshift of $z \sim 3$, the universe it at least 1 Gyr old, and as much as 3 Gyr old. Potentially, in this amount of time there might be some depletion of D in the protogalaxies that comprise the absorption line systems; the question is how large such depletion could be. Also, it is noted that typical absorption line systems are not as metal poor as that studied by Songalia et al. (1994) and Carswell et al. (1994); it is thus desirable to understand the evolution of D as a function of metallicity.

Regarding the depletion of D in the absorption line systems, we note first that if these are protogalaxies, we would expect them to take some time to form; however, we model the Galaxy once it has formed. Thus an object at a universal age of 1 Gyr would correspond to a time earlier than 1 Gyr on our models. And furthermore, a glance at figures 6 and 8 suggest that the D depletion at very early times is minimal.

To address this question more systematically, we have considered the D depletion in all of our models for universes at a redshift of $z = 3$, where we have made the very conservative assumption that the protogalaxies form immediately and so time in our models corresponds to universal time. The correspondence between the observable z and the time t in our models depends on the adopted cosmology, in particular on the value of Ω. To be conservative we have chosen $\Omega = 0$ (i.e. a curvature dominated universe, which has the largest age at $z = 3$), with a Hubble constant of $H_0 = 75$ km/s/Mpc. For each of these cases we run our models to the time corresponding to $z = 3$ and find the D abundance. To get a sense of how this correlates with the metal production, we plot the D abundance for these models against [Fe/H]. Results appear in figure 27. The figure confirms that to a high accuracy ($\gtrsim 20\%$ and usually better than 5%) D may be considered undepleted in these systems. Furthermore, figure 28 illustrates that for metal poor systems with [Fe/H] $\lesssim -1$, and not necessarily at $z = 3$, the D depletion is minimal regardless of the IMF and infall choices.

4.4.2 ^{4}He

The results from the previous section make clear that our ^{4}He options can produce very different ^{4}He abundances at the birth of the solar system and in the ISM. We now turn to the issue of how these features affect ^{4}He at low metallicities, in particular how the model features affect the $Y-$CNO relation studied in extragalactic H II regions. We show this relation for all four ^{4}He model options (all at $\eta = 4 \cdot 10^{-10}$) in figure 29. We see that the $8 - 10M_\odot$ enhancement is effective at increasing the ^{4}He slope, making an enhancement of about a factor of two over the standard case. On the other hand, mass loss is unimportant in this regime. This result is not surprising when one considers that mass loss—at least as we have modeled it following Maeder (1992)—not only increases ^{4}He but also CNO. Thus while the ^{4}He production is enhanced, the tracers are as well and so the net effect on $Y-$CNO is small. A note of caution, however, is that the mass loss calculations are difficult and so the results we use are subject to large uncertainty; also, they are only available for two metallicities. Improved modeling is crucial to help address the issue of the $Y-$CNO relation.

Figure 10 (a) shows effect of secondary N evolution on the low metallicity $Y-$N relation; this relation needs to be well understood to properly extrapolate from the observations to derive the primordial ^{4}He abundance. Oftentimes a linear relation is assumed; we now estimate the error in assuming a linear $Y-$N relation for different cases of N evolution. For each model, we will try to reproduce the empirical fitting procedure by finding the slope of the $Y-$N curve at a point and then extrapolating to get the estimated primordial ^{4}He abundance Y_p^{est}. We can then compare this to the actual Y_p value in the model and thus compute the error $\delta Y_p = Y_p - Y_p^{est}$ in this extrapolation procedure.

A potential complication to this procedure is that those models lacking features which enhance ^{4}He (mass loss and enhanced $8 - 12M_\odot$ production) will have smaller $Y-$N slopes and so will be poor approximations to the extragalactic H II region data. Thus we will also keep track of the average slope one would assume for these regions if one did a linear fit; only the results with a sufficiently high slope will be admissible for this comparison.

We perform the extrapolation at N/H $= 50 \times 10^{-7}$, i.e. at a region surrounded by data and not at low enough metallicity to itself betray the low-N dropoff in ^{4}He. The average slope is not the one used in the extrapolation but is taken at N/H $= 100 \times 10^{-7}$. This quantity serves only as a diagnostic to indicate the goodness of fit of the given model's $Y-$N relation to the observed slope. As such, a central point better quantifies the average behavior over the whole region.

In figure 30 we plot the error δY_p in the ^{4}He linear extrapolation versus the average slope dY/dN one would assume for the region. Note the distribution in slopes: we will only consider models with slopes above 10×10^4, which is a rough lower limit to the slopes derived from the H II region observations. For the models with large slopes, one can

immediately discern the trends seen in figure 10, here writ large. Namely, the models with no secondary N are well fit to a line, showing little error in the extrapolation. Indeed, the errors are fairly evenly spread around zero, with a width of about 0.001 units in the mass fraction. The models with some secondary and some primary N give $\delta Y \sim 0.002 - 0.004$, while models with purely secondary N can have corrections as large as 0.015.

Thus the models with exclusively secondary N give δY_p at the level claimed by Fuller, Boyd, & Kalen (1991), Mathews, Boyd, & Fuller (1993), and Balbes, Boyd, & Mathews (1993). However, as pointed out by Olive, Steigman, & Walker (1991), the N–O relation in extragalactic H II regions demands some degree of primary N; indeed, figure 9 fits the data well with a mixture of primary and secondary N. For this case, the error in Y_p extrapolation is small. Indeed, differences at this level are unimportant compared to the $\delta Y \sim 0.008$ observational uncertainty.

It is amusing to note that linear extrapolations of H II region data often give slightly larger values when using N as a tracer than when using O, with the difference being around 0.002 to 0.003 units, just the level of the effect we see in the primary + secondary N models. Clearly more work on this issue is needed, and the good agreement of our mixed N model may be somewhat fortuitous; recall that we have not explicitly built models of the irregular galaxies in which these observations are made, and so our models may not be appropriate to import directly. Nevertheless, we our models suggest that the the effect of secondary N on ^{4}He extrapolation may not be as pronounced as originally suggested.

5 Conclusions

Our results on the sources of our model sensitivity confirm those of Tosi (1988), as we find that the elemental abundances of our models are most sensitive to the shape and mass range of the IMF. Indeed, the models we tried were incompatible with a very shallow IMF slope for any mass range; this was the only model feature that was completely excluded by our solar system constraints. Furthermore, we find that our "best" models, those fitting the solar CNOFe as well as solar and ISM observations of D, select an intermediate IMF slope, namely the Salpeter (1955) value. We also find significant sensitivity to the presence and timescale of infall. However, infall itself is strongly constrained by the low metallicity G-dwarf distribution. Finally, we do not find our results to depend strongly on the choice of the star formation rate.

We also follow Tosi (1988) in finding that our results are very sensitive to the stellar nucleosynthesis yields employed. We emphasize in particular the effect of systematic effects such as mass loss which are not included in many models. In our models mass loss can be an important source of ^{4}He as well as CNO; more detailed calculations of this affect are needed to address the important question of the ^{4}He contribution of high

mass stars. We also find that our results are sensitive to the behavior of stars in the poorly understood $8 - 12\ M_{\odot}$ range: this too provides an important uncertainty for ^{4}He production. Work on these objects would be as useful as it will be difficult. Finally, we stress the need for a good understanding of the ^{3}He yields in stars of all masses. While it would be quite useful to update the Iben & Truran (1978) calculation of ^{3}He production in low mass stars, it is as important to understand ^{3}He behavior in high mass stars, with emphasis on the effect of winds.

Regarding the viability of light element chemical evolution, it is an important point simply that we do find models which can fit solar and ISM constraints on D, ^{3}He and ^{4}He (with ^{7}Li, Be and B fits being amenable to a variety of stellar and cosmic ray model combinations; see Paper II). This important "existence proof" demonstrates that the framework we have adopted, despite its roughness, is able to fit the data. Thus a consistent picture of light element evolution, from the early universe to the present day, can be drawn.

From the perspective of BBN, it is reassuring that we find the effect of different η so important for D and ^{3}He chemical evolution. We see that the global chemical evolutionary models we have examined, while having a significant degree of model dependence, nevertheless preserve information about the primordial abundances. Thus we are encouraged in our use of solar and ISM data as meaningful constraints on BBN, with the caveat that there remain significant uncertainties arising from chemical evolution. Indeed, as we have show, for D and ^{3}He the model dependences are larger than the observational uncertainties (for solar D and ^{3}He as well as ISM D). Thus BBN constraints coming from the solar and ISM D and ^{3}He are useful but should be regarded with caution.

On the other hand, we do not find D to be subject to significant depletion or chemical evolutionary uncertainty at early epochs probed by measurements of quasar absorption line systems. We find the D abundances at this epoch to be a clean indication of the initial D abundance (and thus of η); this result is independent of the particular cosmology chosen. Thus more observations of these systems should eventually be able to put strong constraints on η and thus on Ω_B.

In contrast to the case of D and ^{3}He, we find ^{4}He evolution to be dominantly sensitive not to its initial abundance but to the uncertainties in its stellar production. However, we do find that within these uncertainties it is possible to find ^{4}He evolution at low metallicity which can fit the $\Delta Y/\Delta$N and $\Delta Y/\Delta$O slopes better than standard models would indicate. Further, we find that the low metallicity $Y-$N trend is indeed sensitive to the prescence of secondary N. However, our models which best fit H II region N and O data require some degree of primary N and consequently do not lead to large deviations from linear $Y-$N relations. This issue, however, merits further study.

Apart from the uncertainties in our calculations which we have already discussed, another source of error is the possible time dependence of the IMF. This issue is not

well understood but is a potentially important one given the crucial role the IMF plays in chemical evolution. It is plausible that the IMF was at early times different from its present form, being sensitive, for example to the low metallicity of the ISM at early times. Unfortunately, arguments for how the IMF might change go in both directions: some favor a bias towards high mass stars in the early Galaxy, some a bias towards low mass stars (see, e.g. Silk (1994)). If there were a disproportionate enhancement of massive stars in the early Galaxy this implies and increased production of heavy elements, and in general a higher return fraction. In terms of the light elements, this means more D depletion, and less ^{3}He production; also, there would be increased cosmic ray activity which would lead to higher early production of LiBeB. The situation for ^{4}He is unclear and depends on the effects of winds from these heavy objects. Note that a very strong early D depletion could lead to a need to correct for evolution in quasar observations of D. On the other hand, a bias towards low mass stars in the early Galaxy would have the opposite effect, lowering the return fraction and metallicity, while making low mass stars which would eventually produce ^{3}He. Such a bias might be motivated by a need to make a population of low mass, substellar objects which would be the microlensing objects observed in the LMC and the Galactic bulge.

Future work in light element chemical evolution in part would refine the framework adopted here, most importantly by the adoption of different models of the halo phase. One might eventually hope to create a self-consistent stellar and chemical evolution scheme for the light elements, along the lines of the approach of Timmes, Woosley, & Weaver (1994). However, there is ultimately a need for a more fundamental understanding of star formation and its relation to the dynamics and chemistry of the Galaxy. In particular, an understanding of the physics behind the SFR and the IMF would be of tremendous value. Nevertheless, while uncertainties in chemical evolution remain, it is encouraging that they still allow models for the light elements to teach us about about BBN.

I thank Dave Schramm for his thoughtful advice on all aspects of this paper. I am grateful to acknowledge Frank Timmes for his support and insight, and Jim Truran for helpful discussions. I would like to acknowledge Stan Woosley, Tom Weaver and Frank Timmes for allowing use of unpublished material. Thanks to Keith Olive, Grant Mathews, and Mike Turner for useful to discussions and to Jeff Harvey and Simon Swordy for their time and energy. Finally, it is a pleasure to acknowledge Craig Copi for his great technical advice. Presented as a thesis to the Department of Physics, the University of Chicago, in partial fulfillment of the requirements for the Ph.D. degree. This work was supported in part by NASA through a GSRP fellowship at the University of Chicago, and by the DOE and by NASA through grant NAGW 2381 at Fermilab.

References

Anders, E., & Grevesse, N. 1989, Geochim et Cosmochim Acta, 53, 197

Audouze, J., & Lequeux, J., & Vigroux, L. 1975, A&A, 43, 71

Audouze, J., & Tinsley, B. 1974, ApJ, 192, 487

Balbes, M.J., Boyd, R.N. & Mathews, G.J. 1993, ApJ, 418, 229

Bania, T.M., Rood, R.T., & Wilson, T.L. 1987, ApJ, 323, 30

Black, D.C. 1972, Geochim Cosmochim Acta, 53, 197

Boesgaard, A.M., & Steigman, G. 1985, ARAA, 23, 319

Brown, G.E. & Bethe, H.A. 1994, ApJ, 423, 659

Cameron, A.G.W., & Truran, J.W., 1971, A&SS, 14, 179

Carswell, R.F. 1994, private communication cited in Copi, C.J. Schramm, D.N., & Turner M.S. 1994, Science submitted

Carswell, R.F., Rauch, M., Weymann, R.J., Cooke, A.J., and Webb, J.K. 1994, MNRAS, in press

Cassé, M., & Vangioni-Flam, E., 1994, ApJ, submitted

Colin, P. & Schramm, D.N. 1993, ApJ, 407, 510

Copi, C.J., Schramm, D.N., & Turner, M.S. 1994, Science, submitted

Davidson, K. & Kinman, T.D. 1985, ApJS, 58, 321

Dearborn, D.S.P., Schramm, D.N., & Stiegman, G. 1986 ApJ, 302, 35

Dearborn, D. Tinsley, B.M., & Schramm, D.N. 1978, ApJ, 223, 557

Deliyannis, C.P., Demarque, P., & Kawaler, S.D. 1990 ApJS, 73, 21

Dicus, D.A., et al. 1982, Phys. Rev. D, 26, 2694

Edvardsson, B., Gustafsson, B., Johansson, S.G., Kiselman, D., Lambert, D.L., Nissen, P.E., and Gilmore,G., 1994, A&A, submitted

Epstein, R., Lattimer, J., & Schramm, D.N. 1976 Nature, 263, 198

Ferrini, F. Matteucci, F., Pardi, C., & Peco, U. 1992, ApJ, 387, 138

Fields, B.D., 1994, in preparation

Fields, B.D., Dodelson, S., & Turner, M.S. 1993, Phys. Rev. D, 47, 4309

Fields, B.D., Olive, K.A., & Schramm, D.N. 1994 ApJ, 435, in press

Fowler, W., Greenstein, J., & Hoyle, F., 1962 Geophys JRAS, 6, 6

Fuller, G., Boyd, R.N., & Kalen, J.D. 1991, ApJ, 371, L11

Geiss, J. 1993, in Origin and Evolution of the Elements, ed. N. Prantzos, E. Vangioni-Flam, & M. Cassé (Cambridge: Cambridge University Press), 89

Geiss, J., & Reeves, H. 1972, A&A, 18, 126

Hogan, C.J. 1994 ApJ, submitted

Hoyle, F. and Tayler, R.J. 1964 Nature, 203, 1108

Hobbs, L., & Thorburn, J. 1994 ApJ, 428, L25

Iben, I., & Truran, J.W. 1978 ApJ, 220, 980

Jakobsen, P. et al. 1994, Nature, 370, 35

Kernan, P.J. 1993, thesis, Ohio State University

Kernan, P.J., & Krauss, L.M. 1994, Phys Rev D, 72, 3309

Linsky, J.L., et al. 1993, ApJ, 402, 694

Maeder 1983 in Proceedings of the ESO Workshop on Primordial Helium, ed. P.A. Shaver, D. Kunth, & K. Kjär (Garching, European Southern Observatory), 89

Maeder, A. 1992 A&A, 264, 105

Maeder, A. 1993 A&A, 268, 833

Malaney, R., & Mathews, G.J. 1993, Phys. Rep., 229, 145

Mathews, G.J., & Bazan, G. 1990, ApJ, 354, 644

Mathews, G.J., Boyd, R.N., & Fuller, G.M. 1993 ApJ, 403, 65

Matteucci, F., & Francois, P. 1989, MNRAS, 239, 885

Matteucci, F., & Greggio, L. 1986 A&A, 154, 279

Olive, K.A., Rood, R.T, Schramm, D.N., Truran, J.W., & Vangioni-Flam, E. 1994, ApJ, submitted

Olive, K.A., & Schramm, D.N. 1981, ApJ, 257, 276

Olive, K.A., & Schramm, D.N. 1992, Nature, 360, 439

Olive, K.A., Steigman, G., & Walker, T.P. 1991, ApJ, 380, L1

Pagel, B.E.J. 1989, Rev. Mex. Astron. Astrof., 18, 161

Pagel, B.E.J., 1993, Phys. Rep., 227, 251

Pagel, B.E.J. & Kazlauskas, A. 1992, MNRAS

Pagel, B.E.J., Simonson, E.A., Terlevich, R.J., & Edmunds, M.G. 1992, MNRAS, 255, 325

Peimbert, M. & Torres-Peimbert, S. 1974, ApJ, 193, 327

Peimbert, M. & Torres-Peimbert, S. 1976, ApJ, 203, 581

Pinsonneault, M., Deliyannis, C.P. & Demarque, P., 1991, ApJS, 78, 179

Prantzos, N. 1994 A&A, submitted

Prantzos, N., Cassé, M., & Vangioni-Flam, E. 1993, ApJ, 403, 630

Rana, N.C., 1991, ARAA, 29, 129

Reeves, H., Audouze, J., Fowler, W.A., & Schramm, D.N. 1973 ApJ, 179, 909

Ryder, C., Reeves, H., Gradstajn, E., & Audouze, J. 1970, A&A, 8, 389

Renzini, A., & Voli, M. 1981 A&A, 94, 175

Rogerson, J.B., & York, D.G. 1973, ApJ, 106, L95

Rood, R.T., Bania, T.M., & Wilson, T.L. 1992 Nature, 355, 618

Salpeter, E.E. 1955, ApJ, 121, 161

Sasselov, D., & Goldwirth, D. 1994, astro-ph/9407019

Scalo, J.M. 1986 Fund Cosmic Phys, 11, 1

Schramm, D.N., & Wagoner, R.V. 1977, Ann. Rev. Nucl. Sci., 27, 37

Seckel, D., 1993, Bartol preprint

J. Silk, 1994 CfA preprint

Skillman, E., & Kennicutt, R.C. 1993, ApJ, 411, 655

Skillman, E., Terlevich, R.J., Kennicutt, R.C., Garnett, D.R., & Terlevich, E. 1994, ApJ, in press

Smith, M.S., Kawano, L.H., & Malaney, R.A., 1993. ApJS, 85. 219

Smith, V.V., Lambert, D.L, & Nissen, P.E. 1992 ApJ, 408, 262

Songalia, A., Cowie, L.L., Hogan, C.J., & Rugers, M. 1994 Nature, 368, 599

Spite, F, & Spite, M. 1982, A&A, 115, 357

Steigman, G., 1994, MNRAS, submitted

Steigman, G., Fields, B. D., Olive, K. A., Schramm, D. N., & Walker, T. P., 1993, ApJ 415, L35

Steigman, G., Gallagher, J.S., & Schramm, D.N. 1989, Comments Astrophys. 14, 97

Steigman, G., Schramm, D.N., and Gunn, J.E. 1977 Phys Lett. B66. 202

Steigman, G., & Tosi, M. 1992 ApJ. 401, 150

Talbot, R.J., & Arnett, W.D. 1971, ApJ, 170, 409

Timmes, F.X., Woosley, S.E., & Weaver, T.W. 1994. ApJ, in press

Tinsley, B. 1972, A&A, 20, 383

Tinsley, B. 1980 Fund Cosm Phys, 5, 287

Tosi, M. 1988 A&A, 197, 33

Thielemann, F.-K., et al 1993, Phys. Rept., 227,269

Thielemann, F.-K., Nomoto, K., & Yokoi, K. 1986 A&A 158, 17

Thomas, D., Schramm, D.N., Olive, K.A., Meyer, B., Mathews, G.J. & Fields, B.D. 1994 ApJ, 430, 291

Thorburn, J.A. 1994, ApJ, 421, 318

Vangioni-Flam, E., Olive, K.A., & Prantzos, N. 1994 ApJ, 427, 618

Vigroux, L., Audouze, J., & Lequeux, J. 1976 A&A, 52, 1

Wagoner, R.V., Fowler, W.A., & Hoyle, F. 1967 ApJ, 148, 3

Walker, T.P., Stiegman, G., Schramm, D.N., Olive, K.A., & Fields, B. 1993, ApJ, 413, 562

Walker, T.P., Steigman, G., Schramm, D.N., Olive, K.A., and Kang, H-S. 1991 ApJ, 376, 51

Weaver, T.A., & Woosley, S.E. 1993 Phys Rep, 227, 65

Wheeler, J., Sneden, C., & Truran, J.W. 1989, ARAA, 27, 279

Wilson, T.L., & Rood, R.T. 1994, ARAA, in press

Woosley, S.E., & Weaver, T.A., 1986, ARAA, 24, 205

Woosley, S.E., & Weaver, T.A., 1994, in preparation

Yang, J., Turner, M.S., Steigman, G., Schramm, D.N., and Olive, K.A. 1984 ApJ, 281, 493

FIGURE CAPTIONS

1. Big bang nucleosynthesis yields as a function of the baryon-to-photon ratio η. The ^{4}He abudance is plotted as a mass fraction Y_p; all other elements given as number relative to hydrogen. Open points show abundance used for the three values of η considered in this study. The dashed lines give the bounds for the Copi, Schramm & Turner (1992) "sensible" bounds on η.

2. The different adopted star formation rates, plotted as a function of time for models without infall.

3. (a) The star formation rate $\psi = \nu\sigma_{tot}$ plotted for the different models of infall. (b) As in (a), for $\psi = \nu\sigma_{tot}\mu^2$.

4. The (a) total and (b) gas mass surface densities as a function of time. Plotted for $\psi \propto \sigma_{tot}$ with an IMF slope of $x = 1.35$, with the four different infall prescriptions.

5. Iron abundance as a function of time for different star formation rates. Data are from Edvardsson et al. (1994).

6. D evolution for three different IMFs, for SFR 5.

7. As in figure 6, for (a) ^{3}He and D+^{3}He, and (b) ^{4}He.

8. D and ^{3}He evolution for the infall prescriptions. Note the enhancement of D and dilution of ^{3}He in the infall models.

9. N versus O abundances at low metallicities: data is for extragalactic H II regions, as reported by Pagel et al. (1992) and Skillman et al. (1994).

10. (a) The ^{4}He mass fraction as a function of O/H at low metallicities. Data from Pagel et al. (1992). (b) ^{4}He as a function of N/H, as in (a), for different treatments of N evolution. Models as in figure 9.

11. Plot of the yields for the full set of 1184 candidate global models. Calculated for $\eta = 3 \times 10^{-10}$ and for a particular set of light element features. Abundances are calculated for the birth of the solar system and compared to observed solar abundances. Solar abundances are from Geiss (1993) for D and ^{3}He, and from Anders & Grevesse (1989) for all other elements; ± 0.4 dex limits to the solar abundances are indicated by the dashed lines.

12. Plot of the yields for the 267 candidate models constrained to have CNOFe within 0.4 dex of solar abundances.

13. The G-dwarf distribution in two candidate global models. The model in (a) passes, the one in (b) does not; see discussion in text. Data is from Rana (1991).

14. Solar abundances for the 2052 allowed global models with all light element model variations. No cut has been made for CNO overabundances due to mass loss in massive stars (see discussion in text).

15. As in figure 14, with the constraint that CNOFe be within 0.4 dex of solar: 1460 models displayed. Note that imposing this constraint makes little change in the light element ranges.

16. As in figure 15, for models with $\eta = 4 \times 10^{-10}$.

17. The data of figure 15 which reproduces CNOFe within 0.3 dex (short dashed line). For comparison, a level of 0.4 dex is shown in a long dashed line.

18. Plot of D and ^{3}He predicted solar abundances for the "final set" of 1460 models.

19. As in figure 18, for D and ^{4}He.

20. Models in figure 19 having no ^{4}He enhacement features.

21. Models in figure 19, having either or both ^{4}He enhacement features.

22. Calculated solar abundances of ^{3}He and ^{4}He. (a) Models with standard ^{4}He yields: (b) for nonstandard ^{4}He yields.

23. Calculated abundances of D and ^{3}He at the present epoch. As discussed in the text, the ISM ^{3}He data does not offer a strong constraint; we have omitted it here. We show the D abundance in the ISM due to Linsky et al. (1993).

24. Deuterium abundances calculated for the solar birth and for the ISM today.

25. Calculated D and ^{3}He abundances at the solar birth. As in figure 18, but models have been constrained to fit both the presolar and the ISM D abundances.

26. As in figure 25, for ^{3}He and ^{4}He.

27. D versus [Fe/H] for out models, plotted at a galactic age equal to universal time at $z = 3$. The redshift-time relation is derived for a cosmology with $\Omega = 0$ and $H_0 = 75$ km/s/Mpc. Dotted lines indicate primordial levels for the three adopted η values.

28. D versus [Fe/H] for the models of figure 6 having different IMFs and for the high infall model 4 of table protect2. Regardless of these model features, the D evolution at low metallicity is minimal.

29. Mass fraction of ^{4}He plotted as a function of (a) C, (b) N, and (c) O abundance in the low metallicity regime. Solid line: no ^{4}He enhancement; dashed line: $8-12$ $M_\odot$ ^{4}He enhancement; dot-dashed line: mass loss: dotted line, both enhancements. For $\eta = 4 \times 10^{-10}$.

30. The error δY_p made in extrapolating the $Y-$N relation linearly to determine the primordial ^{4}He abundance. Plotted for each model as a function of the average slope dY/dN of the $Y-$N relation at low metallicity. Open circles are for models with only primary N, triangles are models with mixed primary and secondary N, squares are models with low secondary N and hexagons are for models with high secondary N. Horizontal line indicates level of observational error; vertical line indicates approximate level of minimum slope for H II region data.

Table 1: Galactic Sources for the Light Elements

NUCLIDE	PRODUCTION SITE	CONTRIBUTION TO OBSERVED ABUNDANCE
D	none	not applicable
^{3}He	low mass ($\lesssim 3 M_\odot$) stars (?)	$\gtrsim 50\%$ (?)*
^{4}He	stars of all masses	$\sim 10 - 20\%$
^{7}Li	cosmic rays	Pop II : $\sim 20\%$ (?) Pop I : $\sim 10\%$
	AGB stars(?) SN II(?)	Pop II : $\sim 0\%$ (?) Pop I : $\sim 90\%$
^{6}Li, Be, ^{10}B	cosmic rays	100%
^{11}B	cosmic rays	$\sim 60\%$ (?)
	SN II (ν-process?)	$\sim 40\%$ (?)

* ^{3}He abundances in the ISM vary with mass of H II region

Table 2: Global Model Features

Model Feature	#	Descrption
SFR	1	$\nu\sigma_{tot}$
	2	$\nu\sigma_g$
	3	$\nu\sigma_{tot}\mu^2$
	4	$a\exp(-t/\tau)$, $\tau = 7.5$ Gyr
	5	$\tau = 15$ Gyr
IMF shape	1	$\phi \propto m^{-(1+x)}$
	2	from PDMF (Scalo 1986)*
IMF slope	1	$x = 1.0$
	2	$x = 1.35$
	3	$x = 1.7$
IMF mass limits	1	$(m_l, m_u) = (0.2,100)$
	2	$(m_l, m_u) = (0.1,60)$
	3	$(m_l, m_u) = (0.4,30)$
infall		$f = f_0\exp(-t/\tau_{inf})$
	1	$f_0 = 0$
	2	$\tau_{inf} = 2$ Gyr; 99.9% σ_{tot}
	3	$\tau_{inf} = 4$ Gyr; 50% σ_{tot}
	4	$\tau_{inf} = 4$ Gyr; 99.9% σ_{tot}
N yields		$X^{ej} = X_0^{ej}(\alpha + \beta(X_C/X_C^{\odot}))$
	1	$\alpha = 1$, $\beta = 0$
	2	$\alpha = 0.5$, $\beta = 1$
	3	$\alpha = 0$, $\beta = 1$
	4	$\alpha = 0$, $\beta = 2$
SN Ia normalization	1	$\lambda = 0.05$
	2	$\lambda = 0.007$

*Only calculable for exponential SFR

Table 3: Model Ranges for Solar D, ^{3}He, and ^{4}He Production

η	10^5 D_{min}	10^5 D_{max}	10^5 $^3He_{min}$	10^5 $^3He_{max}$	Y_{min}	Y_{max}
2×10^{-10}	5.90	11.9	4.26	18.9	0.250	0.313
4×10^{-10}	1.82	3.66	2.00	7.25	0.258	0.322
6×10^{-10}	0.912	1.83	1.44	4.26	0.262	0.326

η	D_{max}/D_{min}	$(D+^3He)_{max}/(D+^3He)_{min}$	$Y_{max} - Y_{min}$
2×10^{-10}	2.02	3.03	0.063
4×10^{-10}	2.01	2.86	0.064
6×10^{-10}	2.01	2.58	0.064

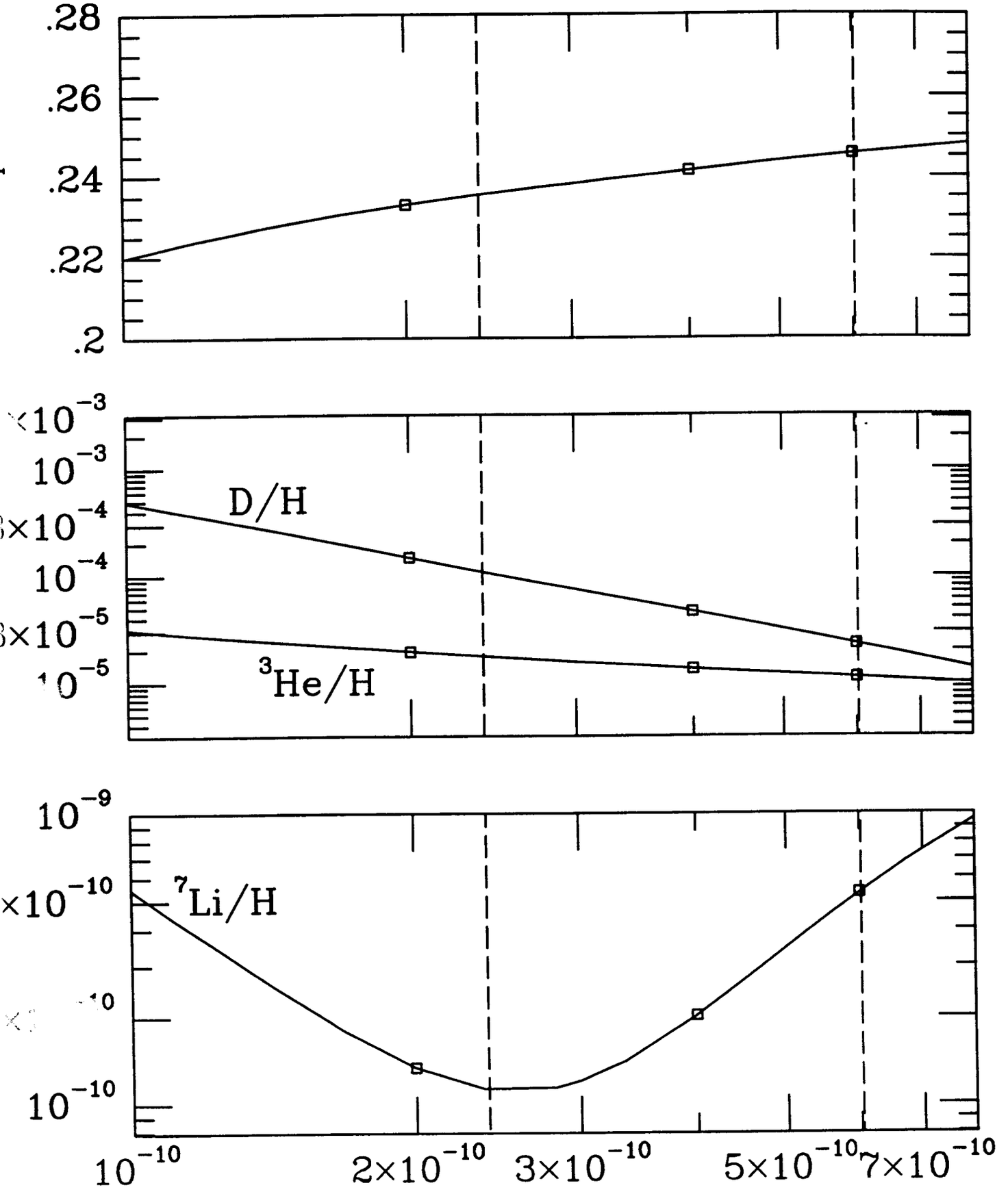
.28
.26
.24
.22
.2
D/H
^{3}He/H
10^{-3}
10^{-4}
10^{-5}
10^{-9}
10^{-10}
^{7}Li/H
10^{-10}
2×10^{-10}
3×10^{-10}
5×10^{-10}
7×10^{-10}
η

FIG 1

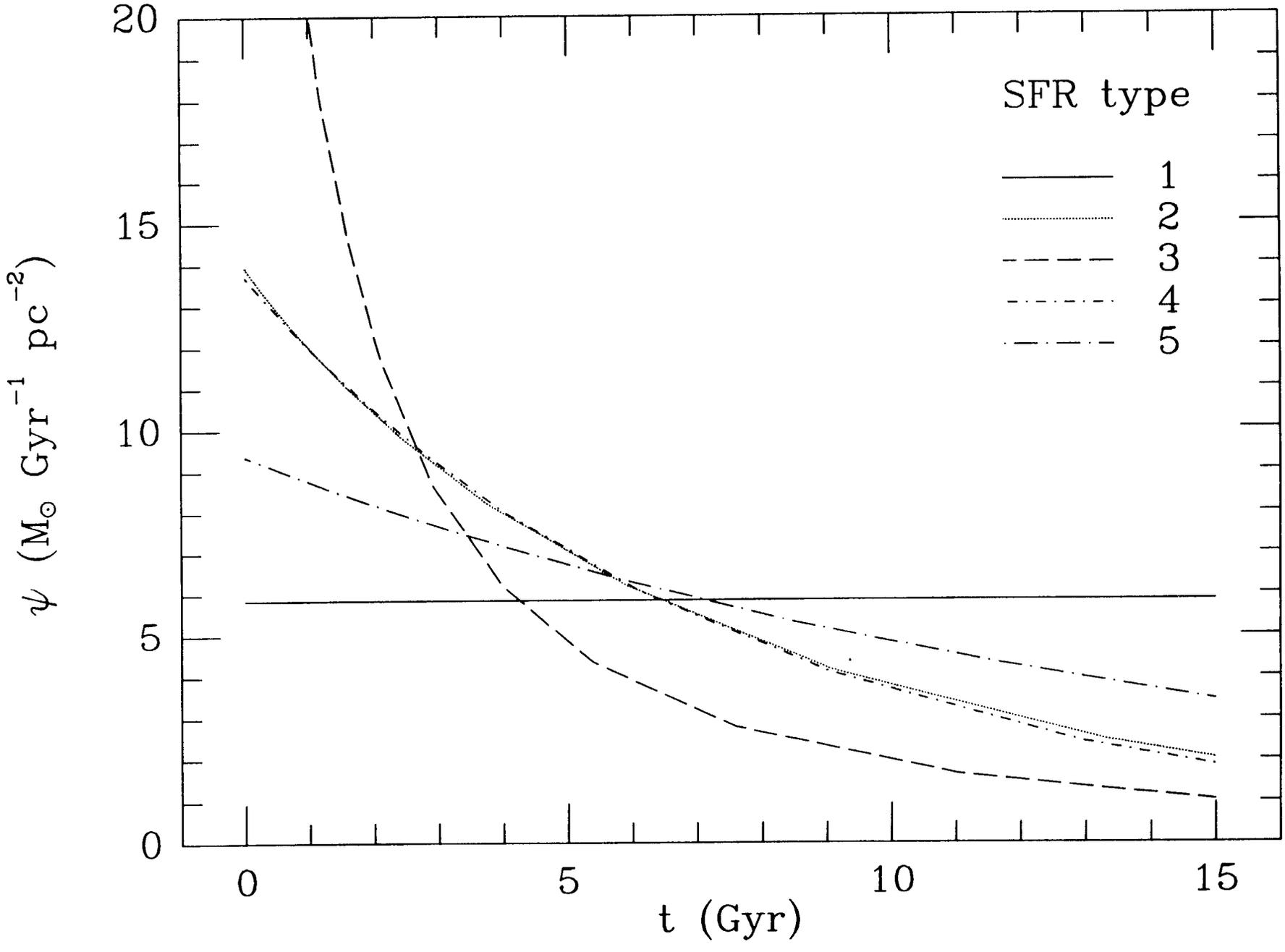

FIG 2

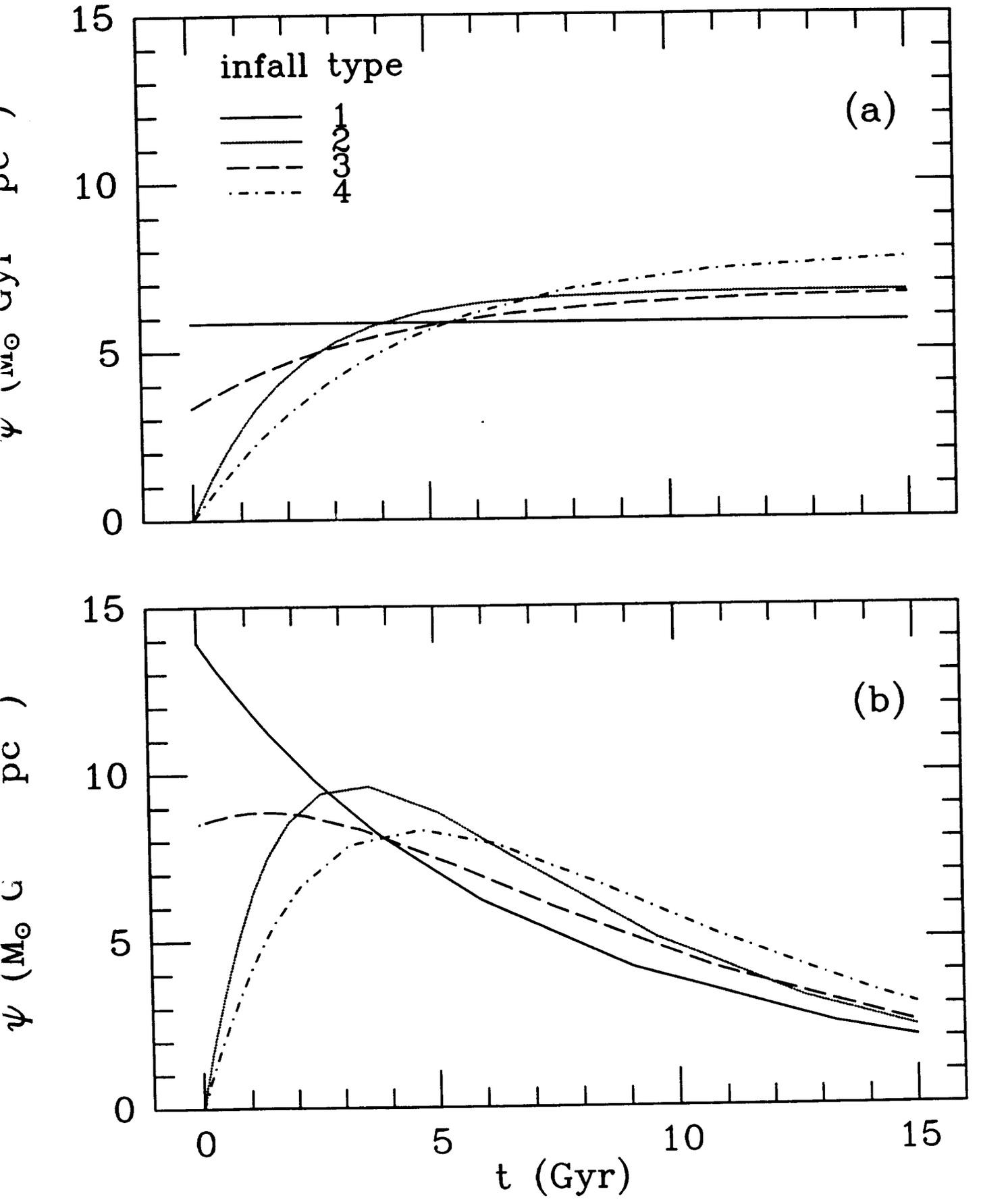

FIG 3

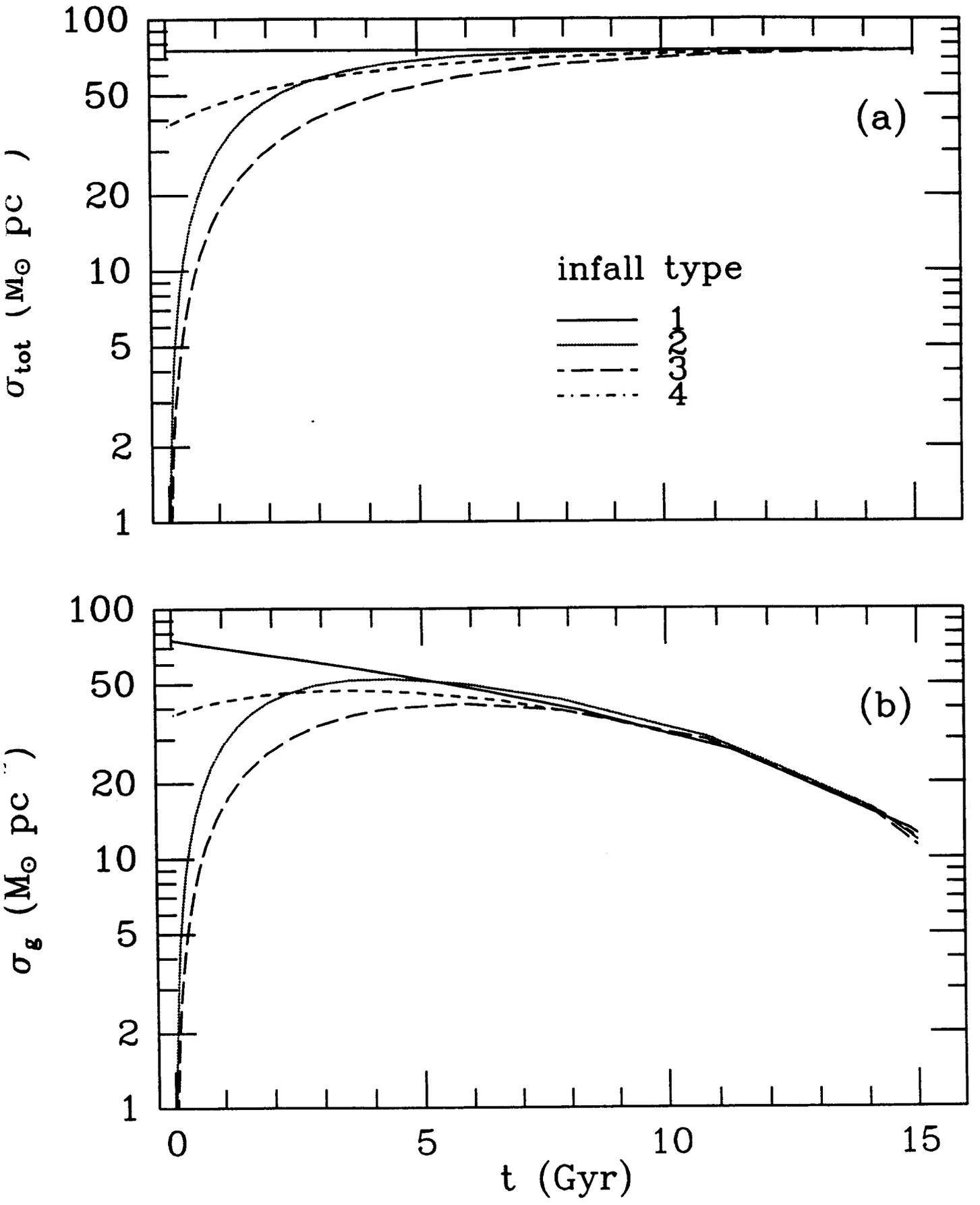
100
50
20
10
5
2
1
σ_{tot} ($M_\odot$ pc^{-2})
(a)
infall type
1
2
3
4
100
50
20
10
5
2
1
σ_g ($M_\odot$ pc^{-2})
(b)
0
5
10
15
t (Gyr)

FIG 4

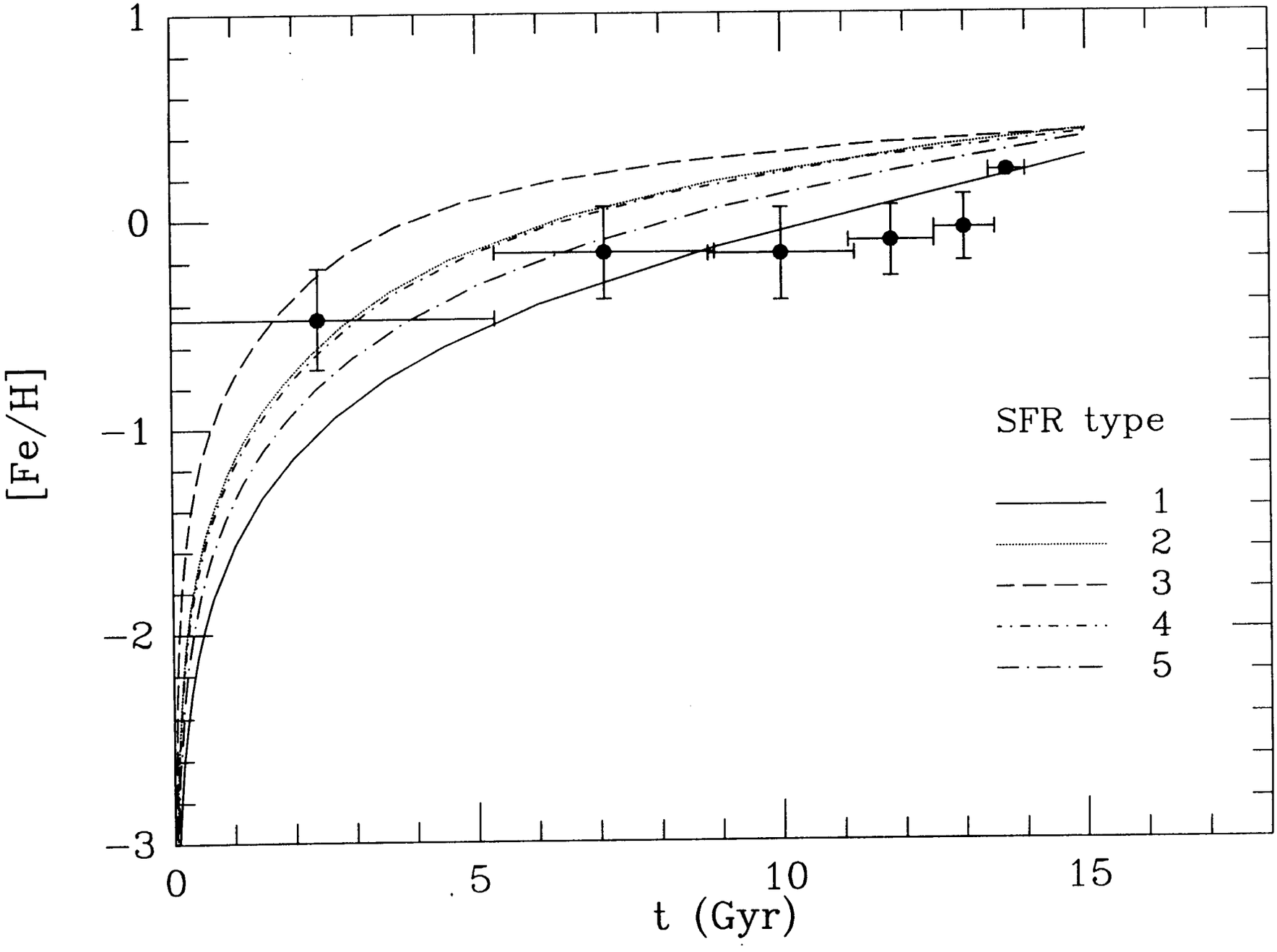

FIG 5

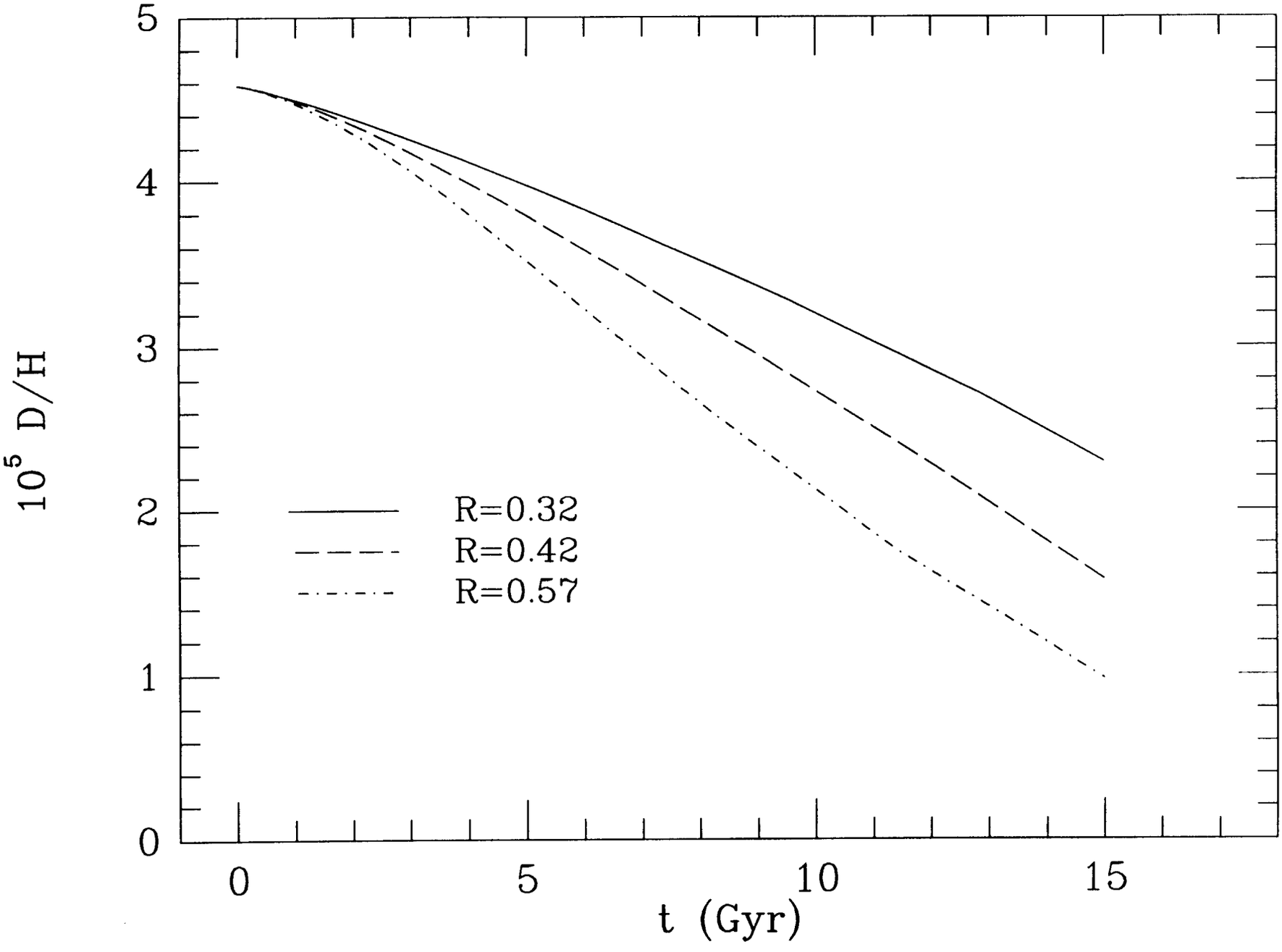

FIG 6

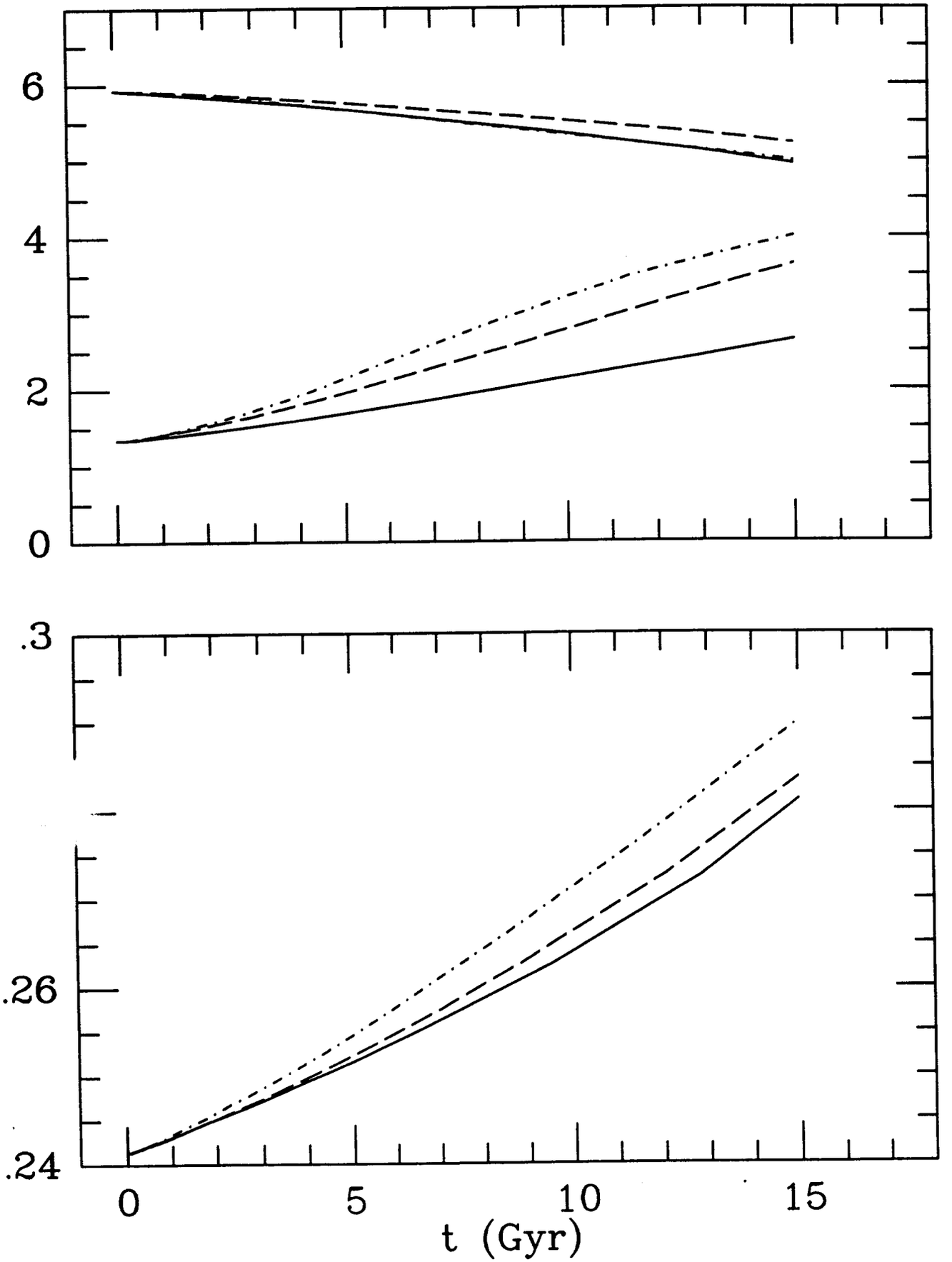

FIG 7

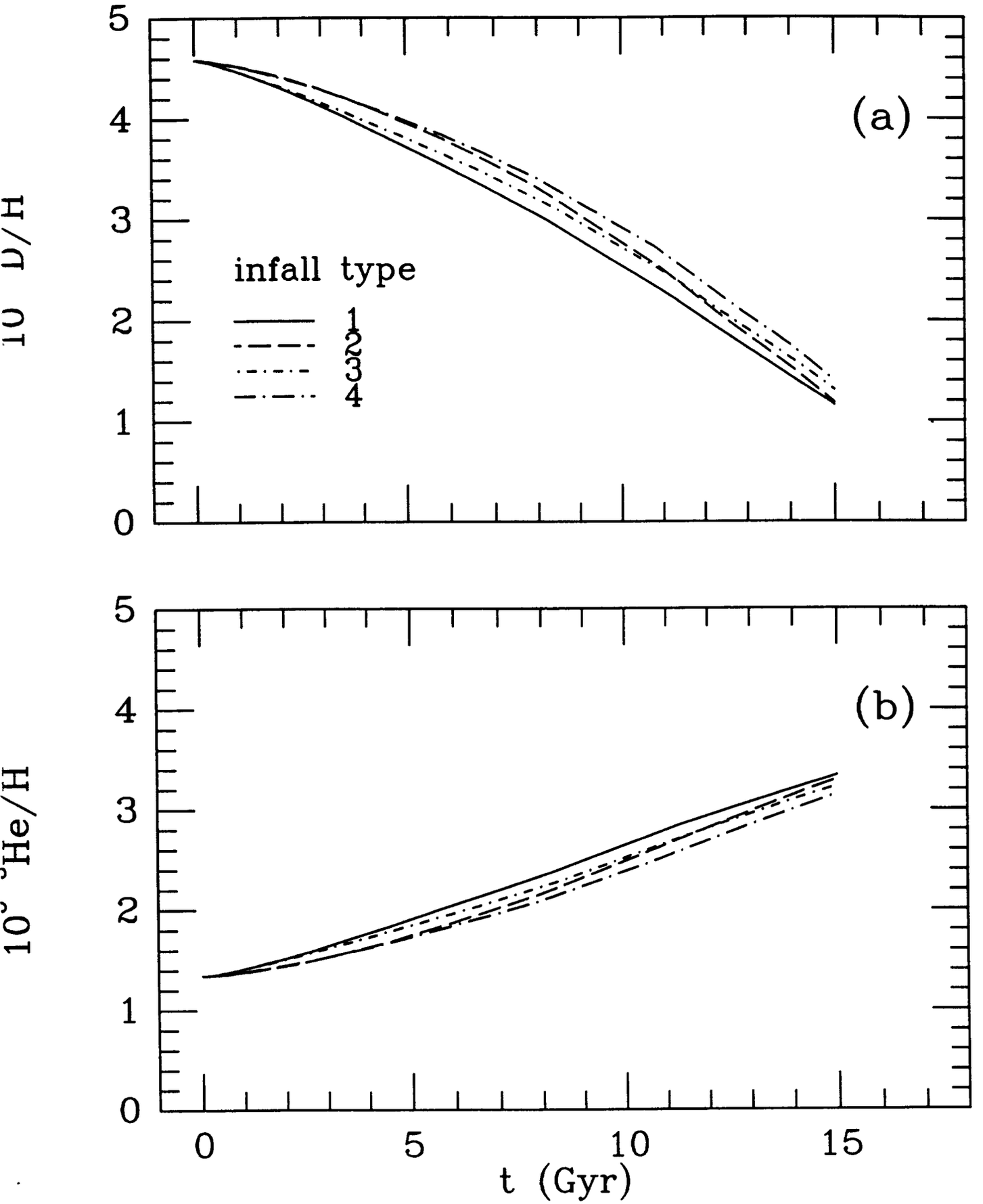

FIG 8

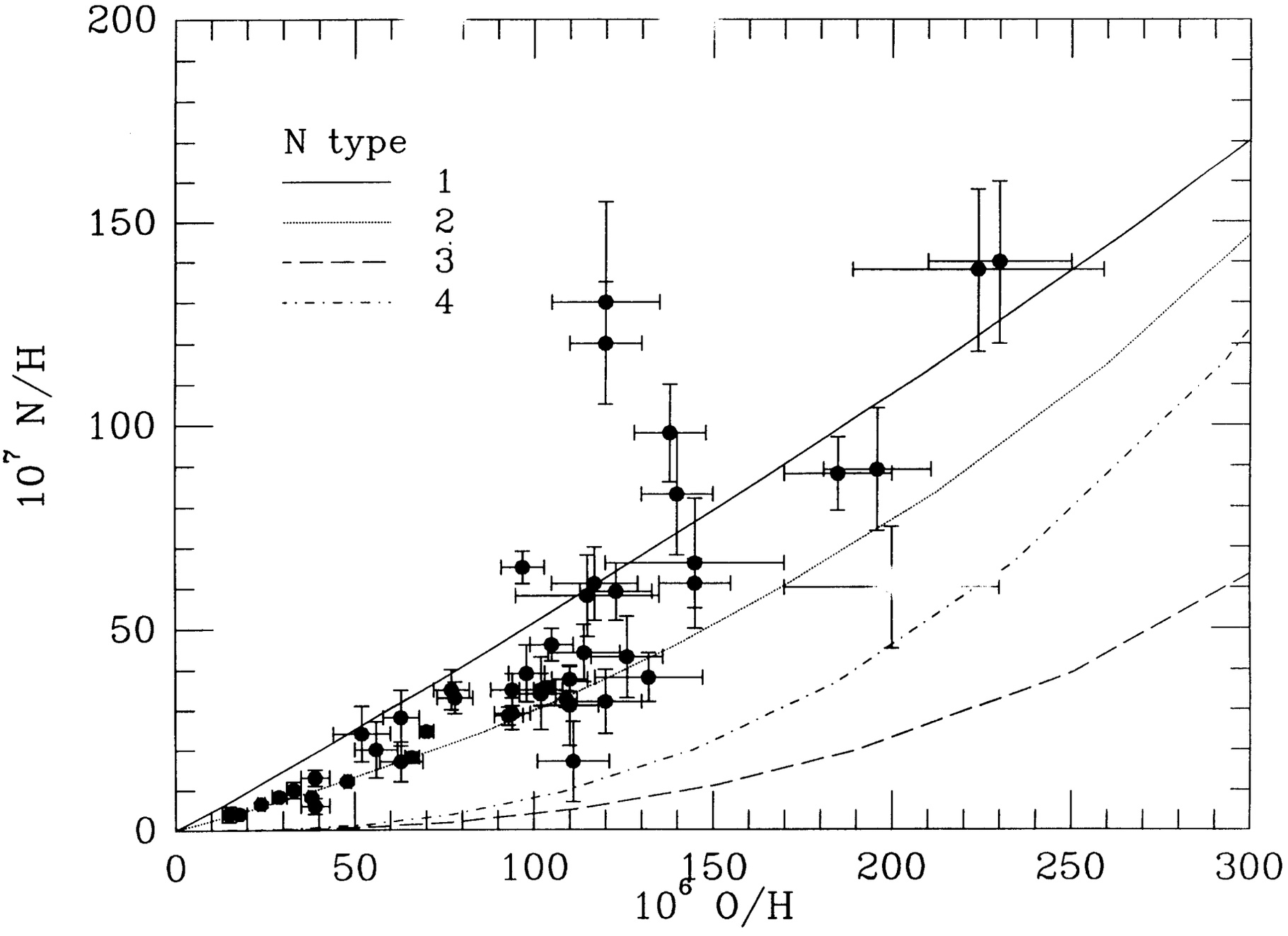

FIG 9

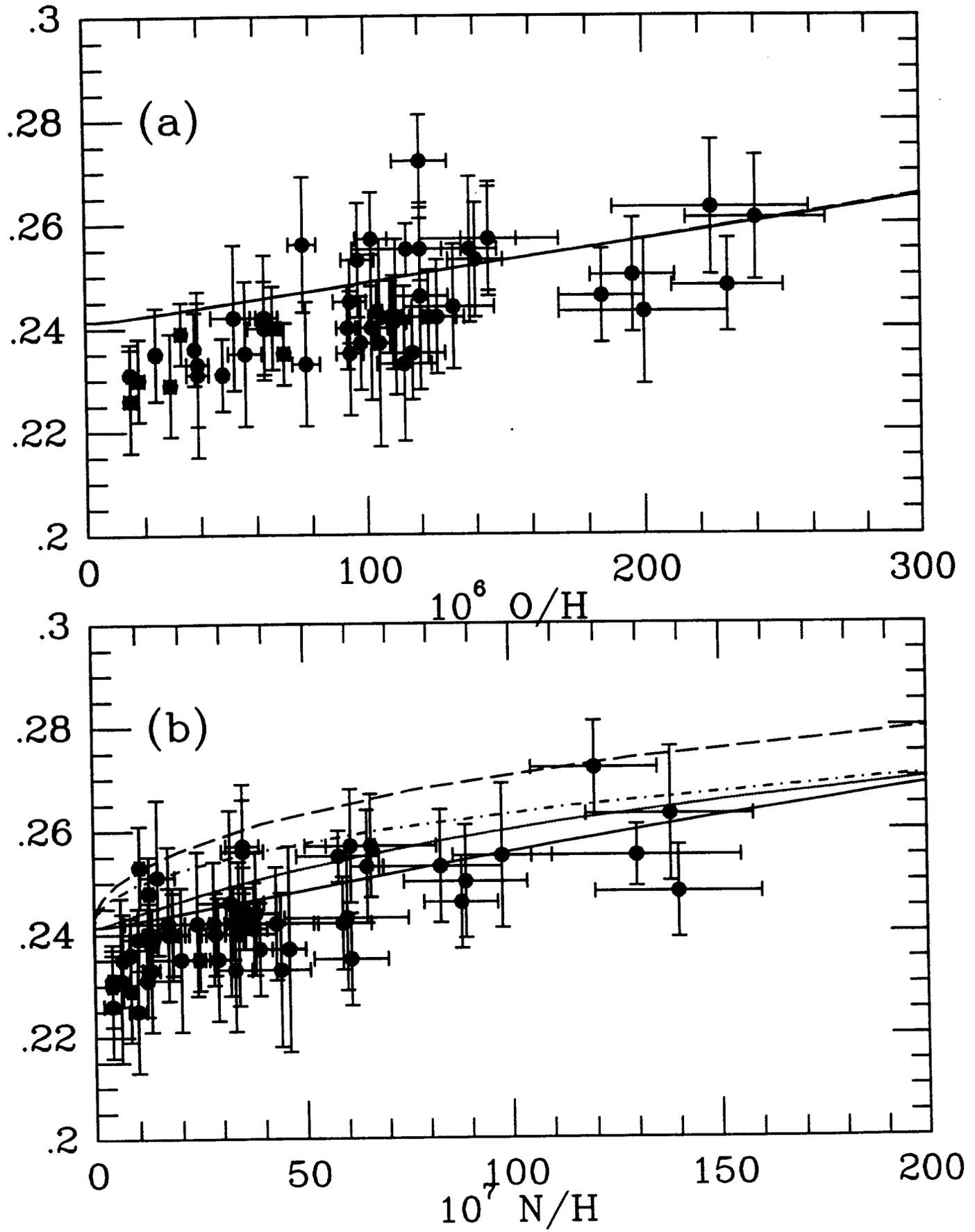
.3
.28
.26
.24
.22
.2
(a)
0
100
200
300
10^6 O/H
.3
.28
.26
.24
.22
.2
(b)
0
50
100
150
200
10^7 N/H
Y

FIG 10

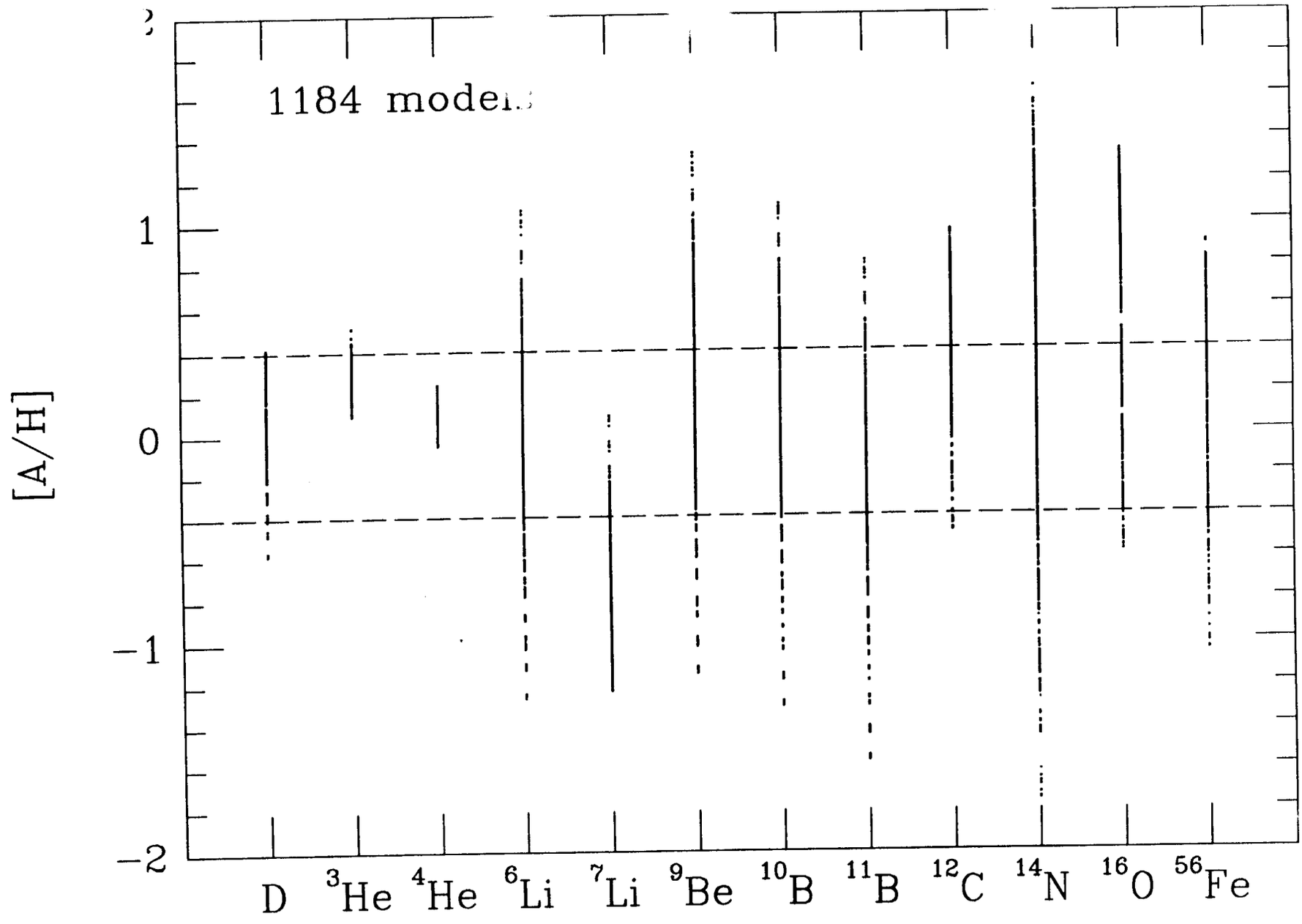
1184 model
[A/H]
2
1
0
−1
−2
D
3He
4He
6Li
7Li
9Be
10B
11B
12C
14N
16O
56Fe

FIG 11

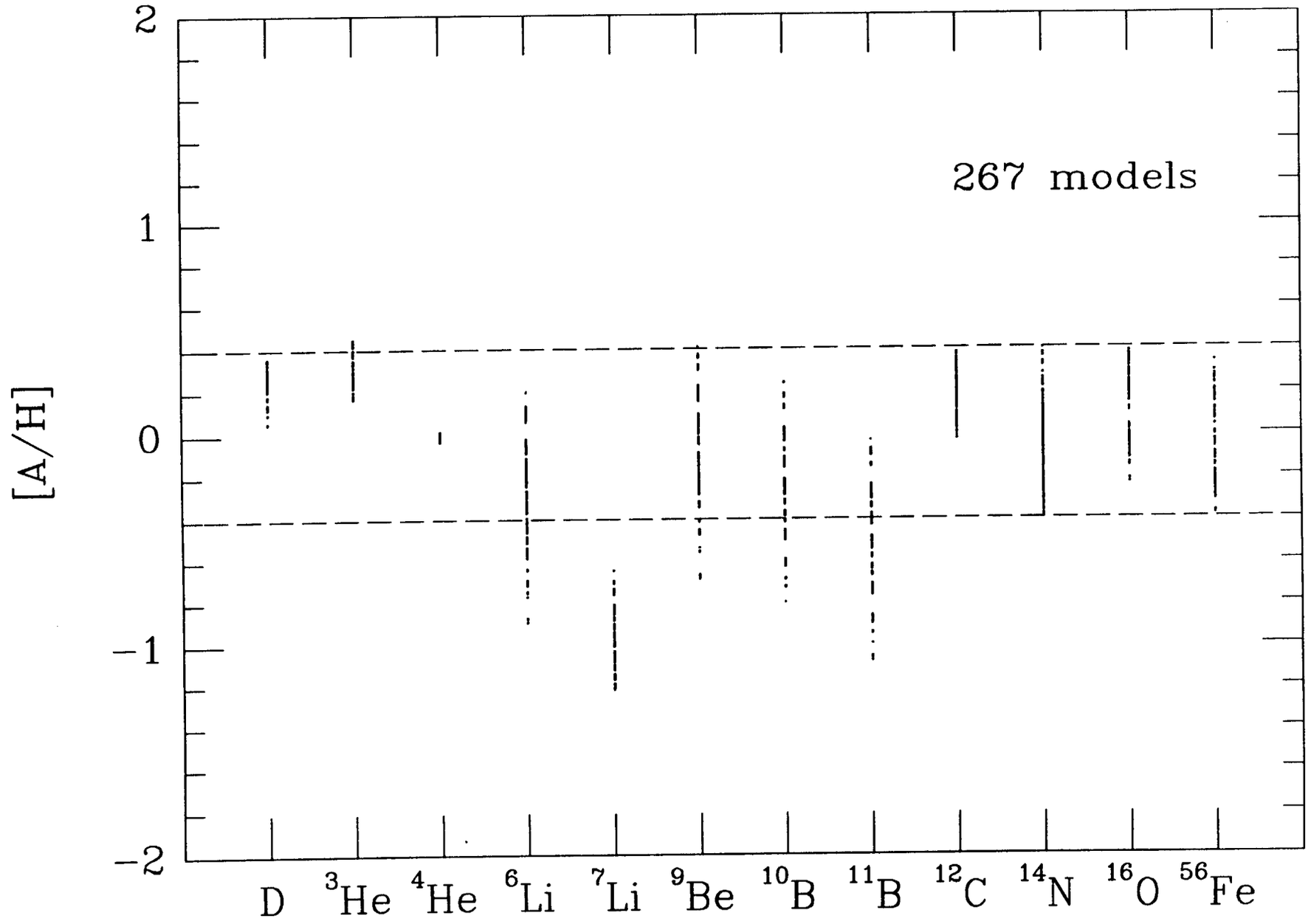
2
1
0
−1
−2
[A/H]
267 models
D
^{3}He
^{4}He
^{6}Li
^{7}Li
^{9}Be
^{10}B
^{11}B
^{12}C
^{14}N
^{16}O
^{56}Fe

FIG 12

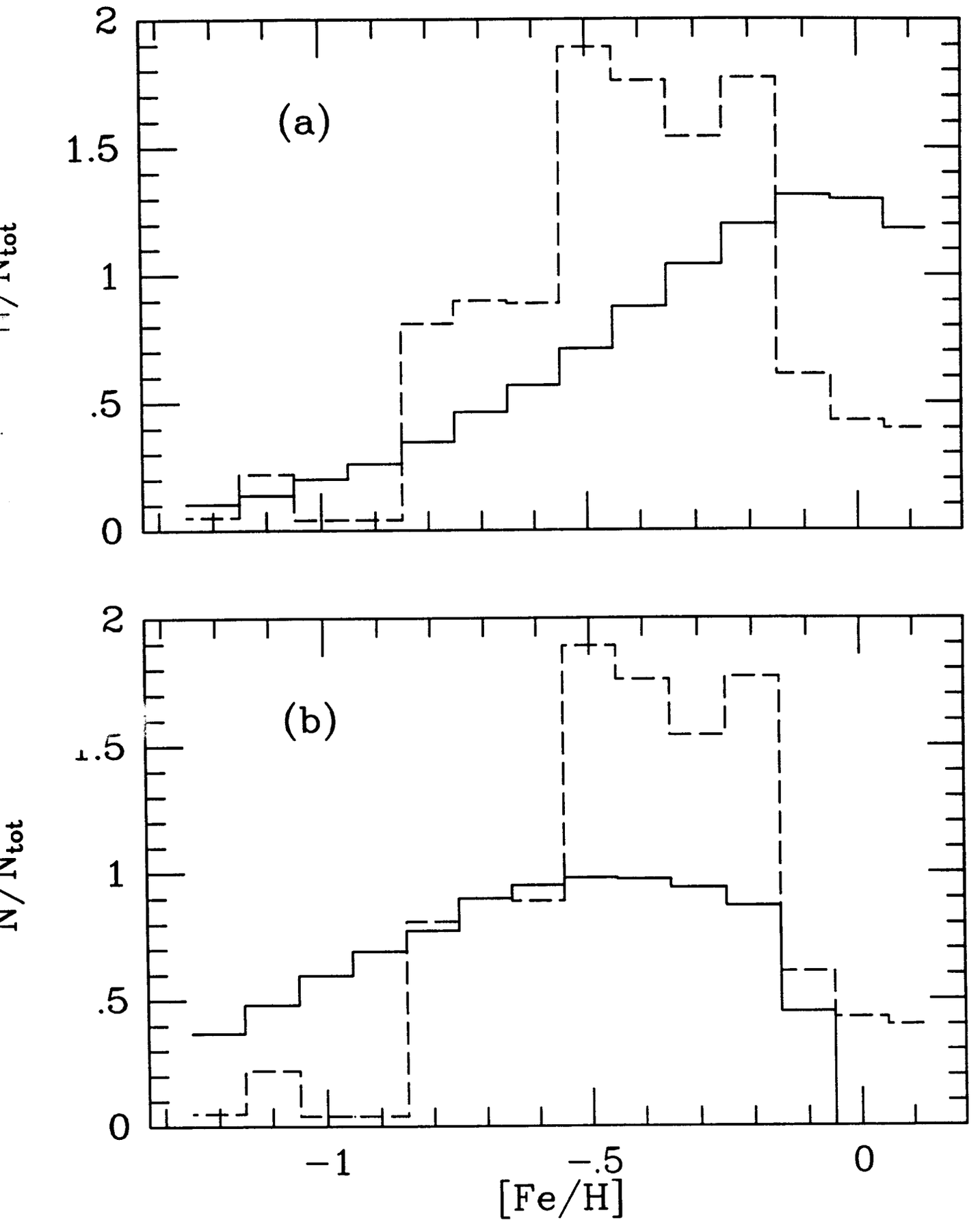

FIG 13

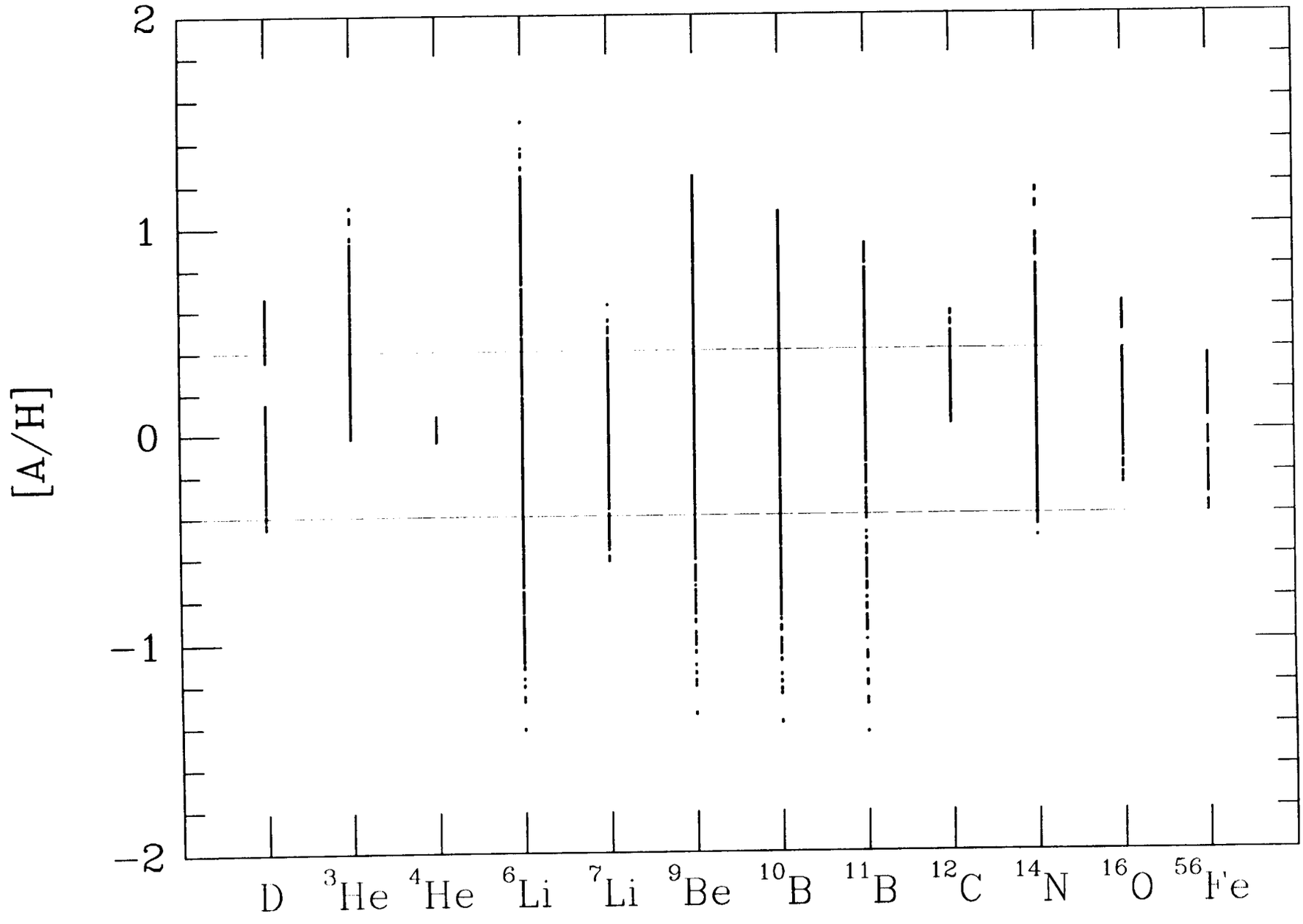

FIG 14

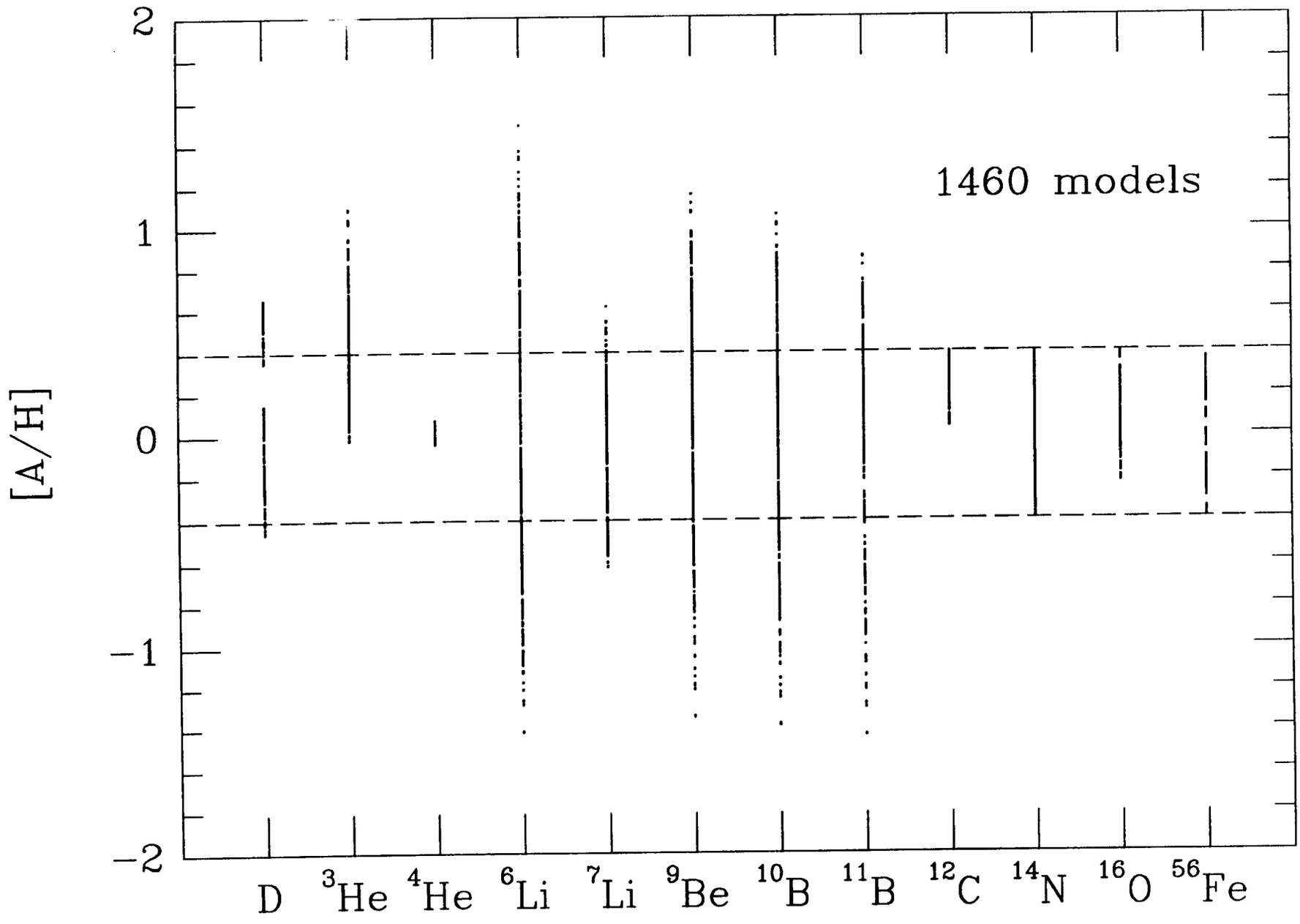
2
1
0
−1
−2
[A/H]
1460 models
D
3He
4He
6Li
7Li
9Be
10B
11B
12C
14N
16O
56Fe

FIG 15

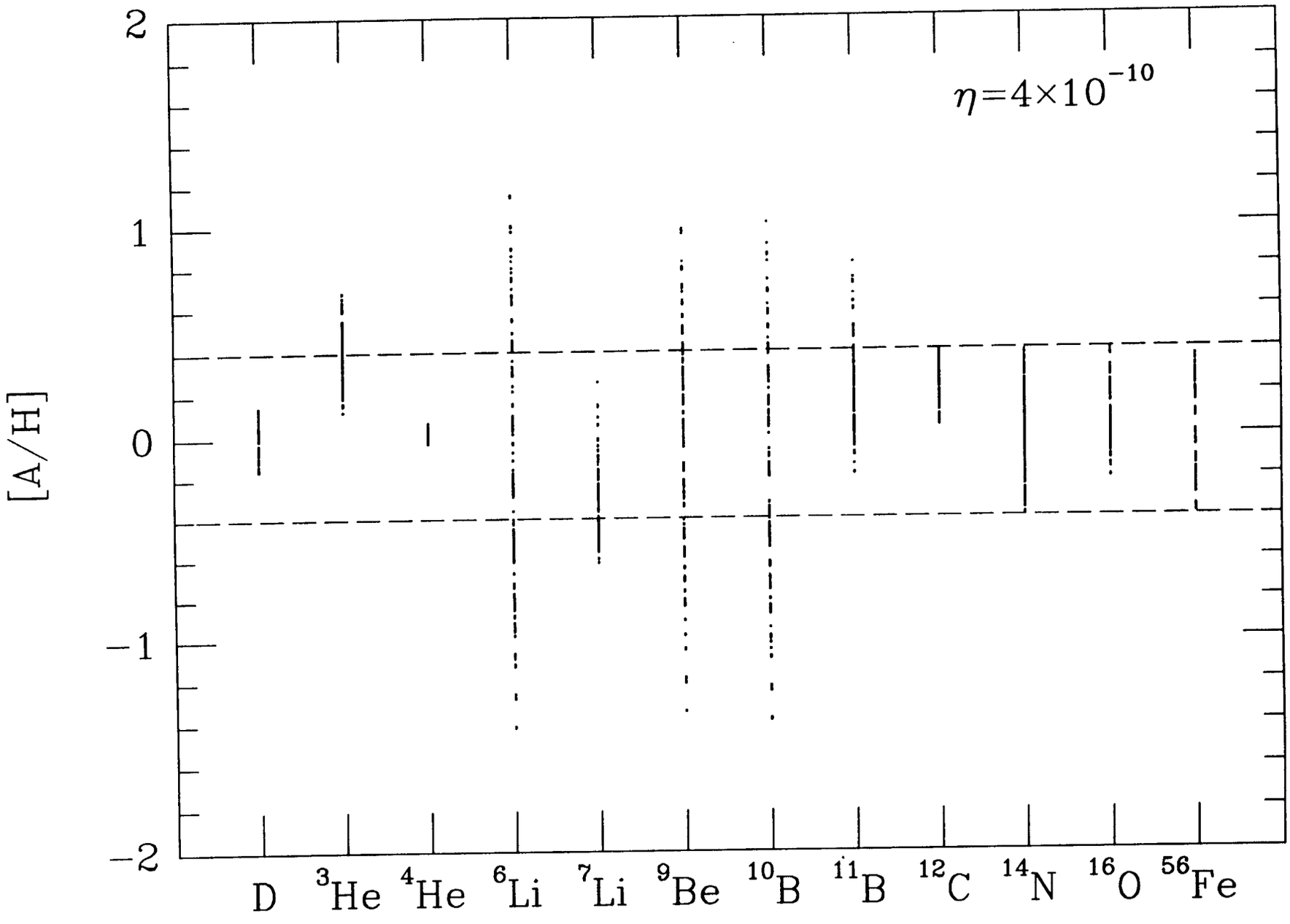
2
1
0
−1
−2
[A/H]
$\eta=4\times10^{-10}$
D
^{3}He
^{4}He
^{6}Li
^{7}Li
^{9}Be
^{10}B
^{11}B
^{12}C
^{14}N
^{16}O
^{56}Fe

FIG 16

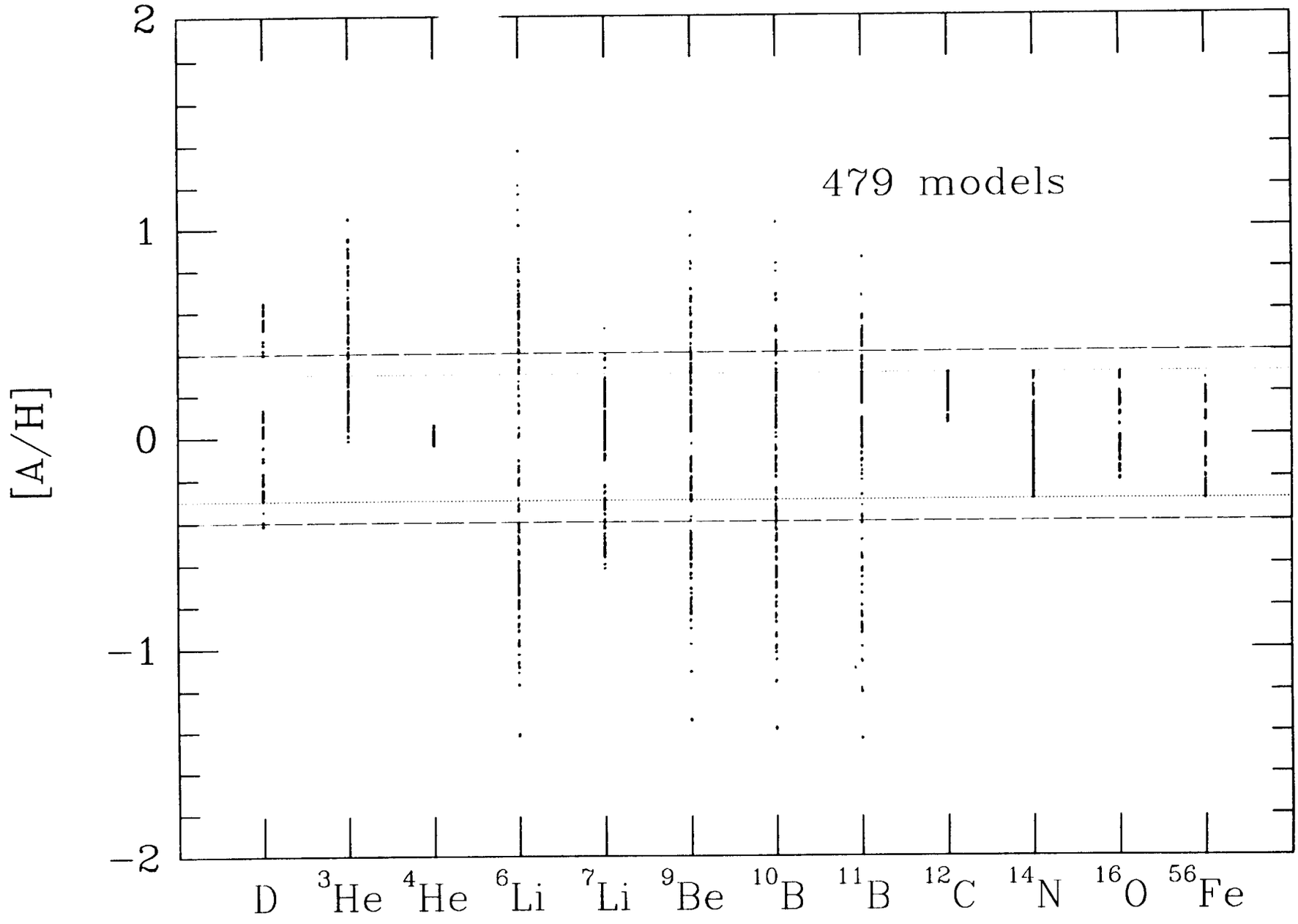
479 models
[A/H]
2
1
0
−1
−2
D
^{3}He
^{4}He
^{6}Li
^{7}Li
^{9}Be
^{10}B
^{11}B
^{12}C
^{14}N
^{16}O
^{56}Fe

FIG 17

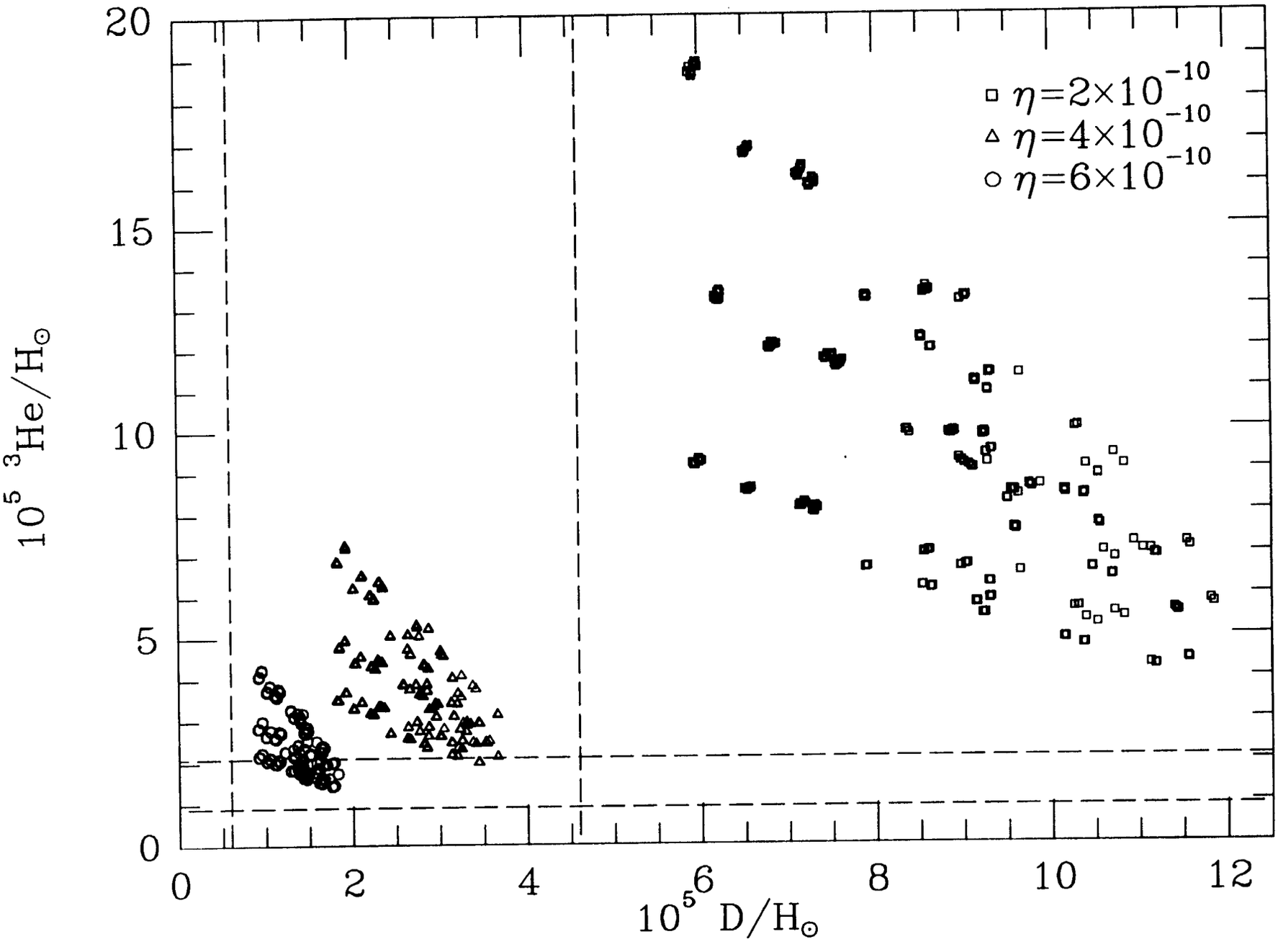
20
15
10
5
0
0
2
4
6
8
10
12
$10^5\ ^3He/H_\odot$
$10^5\ D/H_\odot$
$\square\ \eta=2\times10^{-10}$
$\triangle\ \eta=4\times10^{-10}$
$\circ\ \eta=6\times10^{-10}$

FIG 18

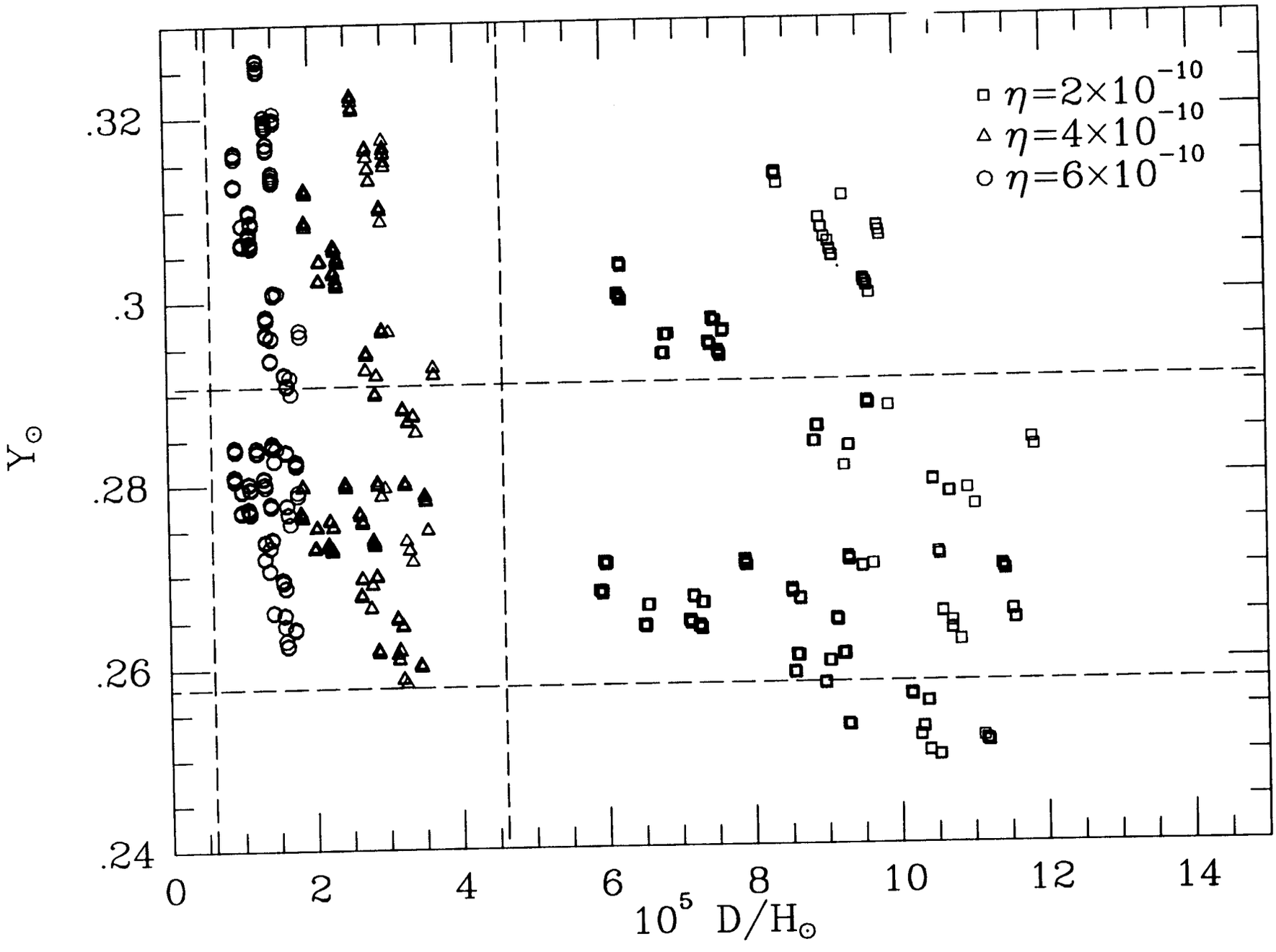
□ $\eta=2\times10^{-10}$
△ $\eta=4\times10^{-10}$
○ $\eta=6\times10^{-10}$
.32
.3
.28
.26
.24
$Y_\odot$
0
2
4
6
8
10
12
14
10^5 D/H$_\odot$

FIG 19

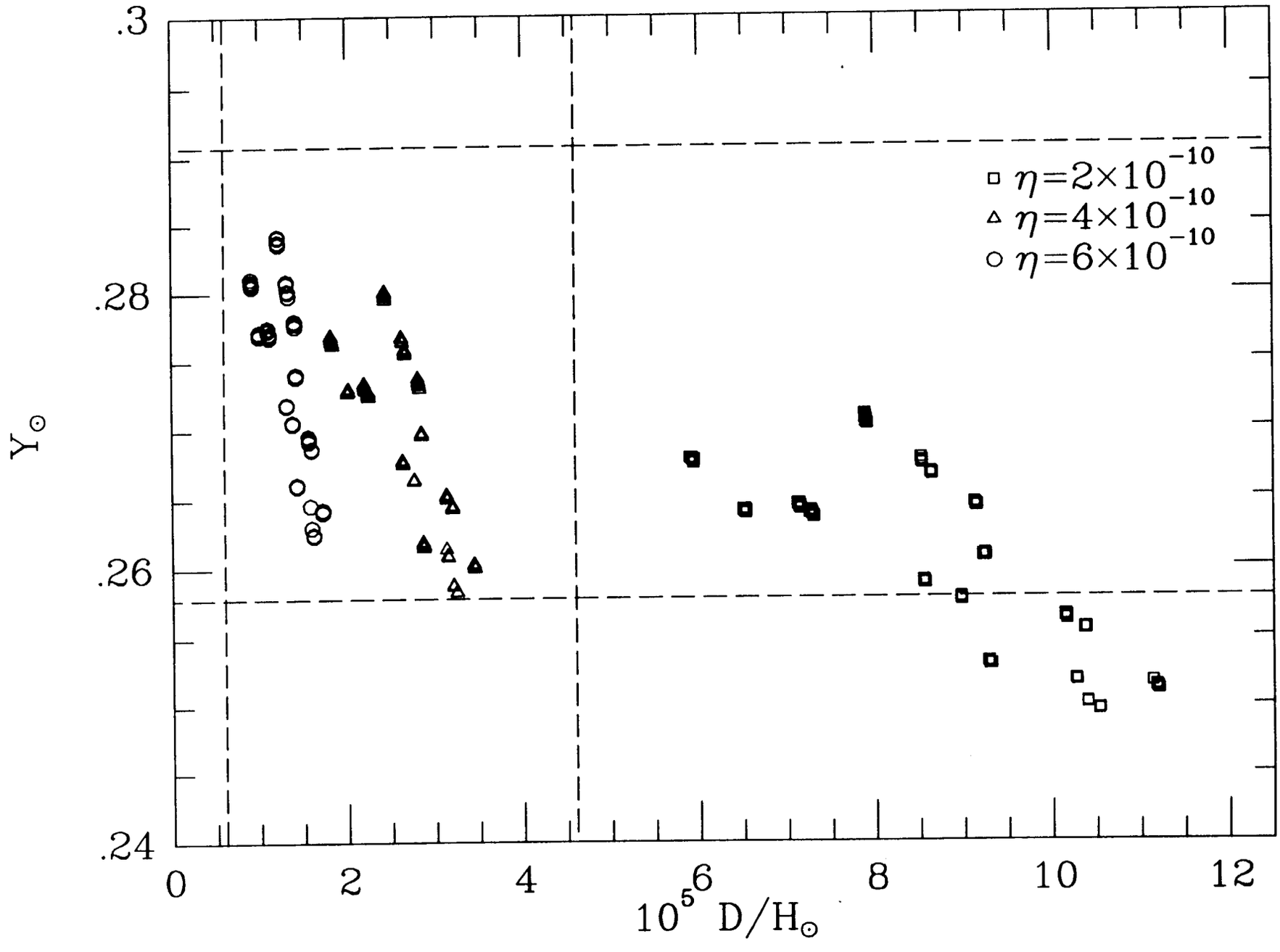
.3
.28
.26
.24
$Y_\odot$
0
2
4
6
8
10
12
10^5 D/H$_\odot$
$\eta=2\times10^{-10}$
$\eta=4\times10^{-10}$
$\eta=6\times10^{-10}$

FIG 20

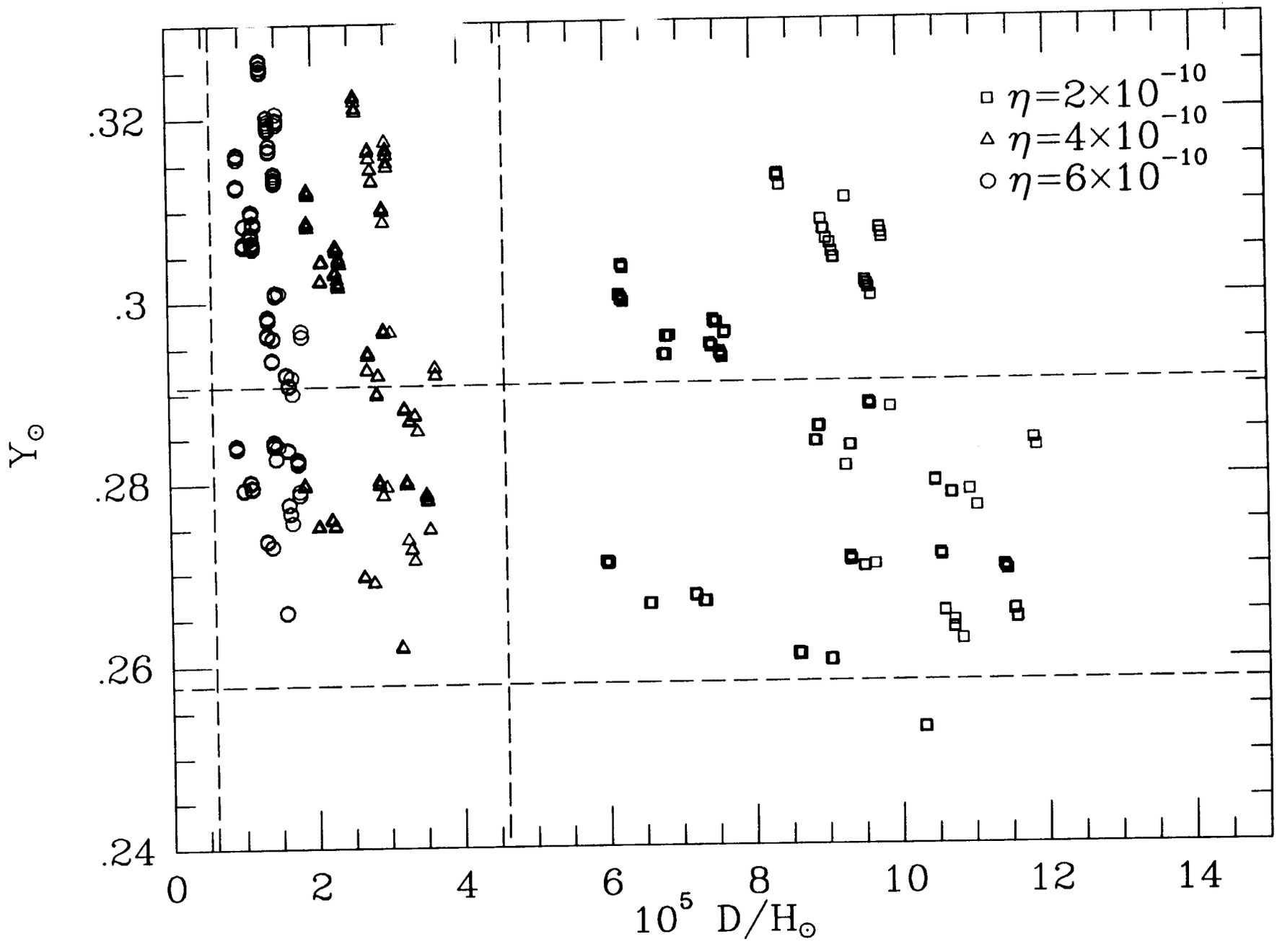
□ $\eta=2\times10^{-10}$
△ $\eta=4\times10^{-10}$
○ $\eta=6\times10^{-10}$
$Y_\odot$
.32
.3
.28
.26
.24
0
2
4
6
8
10
12
14
10^5 D/H$_\odot$

FIG 21

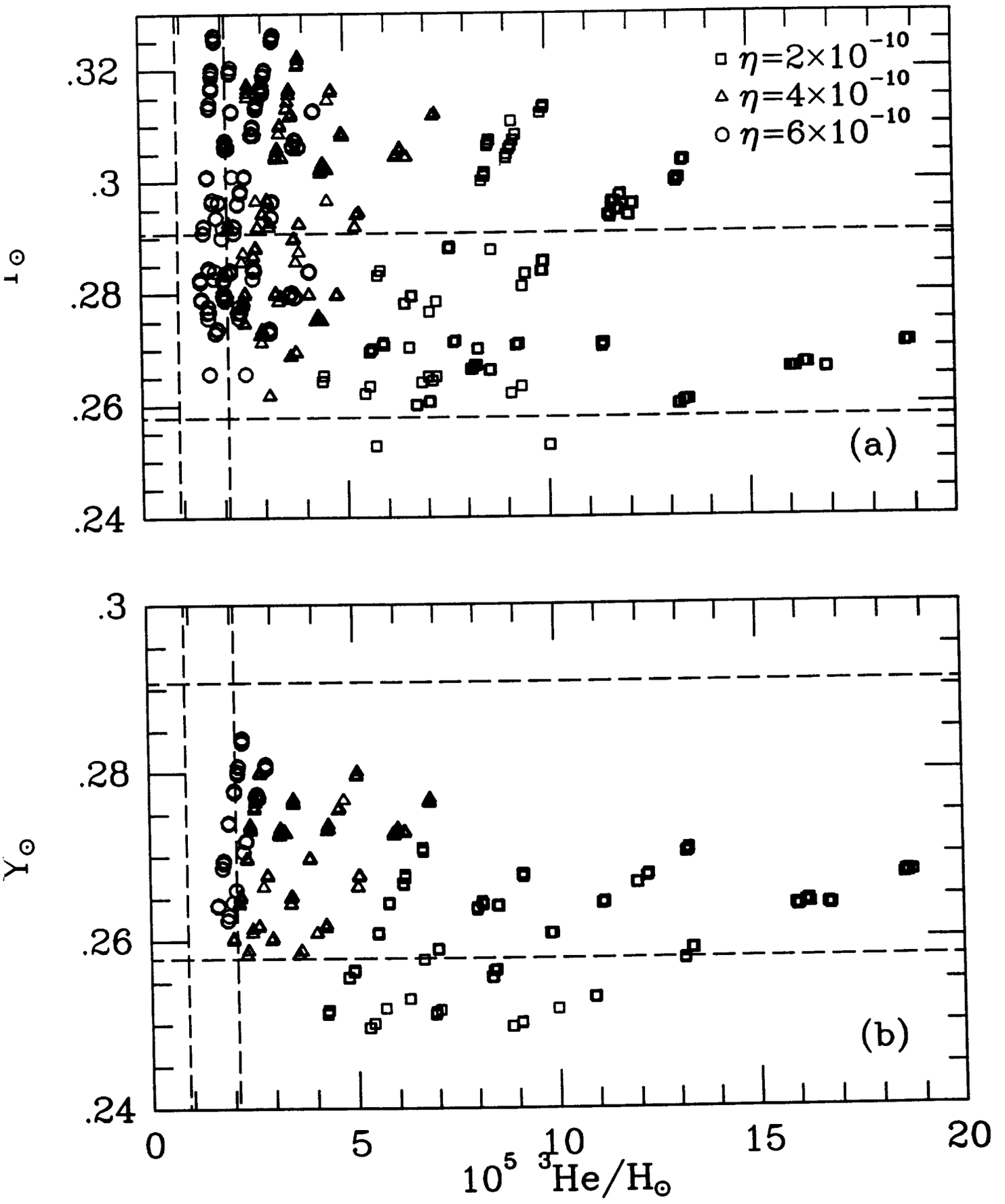
□ $\eta=2\times10^{-10}$
△ $\eta=4\times10^{-10}$
○ $\eta=6\times10^{-10}$
.32
.3
.28
.26
.24
$Y_\odot$
(a)
.3
.28
.26
.24
$Y_\odot$
(b)
0
5
10
15
20
$10^5\ ^3He/H_\odot$

FIG 22

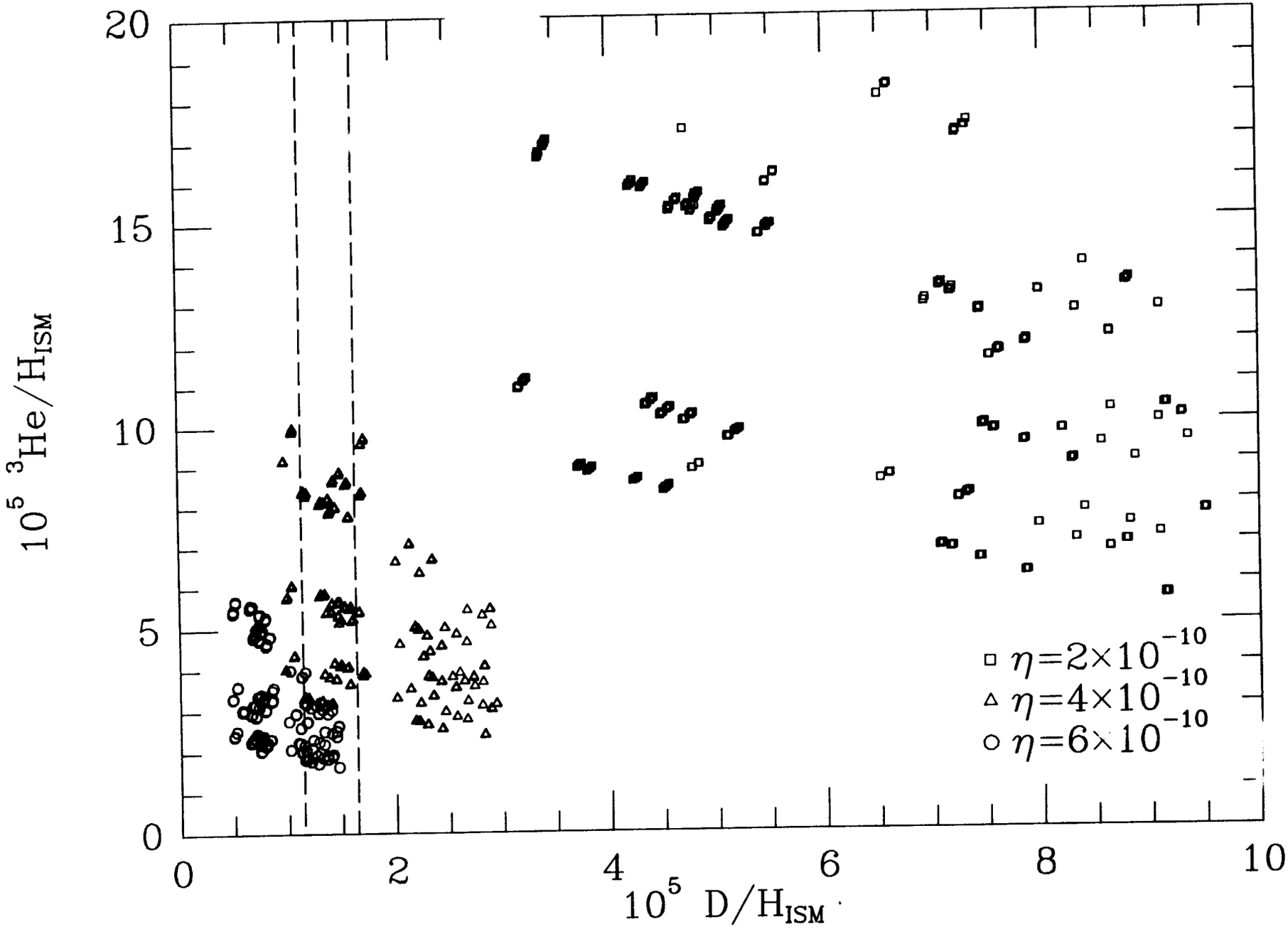
20
15
10
5
0
0
2
4
6
8
10
$10^5\ ^3He/H_{ISM}$
$10^5\ D/H_{ISM}$
$\eta=2\times10^{-10}$
$\eta=4\times10^{-10}$
$\eta=6\times10^{-10}$

FIG 23

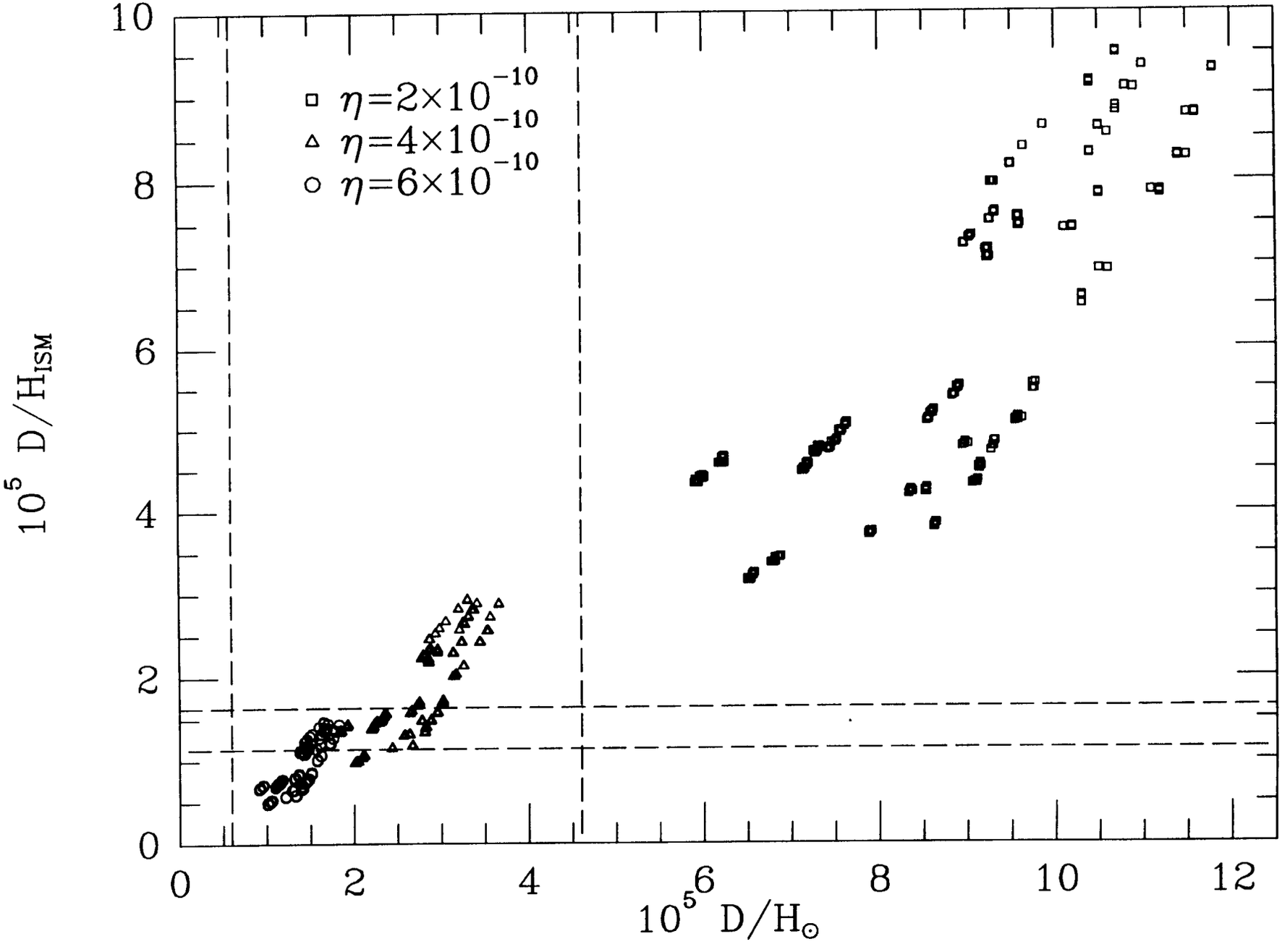
10
8
6
4
2
0
0
2
4
6
8
10
12
$\eta=2\times10^{-10}$
$\eta=4\times10^{-10}$
$\eta=6\times10^{-10}$
10^5 D/H_{ISM}
10^5 D/$H_\odot$

FIG 24

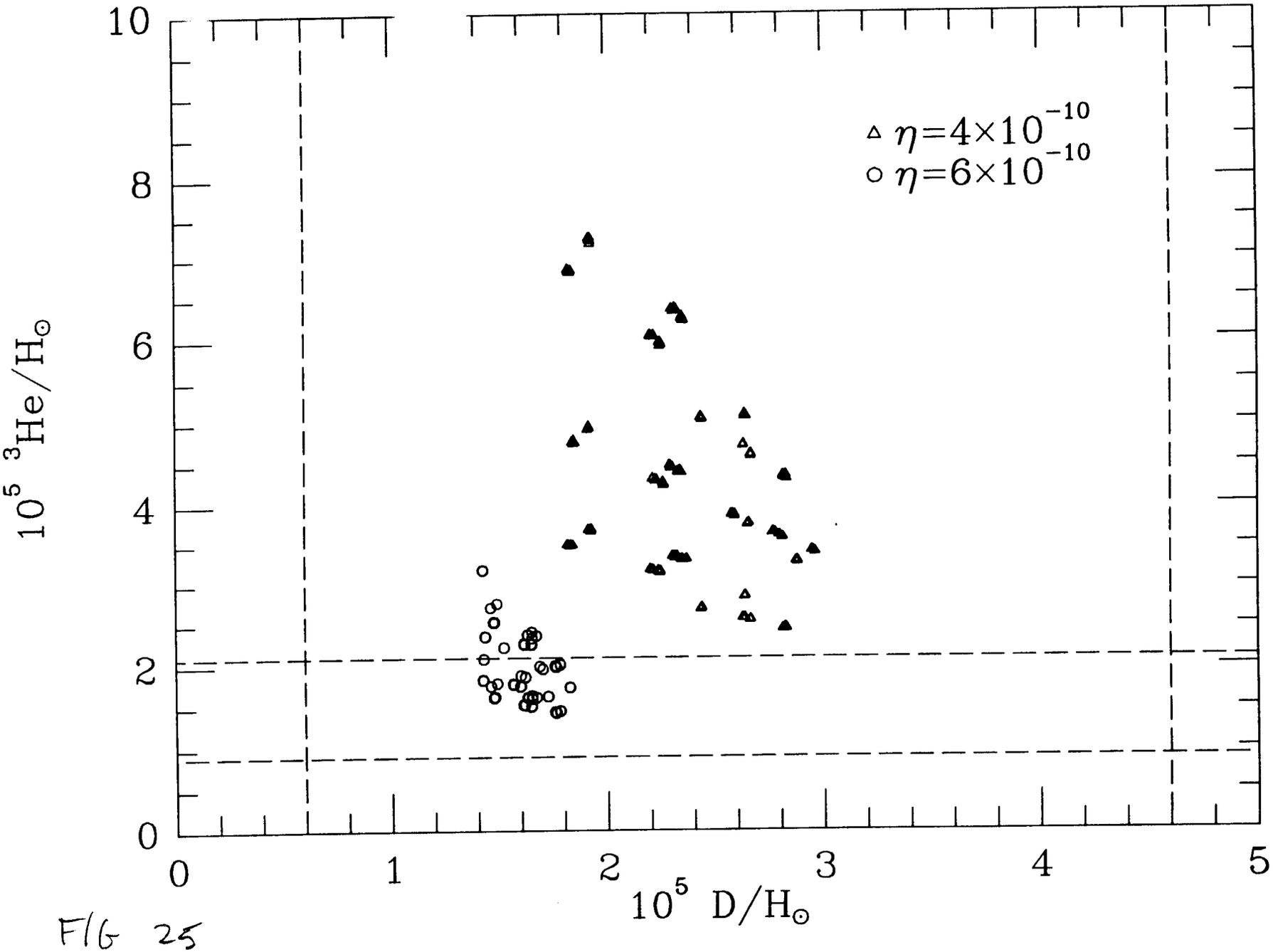
10
8
6
4
2
0
0
1
2
3
4
5
$10^5\ ^3He/H_\odot$
$10^5\ D/H_\odot$
$\triangle\ \eta=4\times10^{-10}$
$\circ\ \eta=6\times10^{-10}$

FIG 25

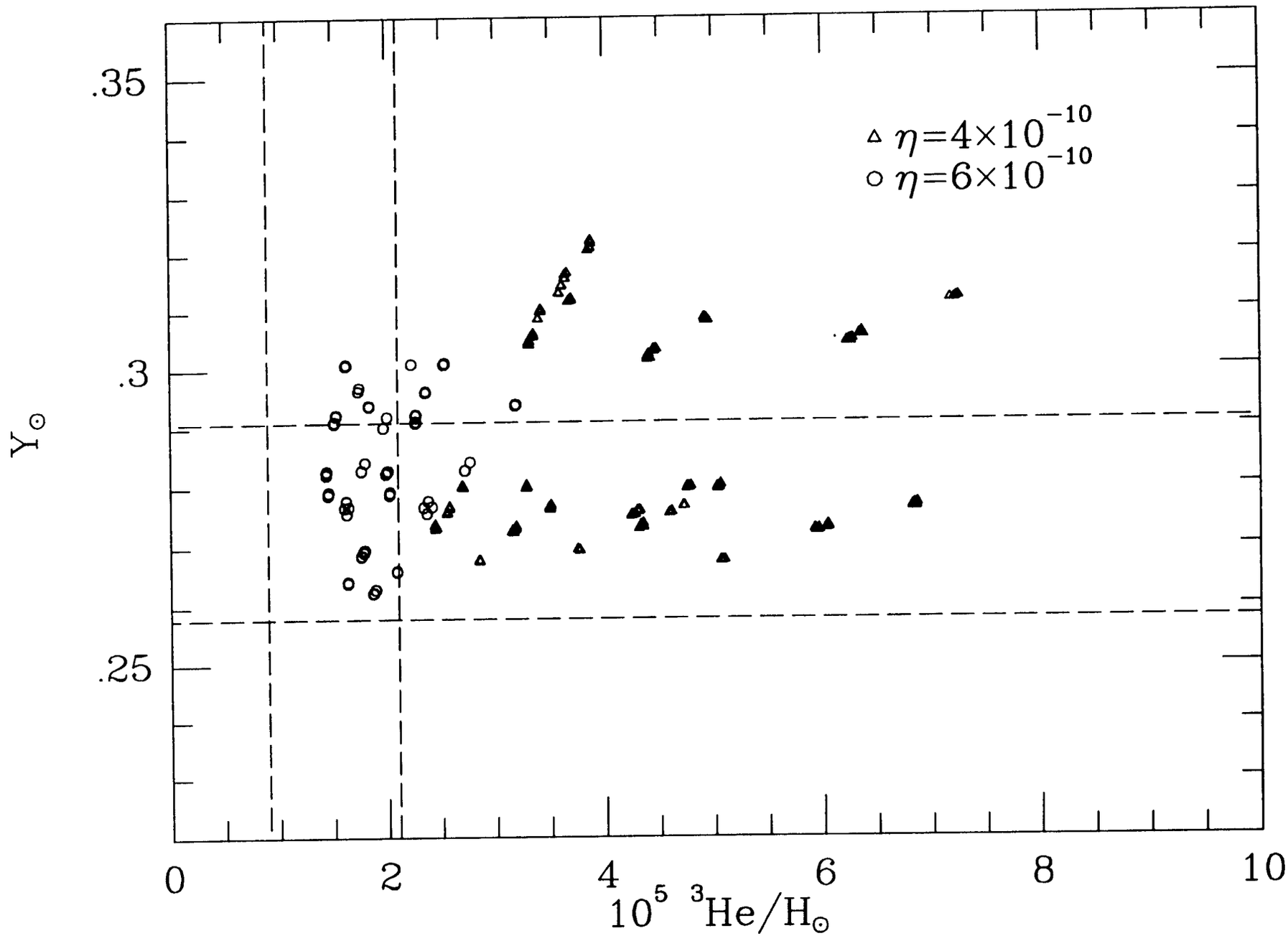
.35
.3
.25
$Y_\odot$
$\triangle\ \eta=4\times10^{-10}$
$\circ\ \eta=6\times10^{-10}$
0
2
4
6
8
10
$10^5\ ^3He/H_\odot$

FIG 26

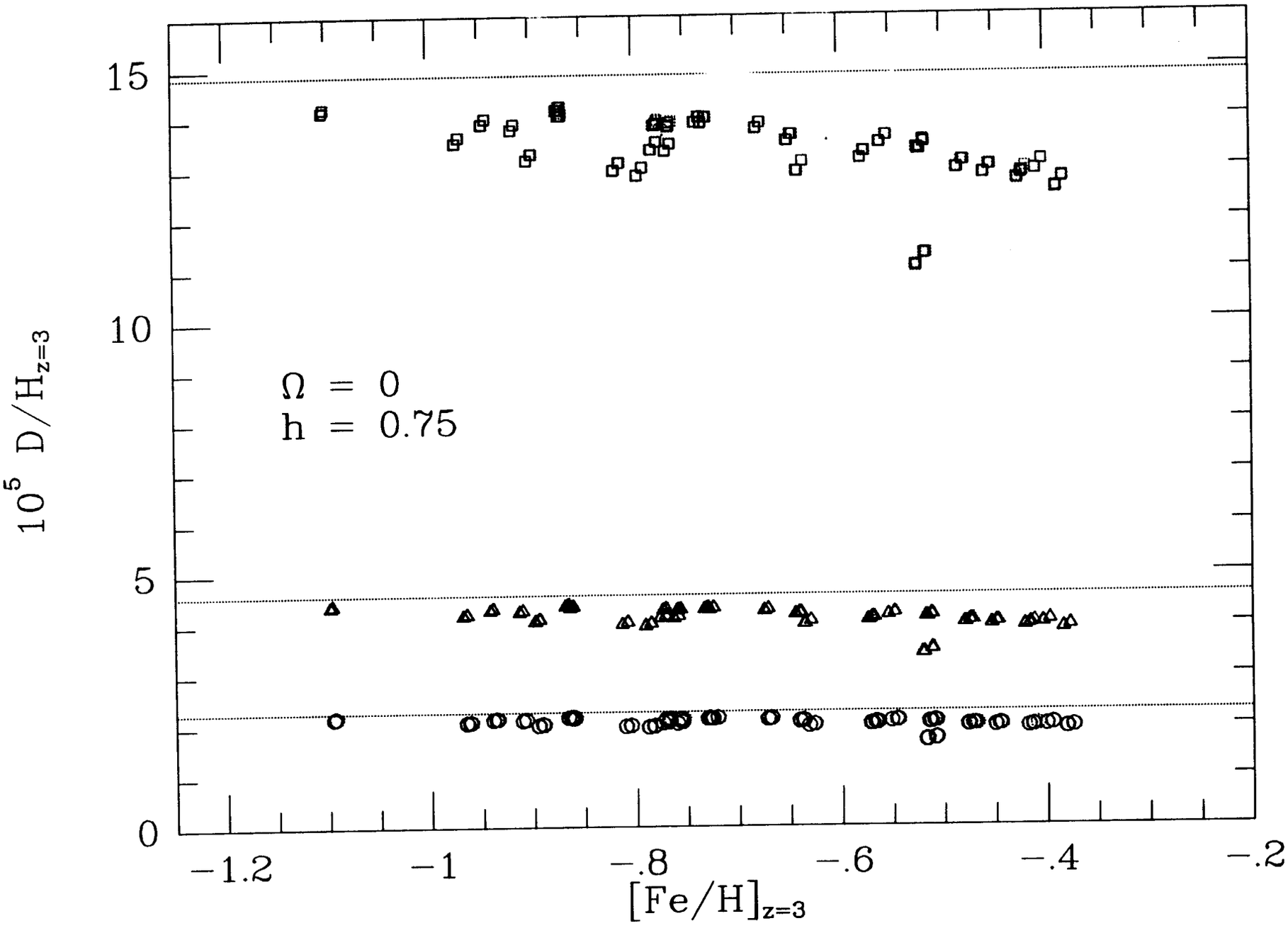

FIG 27

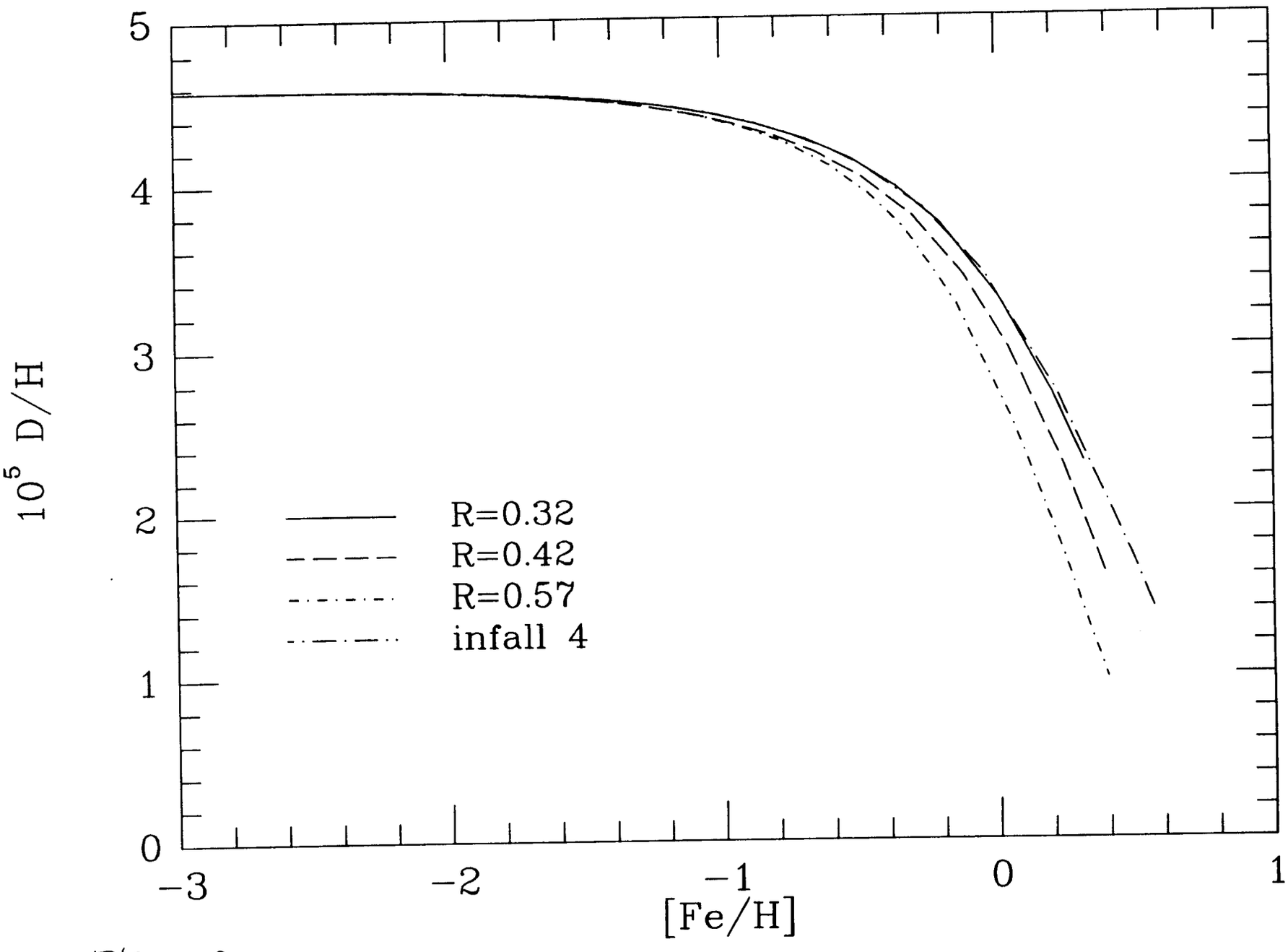

FIG 28

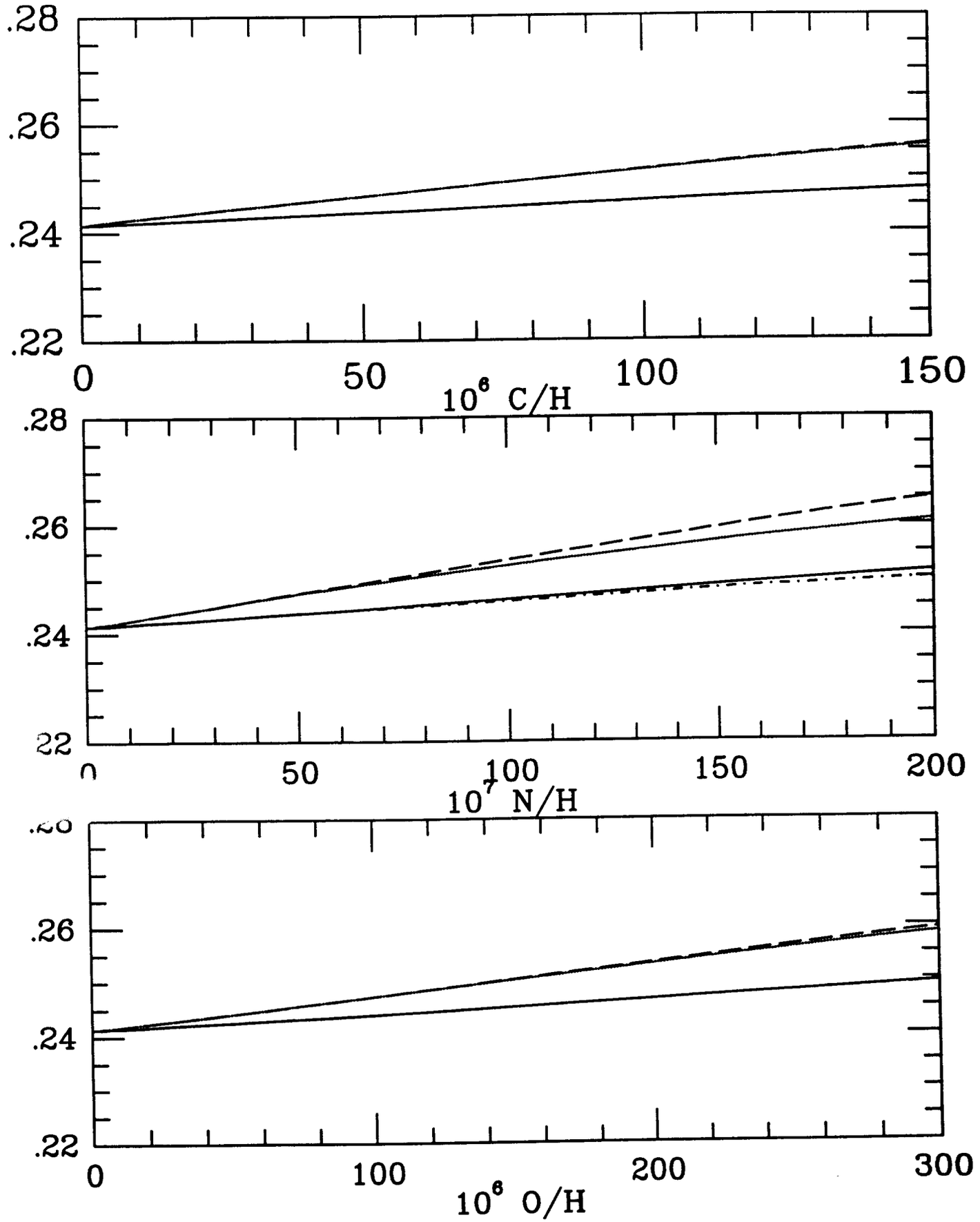
.28
.26
.24
.22
Y
0
50
100
150
10^6 C/H
.28
.26
.24
22
Y
0
50
100
150
200
10^7 N/H
.26
.24
.22
Y
0
100
200
300
10^6 O/H

FIG 29

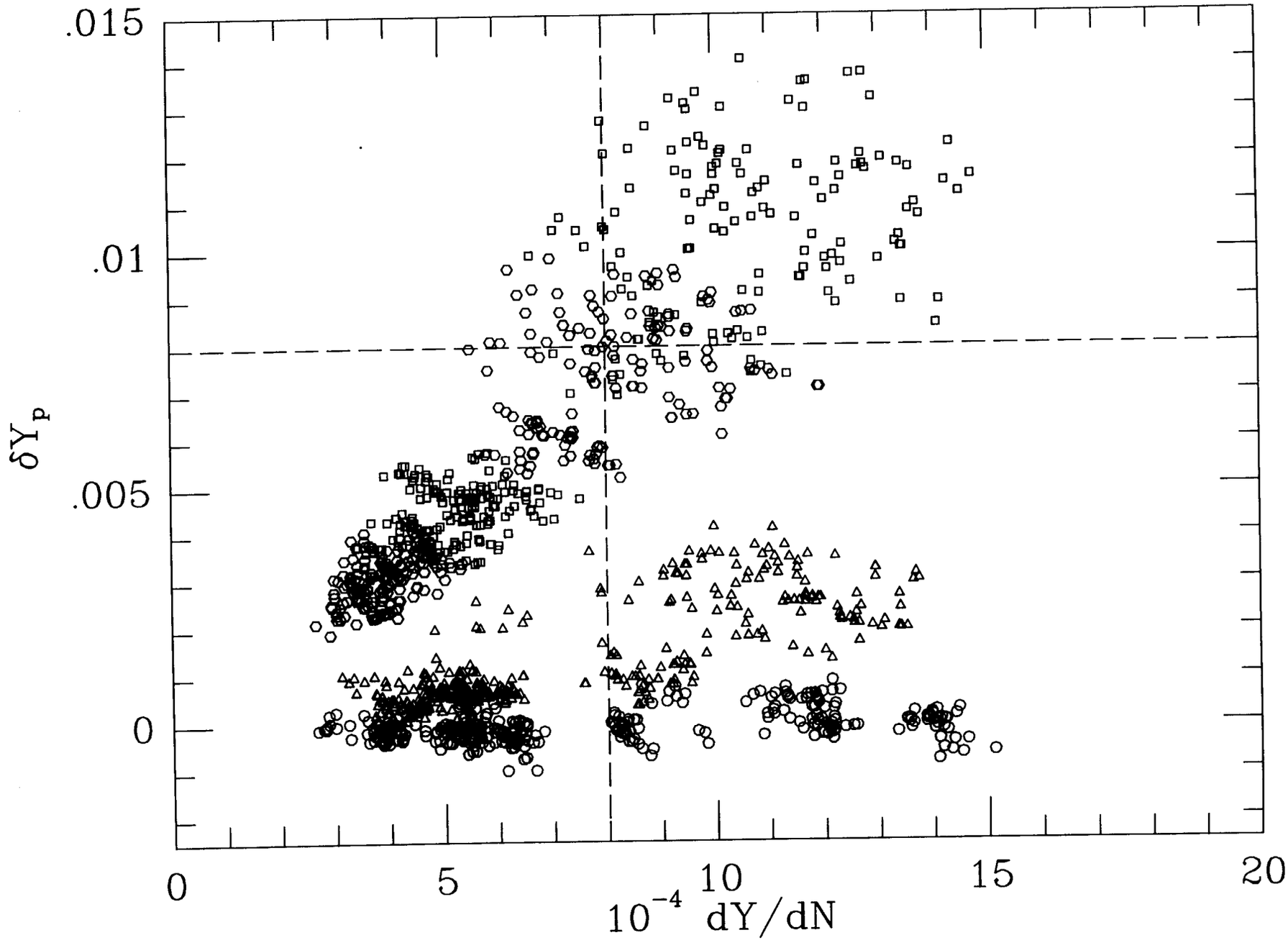

FIG 30